

STOCHASTIC CHARACTERIZATION AND MATHEMATICAL ANALYSIS OF  
FEEDFORWARD LINEARIZERS

A THESIS SUBMITTED TO  
THE GRADUATE SCHOOL OF NATURAL AND APPLIED SCIENCES  
OF  
THE MIDDLE EAST TECHNICAL UNIVERSITY  
BY

ARSLAN HAKAN COSKUN

IN PARTIAL FULFILLMENT OF THE REQUIREMENTS FOR THE DEGREE OF  
DOCTOR OF PHILOSOPHY  
IN  
THE DEPARTMENT OF ELECTRICAL AND ELECTRONICS ENGINEERING

SEPTEMBER 2003

Approval of the Graduate School of Natural and Applied Sciences.

---

Prof. Dr. Canan Özgen  
Director

I certify that this thesis satisfies all the requirements as a thesis for the degree of Doctor of Philosophy.

---

Prof. Dr. Mübeccel Demirekler  
Head of Department

This is to certify that we have read this thesis and that in our opinion it is fully adequate, in scope and quality, as a thesis for the degree of Doctor of Philosophy.

---

Assist. Prof. Dr. Simsek Demir  
Supervisor

Examining Committee Members

Prof. Dr. Canan TOKER (Chair)

Assist. Prof. Dr. Simsek DEMİR

Prof. Dr. Hayrettin KÖYMEN

Prof. Dr. Mete SEVERCAN

Prof. Dr. Altuncan HIZAL

## **ABSTRACT**

### **STOCHASTIC CHARACTERIZATION AND MATHEMATICAL ANALYSIS OF FEEDFORWARD LINEARIZERS**

Coskun, Arslan Hakan

Ph.D., Department of Electrical and Electronics Engineering

Supervisor: Assist. Prof. Dr. Simsek Demir

September 2003, 144 pages

Feedforward is known to be one of the best methods for power amplifier linearization due to its superior linearization performance and broadband stable operation. However feedforward systems have relatively poor power efficiency and are complicated due to the presence of two nonlinear amplifiers and the requirements of amplitude, phase and delay matching within two different loops. In this thesis stochastic characterization of a simple feedforward system with autocorrelation analysis has been presented for Code Division Multiple Access (CDMA) applications taking the amplitude and delay mismatches into consideration. It has been assumed that, the input signal can be represented as Gaussian noise, main and error amplifiers can be modeled with third order AM/AM nonlinearities and there exists no phase mismatch within the loops. Hence closed form expressions, which relate the main channel and distorted adjacent channel power at any point in the feedforward circuitry to the system parameters, have been obtained. Consequently, a mathematical handy tool is achieved towards specifying the circuit parameters

rapidly for optimum linearity performance and efficiency. The developed analytical model has been verified by Radio Frequency (RF) and system simulations. An alternative approach towards modeling feedforward systems for arbitrary signals has also been brought into consideration and has been verified with system simulations.

Keywords: Feedforward, Linearization, Stochastic characterization, System modeling, Autocorrelation analysis, Gaussian noise, CDMA.

## ÖZ

### İLERİBESLEME DOĞRUSALLAŞTIRICILARIN STOKASTİK KARAKTERİZASYONLARI VE MATEMATİKSEL ANALİZLERİ

Coşkun, Arslan Hakan

Doktora, Elektrik ve Elektronik Mühendisliği Bölümü

Tez Yöneticisi: Yrd. Doç. Dr. Şimşek Demir

Eylül 2003, 144 sayfa

İleribesleme, yüksek doğrusallaştırma performansı ve geniş bantlı kararlı çalışması ile güç yükselteç doğrusallaştırmasında bilinen en iyi yöntemlerden biridir. Ancak, ileribesleme sistemleri iki doğrusal olmayan yükseltecin varlığı ve iki ayrı döngü içinde genlik, faz ve gecikme uyumunun gerekliliği yüzünden karmaşıktır ve nispeten düşük güç verimliliği vardır. Bu tezde, basit bir ileribesleme sisteminin genlik ve gecikme uyumsuzlukları dikkate alınarak Kod Bölmeli Çoklu Erişim (CDMA) uygulamaları için otokorolasyon analiziyle stokastik karakterizasyonu sunulmaktadır. Giriş sinyalinin Gauss gürültüsü ile gösterilebildiği, ana ve hata yükselteçlerinin üçüncü dereceden genlik bozukluğu ile modellenebildiği ve döngüler içinde faz uyumsuzluklarının olmadığı varsayılmıştır. Böylelikle, ileribesleme devresinin herhangi bir noktasındaki ana kanal ve bozulmuş yan kanal güç seviyelerini sistem parametrelerine bağlayan kapalı ifadeler elde edilmiştir. Bunun sonucu olarak, optimum doğrusallaştırma performansı ve verimlilik için devre parametrelerini hızlı bir şekilde belirlemeye yönelik matematiksel, kullanışlı bir araç

elde edilmiştir. Geliştirilen analitik model Radyo Frekansı (RF) ve sistem simülasyonları ile doğrulanmıştır. İleribesleme sistemlerini rastgele sinyaller için modellemeye yönelik alternatif bir yaklaşım da dikkate getirilmiş ve sistem simülasyonları ile doğrulanmıştır.

Anahtar kelimeler: İleribesleme, Doğrusallaştırma, Stokastik karakterizasyon, Sistem modelleme, Otokorolasyon analizi, Gauss gürültüsü, CDMA.

*To my parents*

## ACKNOWLEDGMENTS

I would like to express my sincere gratitude to my thesis advisor Assist. Prof. Dr. Simsek Demir for his guidance, support and encouragement throughout the study of this thesis. It was a privilege for me to have an outstanding research experience under his supervision.

I would like to thank my thesis supervision committee members Prof. Dr. Canan Toker, Prof. Dr. Hayrettin Köymen, the former members Prof. Dr. Irsadi Aksun and Prof. Dr. Ayhan Altuntas for their guidance and constructive criticisms at every progress of this research. Special thanks also go to Assist. Prof. Dr. Arzu Koç for her technical and conceptual assistance during this work.

I am grateful to ASELSAN Electronics Industries for not only giving me the opportunity to improve my engineering capabilities but also providing me every kind of software, hardware and financial support throughout the progress of this work. I would like to acknowledge my department manager Dr. Faik Eken and my group leader Ibrahim Cantürk for their support, understanding, tolerance and invaluable discussions. It is also my pleasure to express my appreciation to my colleagues who always supported me spiritually and provided me a nice, friendly office atmosphere.

It is a distinction for me to acknowledge Dr. Murat Eron for sharing his experience and technical facilities with me, lighting the way for the concept of this research and his invaluable suggestions and contributions.

Finally, I would like to deeply appreciate my parents and my brother for their endless love, support, encouragement and patience throughout my life. This thesis would have been impossible without their guidance.

## TABLE OF CONTENTS

<b>ABSTRACT.....</b>	<b>iii</b>
<b>ÖZ.....</b>	<b>v</b>
<b>DEDICATION.....</b>	<b>vii</b>
<b>ACKNOWLEDGMENTS.....</b>	<b>viii</b>
<b>TABLE OF CONTENTS.....</b>	<b>ix</b>
<b>LIST OF FIGURES.....</b>	<b>xii</b>
<b>LIST OF TABLES.....</b>	<b>xvii</b>
<b>CHAPTER</b>	
<b>1. INTRODUCTION.....</b>	<b>1</b>
<b>2. OVERVIEW ON LINEARITY AND LINEARIZATION .....</b>	<b>5</b>
2.1 Concept of linearity .....	5
2.2 Types of nonlinearities – AM/AM and AM/PM .....	6
2.3 Measures of linearity .....	10
2.4 Types and natures of signals.....	12
2.5 Memory effects.....	14
2.6 Methods of linearization.....	16
2.6.1 Cartesian Feedback .....	16
2.6.2 Envelope Elimination and Restoration (EER).....	17
2.6.3 Linear Amplification using Nonlinear Components (LINC).....	18
2.6.4 RF Predistortion.....	19
2.6.5 Other linearization techniques .....	20
<b>3. OVERVIEW ON FEEDFORWARD .....</b>	<b>22</b>
3.1 Principle of operation .....	22
3.2 Delay matching.....	25

3.3 Gain and phase matching – Vector modulators.....	25
3.4 Error amplifier .....	28
3.5 Loop control .....	28
3.6 Efficiency considerations .....	31
3.7 Nested feedforward system .....	34
3.8 Research topics .....	35
3.8.1 Component approach .....	36
3.8.2 System approach .....	37
<b>4. FEEDFORWARD CHARACTERIZATION FOR CDMA SYSTEMS ....</b>	<b>40</b>
4.1 Overview .....	40
4.2 Model analysis .....	44
4.2.1 Transfer function of a feedforward circuit without delay mismatches	44
4.2.2 Main amplifier and feedforward output characterization .....	47
4.2.3 Feedforward output characterization with delay mismatches in the	
second loop .....	53
4.2.4 Feedforward output characterization with delay mismatches in both	
loops.....	54
4.2.5 Error amplifier input characterization with delay mismatch in the first	
loop .....	57
4.3 Verification of the model with simulations .....	59
4.3.1 Verification of the model in MATLAB environment.....	60
<b>5. RF SIMULATIONS .....</b>	<b>70</b>
5.1 Verification of the model using co-simulation .....	70
5.2 Verification of the model using Analog/RF envelope simulation.....	80
5.3 Phase mismatch considerations .....	88
5.4 Efficiency considerations .....	90
5.5 Verification of the model using complex Gaussian CDMA noise .....	91
5.6 Application of the model to a CDMA wideband system design .....	94

<b>6. APPLICATION OF A MULTITONE MODEL TO ANALYZE FEEDFORWARD CIRCUITS.....</b>	<b>99</b>
6.1 Representation of signals with various envelopes.....	100
6.2 Modeling the feedforward system.....	102
6.3 Application of the model to real time signals and discussions.....	103
6.3.1 Random signal.....	104
6.3.2 Wideband CDMA.....	109
6.4 Discussions and future research.....	117
<b>7. CONCLUSION.....</b>	<b>119</b>
<b>REFERENCES.....</b>	<b>125</b>
<b>APPENDIX</b>	
<b>A. COEFFICIENTS FOR THE MODEL PRESENTED IN CHAPTER 4.</b>	<b>130</b>
<b>B. CALCULATED EXPECTED VALUES FOR GAUSSIAN MULTI RANDOM VARIABLES.....</b>	<b>133</b>
<b>C. COEFFICIENTS FOR THE CUBE OF A TONE STREAM.....</b>	<b>142</b>
<b>VITA.....</b>	<b>144</b>

## LIST OF FIGURES

### FIGURES

2.1 Distortion products via a nonlinear amplifier.....	6
2.2 Block diagram for Cartesian Feedback. ....	17
2.3 Block diagram for EER. ....	18
2.4 Block diagram for LINC.....	19
2.5 Production of the inverse characteristic of an amplifier.....	20
3.1 Schematic of a feedforward circuit.....	23
3.2 Block diagram for a typical vector modulator.....	27
4.1 A simplified form of a feedforward circuit. ....	44
4.2 a) Response of (4.17) for various $IP3^e$ values( $IP3^m=45.5$ dBm, $G_m=20$ dB, $G_e=40$ dB, $C_1=C_3=C_4=10$ dB, $C_2=20$ dB) b) Response of (4.17) for various $C_2$ values ( $IP3^m=45.5$ dBm, $G_m=20$ dB, $IP3^e=50$ dBm, $G_e=40$ dB, $C_1=C_3=C_4=10$ dB). ....	46
4.3 Generation of the input data. ....	59
4.4 a) ADS simulation for main amplifier output. b) ADS simulation for feedforward output ( $C_1 = 10$ dB, $C_2 = 20$ dB, $C_3 = 10$ dB, $C_4 = 10$ dB, $G_m = 20$ dB, $IP3^m = 46$ dBm, $G_e = 40$ dB, $IP3^e = 50$ dBm).....	61
4.5 a) MATLAB simulation for main amplifier output. b) MATLAB simulation for feedforward output ( $C_1 = 10$ dB, $C_2 = 20$ dB, $C_3 = 10$ dB, $C_4 = 10$ dB, $G_m = 20$ dB, $IP3^m = 46$ dBm, $G_e = 40$ dB, $IP3^e = 50$ dBm)...	62
4.6 Comparison of MATLAB simulation and closed form expressions for a) main amplifier output b) feedforward output ( $C_1 = 10$ dB, $C_2 = 20$ dB, $C_3 = 10$ dB, $C_4 = 10$ dB, $G_m = 20$ dB, $IP3^m = 46$ dBm, $G_e = 40$ dB, $IP3^e = 50$ dBm, $P_{out} = 28.5$ dBm. ....	63

4.7 (a) Time domain data at the input of the main amplifier for IP3 <sup>m</sup> = 45.8 dBm. (b) Time domain data at the input of the error amplifier for IP3 <sup>m</sup> = 45.8 dBm. ....	66
4.8 Comparison of MATLAB simulation and closed form expressions for feedforward output (C <sub>1</sub> = 10 dB, C <sub>2</sub> = 20 dB, C <sub>3</sub> = 10 dB, C <sub>4</sub> = 10 dB, G <sub>m</sub> = 20 dB, IP3 <sup>m</sup> = 46 dBm, G <sub>e</sub> = 40 dB, IP3 <sup>e</sup> = 50 dBm, P <sub>out</sub> = 28.5 dBm, t <sub>2</sub> =270 nsec) .....	67
4.9 Comparison of the closed form and simulation results a) t <sub>1</sub> =1, t <sub>2</sub> =0 b) t <sub>1</sub> =1, t <sub>2</sub> =1 samples. ....	68
5.1 Schematic of the feedforward system in DSP co-simulation environment. .....	71
5.2 Schematic of the main amplifier – d2001uk_amp.....	73
5.3 SPICE model of D2001UK. ....	73
5.4 (a) Phase variation (b) gain variation of the main amplifier at 300 MHz	74
5.5 (a) Phase variation (b) gain variation of the main amplifier at 350 MHz. .....	75
5.6 (a) Phase variation (b) gain variation of the error amplifier at 350 MHz.	75
5.7 Schematic of the error amplifier. ....	76
5.8 Main amplifier output power spectrum at 350 MHz for C <sub>1</sub> =C <sub>3</sub> =C <sub>4</sub> =10, C <sub>2</sub> =13 dB, t <sub>1</sub> = t <sub>2</sub> =0 a) Model b) ADS co-simulation. ....	77
5.9 Feedforward output power spectrum at 350 MHz for C <sub>1</sub> =C <sub>3</sub> =C <sub>4</sub> =10, C <sub>2</sub> =13 dB, t <sub>1</sub> = t <sub>2</sub> =0 a) Model b)ADS co-simulation. ....	78
5.10 Power spectrum at the feedforward output at 350 MHz for C <sub>1</sub> =11dB, C <sub>2</sub> =12dB, C <sub>3</sub> =10.5dB, C <sub>4</sub> =9dB, t <sub>1</sub> = t <sub>2</sub> =0 a) Model b) ADS co-simulation .....	78
5.11 Feedforward output power spectrum at the at 350 MHz for C <sub>1</sub> =C <sub>3</sub> =C <sub>4</sub> =10, C <sub>2</sub> =13dB, t <sub>1</sub> =0, t <sub>2</sub> =270 nsec a) Model b) ADS co- simulation. ....	78
5.12 Error amplifier input power spectrum at 350 MHz for C <sub>1</sub> =C <sub>3</sub> =C <sub>4</sub> =10, C <sub>2</sub> =13 dB, t <sub>1</sub> =270 nsec, t <sub>2</sub> =0 nsec a) Model b) ADS co-simulation.....	79
5.13 Feedforward output power spectrum at 350 MHz for C <sub>1</sub> =C <sub>3</sub> =C <sub>4</sub> =10, C <sub>2</sub> =13 dB, t <sub>1</sub> =270 nsec, t <sub>2</sub> =0 nsec a) Model b) ADS co-simulation.....	79
5.14 Feedforward output power spectrum at 350 MHz for C <sub>1</sub> =C <sub>3</sub> =C <sub>4</sub> =10, C <sub>2</sub> =13dB, t <sub>1</sub> =270 nsec, t <sub>2</sub> =270 nsec a) Model b) ADS co-simulation.....	79

5.15 Schematic of the feedforward system in Analog/RF envelope simulation environment.....	82
5.16 Comparison of the model and envelope simulation results for varying $C_1$ at 350MHz. $C_3=C_4=10$ dB, $C_2=13$ dB, $t_1=0$ , $t_2=0$ .....	85
5.17 Comparison of the model and envelope simulation results for varying $C_4$ at 350MHz. $C_1=C_3=10$ dB, $C_2=13$ dB, $t_1=0$ , $t_2=0$ a) $IP3^m=31.6$ dBm, $IP3^e=38$ dBm b) $IP3^m=31.9$ dBm, $IP3^e=38.5$ dBm.....	85
5.18 Comparison of the model and envelope simulation results for varying $IP3^e$ at 350MHz. $C_1=C_4=10$ dB, $C_3=11$ dB, $C_2=13$ dB, $t_1=0$ , $t_2=0$ .....	86
5.19 Comparison of the model and envelope simulation results for varying $IP3^e$ at 350MHz. $C_1=C_4=C_3=10$ dB, $C_2=13$ dB, $t_1=0$ , $t_2=0$ .....	86
5.20 Comparison of the model and envelope simulation results for varying $t_1$ at 350MHz. $C_1=C_4=10$ dB, $C_3=11$ dB, 9 dB, $C_2=13$ dB, $IP3^e=34$ dBm, $t_2=0$ .....	87
5.21 Comparison of the model and envelope simulation results for varying $t_1$ at 350MHz. $C_1=11$ dB, $C_3=9$ dB, $C_4=10$ dB, $C_2=13$ dB, $IP3^e=34$ dBm, $t_2=0$ .....	87
5.22 Comparison of the model and envelope simulation results for varying $t_2$ at 350MHz. $C_1=C_4=C_3=10$ dB, $C_2=13$ dB, $t_1=0$ .....	88
5.23 Power spectrum a) at the feedforward input b) main amplifier output. ..	91
5.24 Power spectrum at the feedforward output at 350 MHz for $C_1=C_3=C_4=10$ , $C_2=13$ dB, $t_1=t_2=0$ a) Model b) ADS co-simulation.....	92
5.25 Power spectrum at the feedforward output at 350 MHz for $C_1=11$ dB, $C_2=12$ dB, $C_3=10.5$ dB, $C_4=9$ dB, $t_1=t_2=0$ a) Model b) ADS co-simulation.....	92
5.26 Power spectrum at the feedforward output at 350 MHz for $C_1=C_3=C_4=10$ , $C_2=13$ dB, $t_1=0$ , $t_2=270$ nsec a) Model b) ADS co-simulation.....	92
5.27 Power spectrum at the error amplifier input at 350 MHz for $C_1=C_3=C_4=10$ , $C_2=13$ dB, $t_1=270$ nsec, $t_2=0$ nsec a) Model b) ADS co-simulation .....	93
5.28 Power spectrum at the feedforward output at 350 MHz for $C_1=C_3=C_4=10$ , $C_2=13$ dB, $t_1=270$ nsec, $t_2=0$ nsec a) Model b) ADS co-simulation.....	93
5.29 Power spectrum at the feedforward output at 350 MHz for $C_1=C_3=C_4=10$ , $C_2=13$ dB, $t_1=270$ nsec, $t_2=270$ nsec a) Model b) ADS co-simulation.....	93

5.30 a) Main amplifier output b) Feedforward output (ADS simulation for nominal parameter values around 300 MHz). .....	96
5.31 Comparison of the model and simulation results for $P_{out}$ and $P_{outacp}$ for the parameter variations listed in Table 5.8.....	98
5.32 Comparison of the model and simulation results for $P_{out}$ and $P_{outacp}$ for the parameter variations listed in Table 5.9.....	98
6.1 a) Time domain envelope b) Envelope histogram of the generated random signal.....	104
6.2 Power spectrum of the random signal a) Main amplifier output b) Feedforward output - $C_1=C_2=C_3=C_4=10$ dB, $IP3^m=33$ dBm, $IP3^e=33$ dBm, $G_m=10$ dB and $G_e=30$ dB.....	104
6.3 Feedforward output power and ACP for various $C_1$ - $m_1=0.55$ , $m_2=0.9$ $m_3=0.1$ - $C_2=C_3=C_4=10$ dB, $G_m=10$ dB, $IP3^m=33$ dBm, $G_e=30$ dB, $IP3^e=35$ dBm. ....	107
6.4 Feedforward output power and ACP for various $C_4$ - $m_1=0.55$ , $m_2=0.9$ $m_3=0.1$ - $C_1=C_2=C_3=10$ dB, $G_m=10$ dB, $IP3^m=33$ dBm, $G_e=30$ dB, $IP3^e=35$ dBm. ....	107
6.5 Feedforward output power and ACP for various $C_3$ - $m_1=0.55$ , $m_2=0.9$ $m_3=0.1$ - $C_1=C_2=C_4=10$ dB, $G_m=10$ dB, $IP3^m=33$ dBm, $G_e=30$ dB, $IP3^e=35$ dBm. ....	108
6.6 a) Time domain envelope b) Envelope histogram of the generated real WCDMA data.....	110
6.7 Power spectrum of the real WCDMA signal a) Main amplifier output b) Feedforward output - $C_1=C_2=C_3=C_4=10$ dB, $IP3^m=36$ dBm, $IP3^e=35$ dBm, $G_m=10$ dB and $G_e=30$ dB.....	110
6.8 Feedforward output power and ACP for various $C_1$ - $m_1=0.9$ , $m_2=0.4$ $m_3=0.15$ - $C_2=C_3=C_4=10$ dB, $G_m=10$ dB, $IP3^m=36$ dBm, $G_e=30$ dB, $IP3^e=40$ dBm. ....	111
6.9 Feedforward output power and ACP for various $C_4$ - $m_1=0.9$ , $m_2=0.4$ $m_3=0.15$ - $C_1=C_2=C_3=10$ dB, $G_m=10$ dB, $IP3^m=36$ dBm, $G_e=30$ dB, $IP3^e=35$ dBm. ....	112
6.10 Feedforward output power and ACP for various $C_3$ - $m_1=0.9$ , $m_2=0.4$ , $m_3=0.15$ - $C_1=C_2=C_4=10$ dB, $G_m=10$ dB, $IP3^m=36$ dBm, $G_e=30$ dB, $IP3^e=40$ dBm. ....	112

6.11 a) Time domain envelope b) Envelope histogram of the generated complex WCDMA data. ....	113
6.12 Power spectrum of the complex WCDMA signal a) Main amplifier output b) Feedforward output - $C_1=C_2=C_3=C_4=10$ dB, $IP3^m=36$ dBm, $IP3^e=40$ dBm, $G_m=10$ dB and $G_e=30$ dB. ....	114
6.13 Feedforward output power and ACP for various $C_1 - m_1=0.9, m_2=m_3=0, m_4=0.3 - C_2=C_3=C_4=10$ dB, $G_m=10$ dB, $IP3^m=36$ dBm, $G_e=30$ dB, $IP3^e=40$ dBm. ....	115
6.14 Feedforward output power and ACP for various $C_4 - m_1=0.9, m_2=m_3=0, m_4=0.3 - C_1=C_2=C_3=10$ dB, $G_m=10$ dB, $IP3^m=36$ dBm, $G_e=30$ dB, $IP3^e=35$ dBm. ....	116
6.15 Feedforward output power and ACP for various $C_3 - m_1=0.9, m_2=m_3=0, m_4=0.3 - C_1=C_2=C_3=10$ dB, $G_m=10$ dB, $IP3^m=36$ dBm, $G_e=30$ dB, $IP3^e=40$ dBm. ....	116

## LIST OF TABLES

### TABLES

4.1 Quantitative comparison of the closed form and simulation results ( $C_1 = 10$ dB, $C_2 = 20$ dB, $C_3 = 10$ dB, $C_4 = 10$ dB, $G_m = 20$ dB, $IP3^m = 46$ dBm, $G_e = 40$ dB, $IP3^e = 50$ dBm, $P_{out} = 28.5$ dBm).....	64
4.2 Quantitative comparison of the closed form and simulation results for different loop mismatches ( $l_1=l_2=l_3=l_4=0.3$ dB, $C_1 = 10$ dB, $C_2 = 20$ dB, $C_3 = 10$ dB, $C_4=10$ dB, $G_m = 20$ dB, $IP3^m = 46$ dBm, $G_e = 40$ dB, $IP3^e = 50$ dBm, $P_{out} = 28.5$ dBm). .....	64
4.3 Quantitative comparison of the closed form and simulation results for $t_2=270$ nsec ( $C_1 = 10$ dB, $C_2 = 20$ dB, $C_3 = 10$ dB, $C_4 = 10$ dB, $G_m = 20$ dB, $IP3^m = 46$ dBm, $G_e = 40$ dB, $IP3^e = 50$ dBm, $P_{out} = 28.5$ dBm). .....	68
4.4 Main amplifier and feedforward outputs for various fifth order nonlinearities – $a_5$ values ( $C_1 = 10$ dB, $C_2 = 20$ dB, $C_3 = 10$ dB, $C_4 = 10$ dB, $G_m = 20$ dB, $IP3^m = 46$ dBm, $G_e = 40$ dB, $IP3^e = 50$ dBm, $P_{out} = 28.5$ dBm). .....	69
4.5 Equivalent third order model $a_3$ coefficients and $IP3^m$ values for the fifth order nonlinearities presented in Table 4.4 ( $C_1 = 10$ dB, $C_2 = 20$ dB, $C_3 = 10$ dB, $C_4 = 10$ dB, $G_m = 20$ dB, $G_e = 40$ dB, $IP3^e = 50$ dBm, $P_{out} = 28.5$ dBm). .....	69
5.1 Variation of gain and $IP3$ of the main amplifier for different gate voltages at 350 MHz. ....	74
5.2 Comparison of the co-simulation and model results for different cases at 350 MHz. ....	80

5.3 Effect of the phase mismatch in the first loop at 350MHz - $IP3^e=38$ dBm, $IP3^m = 31.6$ dBm, $C_1=C_3=C_4=10$ dB, $C_2=13$ dB. ....	88
5.4 Effect of the phase mismatch in the first loop at 350MHz - $IP3^e=38$ dBm, $IP3^m=31.6$ dBm, $C_1=C_4=10$ dB, $C_3=11$ dB, $C_2=13$ dB. ....	89
5.5 Effect of the phase mismatch in the first loop at 350MHz - $IP3^e=34$ dBm, $IP3^m=31.6$ dBm, $C_1=C_4=10$ dB, $C_3=11$ dB, $C_2=13$ dB, $t_1=100$ nsec. ....	89
5.6 Effect of the phase mismatch in the second loop at 350 MHz - $IP3^e=38$ dBm, $IP3^m=31.6$ dBm, $C_1=C_4=10$ dB, $C_3=11$ dB, $C_2=13$ dB.....	89
5.7 Comparison of the co-simulation and model results for different cases at 350MHz.....	94
5.8 Initial parameter variations in the feedforward circuit. ....	95
5.9 Optimized parameter variations in the feedforward circuit.....	98
6.1 Different harmonic sets to model the random signal $C_1=C_2=C_3=C_4=10$ dB, $IP3^m=33$ dBm, $IP3^e=33$ dBm, $G_m=10$ dB, $G_e=30$ dB.....	106
6.2 Comparison of the simulation and model results for different $IP3^e$ values, $C_1=C_2=C_3=C_4=10$ dB, $IP3^m=33$ dBm, $G_m=10$ dB, $G_e=30$ dB.....	108
6.3 Comparison of the simulation and model results for different $IP3^m$ values, $C_1=C_2=C_3=C_4=10$ dB, $IP3^e=33$ dBm, $G_m=10$ dB, $G_e=30$ dB.....	109
6.4 Different harmonic sets to model the real WCDMA signal $C_1=C_2=C_3=C_4=10$ dB, $IP3^m=36$ dBm, $IP3^e=35$ dBm, $G_m=10$ dB, $G_e=30$ dB .....	111
6.5 Comparison of the simulation and model results for different $IP3^e$ values, $C_1=C_2=C_3=C_4=10$ dB, $IP3^m=36$ dBm, $G_m=10$ dB, $G_e=30$ dB.....	113
6.6 Different harmonic sets to model the complex WCDMA signal $C_1=C_2=C_3=C_4=10$ dB, $IP3^m=36$ dBm, $IP3^e=40$ dBm, $G_m=10$ dB, $G_e=30$ dB. ....	115

# CHAPTER 1

## INTRODUCTION

Modern communication systems use digital modulation techniques to transmit more data at high data rates and preserve the quality of the signal without loss of information. Digital modulation involves individual bits or symbols with finite time duration in baseband, which are produced as a result of sampling analog data at a given sampling rate. Since baseband waveform is time limited its power spectral density extends effectively over a very wide frequency spectrum. In order to avoid frequency components fall outside the channel bandwidth (interchannel interference) the signal is lowpass filtered so that its spectrum can be frequency limited [1]. However this process results with time spreading of individual bits and symbols which cause them to overlap. This is called Inter Symbol Interference (ISI). Hence there is a trade off between frequency occupation of the signal and ISI. To minimize ISI usually raised cosine filters are used. Another disadvantage of filtering process is the fluctuation of the envelope when the baseband is modulated onto an RF signal. In other words the signal is no more a constant amplitude one [2]. Another source of non-constant envelope signals is the multicarrier transmission which can be seen in basestation applications. Amplification of non-constant envelope signals requires power amplifiers whose back-off powers are determined by the envelope peak-to-average ratio of the signal, namely crest factor to avoid intermodulation distortion for multi-carrier signals and spectral regrowth for digitally modulated signals. If linearity cannot be achieved to an adequate level then unwanted spurious signals would allocate adjacent channels resulting with reduction in number of useful

channels and poor performance in sensitivity and bit error rate. If the RF signal to be modulated were a constant envelope one then a nonlinear type of amplifier would work well and it would be power efficient since no bias (or a very small amount of) current is required. However in the case of linear amplification Class A type amplifiers are required where bias current level is high resulting with high DC power consumption and extremely low power efficiency. Moreover the amplifier should operate several dB below saturation (backed off) depending on the nature of the signal and required linearity level. For a linear 50W output for instance, if 7 dB back-off power is required then an amplifier that has an output power capacity of more than 200W is required which may require several output transistors working in parallel. These limitations increase the cost and complexity of the circuitry.

In order to overcome efficiency and output power capability problems and improve efficiency some auxiliary circuitries (linearizers) are used. There are several techniques to accomplish this task. The most popular ones are Cartesian feedback, predistortion, Envelope Elimination and Restoration (EER), Linearization using Nonlinear Components (LINC) and feedforward. Among these methods, feedforward has a better linearization performance and provides a more broadband stable operation since it carries no feedback path whereas it has the limitation of efficiency [2].

Feedforward linearizers involve two cancellation loops. Linearity performance of the linearizer depends on how well amplitude, delay and phase matching are maintained within these two loops. The system has lots of parameters to be optimized for the best efficiency and a given linearity performance. Hence analytical tools which relate the power spectral density and absolute power at any point in the system to the system parameters are essential in order to adjust component tolerances particularly for broadband performance. In this thesis, an analytical model of a feedforward system including amplitude and delay mismatches has been proposed for Code Division Multiple Access (CDMA) applications. The reasons for focusing on CDMA are the facts that CDMA is one of the most popular schemes used in cellular communication systems because of its spectral efficiency and stochastic characterization for CDMA signal for a large number of users is

relatively simple to model. Consequently, a flexible, mathematical and handy tool has been developed for the designer to work out the complexity of the system and observe the impact of different combination of parameter variations particularly at the beginning of the design. The superiority of the model over other classical simulation tools is its capability of providing the correct results instantly and hence decreasing design durations dramatically. Additionally an alternative mathematical analysis has also been proposed to model feedforward systems for arbitrary waveforms.

In literature there have been various works towards characterizing amplifier nonlinearities for CDMA Gaussian processes and bandlimited white Gaussian noise. These activities involve relating output and input envelopes to each other and characterizing the amplifier using autocorrelation analysis. A brief overview on these research activities has been presented at the beginning of Chapter 4. There has also been a lot of research on analyzing and improving the feedforward components and system performance. Main aspect and novelty of the research presented in this thesis is to extend the autocorrelation analysis to a complete feedforward system including nonlinearities and delay mismatches existing in two different loops. Since nonlinearities and delay mismatches are coupled to each other, the resulting analysis becomes very complex and the order of nonlinearity is higher than those of individual nonlinear amplifiers. Nevertheless, by working out this complexity some handy mathematical relationships and closed form equations have been obtained.

To summarize, the concept of this thesis includes constructing a precise and realistic mathematical amplifier model analyzing an arbitrary input waveform stochastically and defining an effective peak to average ratio and based on these analyses constructing a mathematical model for the overall feedforward circuitry and optimizing the specifications of the active and passive components for IMD performance, bandwidth and efficiency.

In Chapter 2, first, concept of linearity and linearization is going to be discussed, and then popular linearization techniques will be mentioned. In Chapter 3, feedforward linearizer will be analyzed in details and research topics will be discussed. For the sake of completeness, literature survey on linearity and

linearization, and feedforward linearization techniques are present in these chapters, Chapters 2 and 3 respectively. In Chapter 4, a mathematical analysis and characterization of a simple feedforward circuit is going to be presented for CDMA applications. The validity range of the model and verifications will be discussed. Verification of the model with RF simulations will be performed in Chapter 5. In Chapter 6, an alternative approach to analyze feedforward linearizers for an arbitrary source signal will be proposed. In Chapter 7, we are going to conclude the results that have been obtained.

## CHAPTER 2

### OVERVIEW ON LINEARITY AND LINEARIZATION

#### 2.1 Concept of linearity

An ideal linear amplifier has constant gain and linear phase characteristics over the bandwidth of interest and output voltage is proportional to the input voltage, that is:

$$V_{out} = GV_{in} \quad (2.1)$$

where  $G$  is the gain of the amplifier. In other words a certain percentage of increase in input voltage results with the same percentage of increase in the output voltage. However in real life there is no such a linear relationship and deviation from this linearity can be expressed as follows [2]:

$$V_{out} = G_1V_{in} + G_2V_{in}^2 + G_3V_{in}^3 + \dots + G_nV_{in}^n \quad (2.2)$$

The power series expansion (2.2) approximates the nonlinear behavior of the amplifier in the immediate vicinity of a particular DC operating point. If the input signal is a single tone (a sinusoid at a single frequency), this nonlinearity will produce harmonics, which can be eliminated using harmonic filters. However, if the input is a multitone signal then the output signal will contain side products by the fundamental tones in addition to harmonics as seen in Figure 2.1. These side products are called intermodulation products and unfortunately cannot be filtered out since they are very close to frequency of interest [3]. The first order coefficient represents the linear gain while the third, fifth and seventh order coefficients become

more dominant as the amplifier gets into compression. Eventually, for instance the fifth degree term contributes to not only fifth order but also third order IMD products.

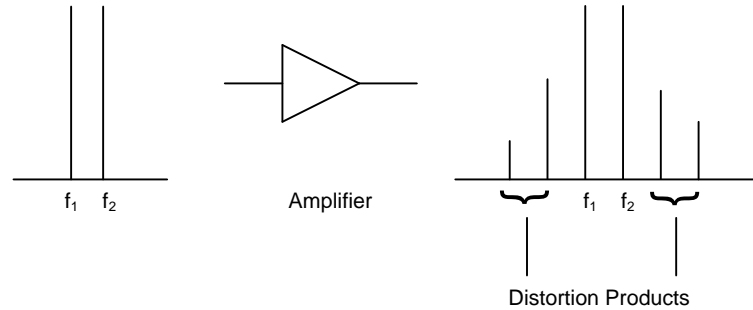


**Figure 2.1** Distortion products via a nonlinear amplifier.

These coefficients are sensitive to changes in input and output tuning and to the bias levels at input and output. The power series expansion is particularly useful in analyzing the weakly nonlinear properties of the amplifier. Strongly nonlinear effects can be expressed in terms of the nonlinear relationships between the drain current and the gate voltage in a typical FET transistor. A realistic relationship can be derived in a form of power series [4]:

$$I_d = g_0 + g_1V_g + g_2V_g^2 + g_3V_g^3 \quad (2.3)$$

where  $I_d$  and  $V_g$  represent the drain current and gate voltage of a MOSFET, respectively. The IMD products are due to not only amplitude (AM/AM) but phase (AM/PM) nonlinearities of the amplifiers as well.

## 2.2 Types of nonlinearities – AM/AM and AM/PM

The AM/AM characteristic represents the amplitude characteristics of the amplifier. At low power levels output power follows the input with a linear function. As the input power increases output power begins to deviate from this linearity and gets into compression. There is a certain input power level where the output power level is 1 dB less than the expected. Output power at this point is called 1 dB

compression (COMP) point and is an important measure of the amplifier. The higher 1 dB compression is, the better linearity for a given power level. As the input power is increased even more, the amplifier gets into a region where no more output power comes out. This point is called the Saturation (SAT) point. The difference between the SAT point and 1-dB COMP point gives us an idea about the linearity of the amplifier. As the 1dB COMP point converges to SAT the degree of the linearity of the amplifier increases [3]. There is a theoretical point where the power levels of the fundamental tone and the third order distortion product meet. This point is called IP3 point and is another important measure of linearity of the amplifier [2]. If the nonlinearity of the amplifier is assumed to be limited by only the third order effects, it can be derived that [5]:

$$IP3 = P_{out} + IM_3 / 2 \quad (2.4)$$

where,  $P_{out}$  is the output power per tone (for a two tone test) and  $IM_3$  is the third order intermodulation distortion below one of the tones (dBc). Hence for a given output power level, the higher IP3, the less IMD. Keeping the same assumptions in mind, it can be shown that IP3 point turns out to be about 10 dB above the 1dB compression point for a single tone (in a two tone analysis) and 13 dB for the total power [4]. Although it is impossible for an amplifier to produce IMD power at 10 dB above its 1dB compression point, using this approach one can estimate about the amount of third order IMD within a few decibels at a low output power level in the linear region. If higher order terms can be included in this analysis then a more realistic and precise relationship can be derived. A similar two tone test can be applied to obtain the fifth order intercept point -IP5- using the following relationship [6]:

$$IP5 = P_{out} + IM_5 / 4 \quad (2.5)$$

where  $IM_5$  is the fifth order intermodulation product.

The nth order IM Intercept point of a cascaded system in terms of IPs of individual stages can be expressed as follows [7]:

$$IP_n^{(1-n)/2} = IP_{n,M}^{(1-n)/2} + (G_M IP_{n,M-1})^{(1-n)/2} + (G_M G_{M-1} IP_{n,M-2})^{(1-n)/2} + \dots \quad (2.6)$$

where,  $IP_{n,m}$  is the  $n^{\text{th}}$  order intercept point of the  $m^{\text{th}}$  stage and  $G_m$  is the gain of the  $m^{\text{th}}$  stage. This expression assumes that distortion voltages produced by each stage are combined in phase. Hence it is a worst case since IM products are not necessarily in phase in especially long cascade of stages. Using Volterra analysis it can be shown that the worst case is valid if  $n^{\text{th}}$  order nonlinear characteristics of the stages are identical and excitation frequencies in two tone analysis are closed to each other.

The AM/PM characteristics represent the phase nonlinearities of the amplifier. Ideally, the amount of phase shift or time delay introduced by the amplifier should be independent of input power level. However in practical amplifiers, phase shift can be a function of the input power level and can convert the amplitude variations in signal level to frequency modulation [3]. Hence distortion products similar to FM sidebands appear near to the fundamental tones. IMD terms generated due to the phase nonlinearities can be 180 degrees out of phase, which cause asymmetry between the upper and lower IMD products. This phenomenon may also cause the fifth or higher order distortion products become higher than the third order ones which are expected to be dominant. AM/PM conversion factor ( $K_p$ ) can be found out using a two tone test, where one of the tones is 20-30 dB lower than the other one. A general equation for  $K_p$  ( $^{\circ}/\text{dB}$ ) is [8]:

$$K_p = \frac{2}{0.152} \sqrt{S_1^2 - \left( \frac{1 + S_1^2 - S_2^2}{2} \right)^2} \quad (2.7)$$

where

$$S_1 = \log^{-1} \left( \frac{\Delta P - \Delta P_{2,out}}{20} \right) \quad (2.8)$$

$$S_2 = \log^{-1} \left( \frac{\Delta P - \Delta P_{3,im}}{20} \right) \quad (2.9)$$

$\Delta P$  is the input tone difference in dB,  $\Delta P_{2,out}$  is output tone difference in dB,  $\Delta P_{3,im}$  is the tone difference between output larger tone and larger third order IMD product in

dB. In [8] an alternative equation to get  $K_p$  for small signal systems, is derived as follows:

$$K_p = 13.2 \log^{-1} \left( \frac{P_{1,in} + G - P_{int}}{10} \right) \quad (2.10)$$

where  $P_{1,in}$  is the larger input signal in dBm,  $G$  is the gain of the amplifier and  $P_{int}$  is the third order intercept point of the amplifier.

An alternative approach to determine gain compression and AM/PM conversion factors is proposed in [9]. If the input signal is a low index AM signal whose AM sidebands are in phase, then the power amplifier will compress these sidebands due to AM/AM nonlinearity and additionally PM sidebands will be generated with a 90 degrees phase difference with AM sidebands due to AM/PM nonlinearity. At the output, the sideband at the same frequency is the vector sum of AM sideband with the quantity  $G(1-c)\alpha A_0/2$  and the generated PM sideband with a 90 phase difference and a quantity  $Gk_p\alpha A_0/2$ , where  $A_0$  is the amplitude of the input signal,  $\alpha$  is the modulation index,  $c$  is the AM-AM compression factor,  $k_p$  is the AM-PM conversion coefficient and  $G$  is the gain, respectively. Similarly for a low-phase deviation PM input signal whose sidebands are out of phase with the quantity  $\beta A_0/2$ , where  $\beta$  is the phase deviation of the PM signal, the sideband at the output of the amplifier will have a quantity  $G\beta A_0/2$  and the same phase with the input sideband. By measuring the sidebands at the input and output of an amplifier with an input signal as superposition of a low-index AM signal and low-phase deviation PM signal, the coefficients  $c$  and  $k_p$  can be computed.

A nonlinear amplifier can be modeled by a cascade of two nonlinear elements. The first one represents AM/PM and the other one AM/AM nonlinearity. AM/PM nonlinearity corresponds to the change of the phase of the amplifier output with the varying amplitude of the amplifier input. Hence if the input signal  $V_{in}$  is:

$$V_{in} = A \cos \omega t \quad (2.11)$$

then the output of the AM/PM nonlinearity can be expressed as:

$$V_{pm} = A \cos \left[ \omega t + \kappa \left( \frac{A^2}{2} \right) \right] \quad (2.12)$$

and the output of the AM/AM nonlinearity can be written as:

$$V_{out} = \sum_{n=1}^{\infty} a_n V_{pm}^n = \sum_{n=1}^{\infty} a_n A^n \cos^n \left[ \omega t + \kappa \left( \frac{A^2}{2} \right) \right] \quad (2.13)$$

If (2.13) is expanded for a two-tone analysis it can be shown that if IMD caused by AM/PM is negligibly small compared with AM/AM then phase of the carrier and third order IMD (IM3) are relatively the same. To take the effect of AM/PM into account the original time-domain input signal can be modulated by using single tone AM/AM and AM/PM characteristics of the amplifier and Discrete Fourier Transform of the resulting signal can be taken. Hence, phase of the carrier and the third order IMD can be observed. Simulations and measurements have shown that phase of the IM3 changes rapidly relative to the carrier as the input voltage begins to drive the amplifier to saturation meaning IM3 caused by AM/PM should be considered. This observation is important especially for predistortion linearizers [10].

### 2.3 Measures of linearity

To have an idea about linearity characteristics of an amplifier, a two tone test is applied. The amount of IMD products (third, fifth order) near to the tones is a measure of linearity. As the number of tones is increased, it can be observed that IMD products fall not only out of band but also inside. These are called inband IMD products and the one at the center of these tones is the most dominant one. To be able to measure this IMD product, tones are applied at a spacing of  $\Delta f$  and a gap of  $\Delta f$  is left blank in the middle of the band. The amount of IMD measured in that gap is referred as Noise Power Ratio (NPR) and it is another useful measure of linearity [3].

An alternative approach to model the Pout-Pin characteristic of an amplifier (other than power series) is to describe the characteristic as a linear line ( $y = x$ ) until the point  $P_{LIN}$  where the amplifier exhibits a perfect linearity and the rest of it where the amplifier gets into compression in the form of a curve whose expression is given as  $y = x - ax^n$ . For power levels below  $P_{LIN}$  weakly nonlinear effects will dominate and the IMD products will approximate to a line of slope 3 which intersects the IP3

point, however as the output power gets into compression, strongly nonlinear effects will be in consideration and the IMDs computed from the third harmonic of the modulating waveform will be somewhat different from the simple line considered for low power levels.

Another alternative to amplifier characterization is brought in [11]. Hence,  $P_{out} - P_{in}$  relationship for a Class A amplifier can be given by following:

$$P_{out} = P_{in} + G_{ss} - K \log_{10} \left[ 1 + 10^{\left( \frac{P_{in} + G_{ss} - P_{sat}}{K} \right)} \right] \quad (2.14)$$

where  $G_{ss}$  is the small signal gain,  $P_{sat}$  is the saturated power and  $K$  is the compression coefficient whose expression can be given as follows:

$$K = \frac{P_{sat} - P_{out}(K)}{0.301} \quad (2.15)$$

where  $P_{out}(K)$  is the measured output power when the input power is set to the value of  $P_{in} = P_{sat} - G_{ss}$ . The parameter  $K$  specifies the sharpness of the compression of the amplifier. As  $K$  becomes smaller, the compression becomes sharper.

Spectral regrowth (SR) is an undesired distortion for transmission of digitally modulated signals. As described in introduction effective bandwidth of digitally modulated signals can be wider than expected and may spread out of the channel. To reduce this bandwidth digital waveforms are filtered before modulation process which creates undesired amplitude modulation. This amplitude modulation causes SR. The change in phase with amplitude also converts the variations in the signal level to angle modulated sidebands broadening SR. The ratio of the Adjacent Channel Power to Main Channel Power is called ACPR and this is another measure of linearity for digitally modulated signal transmission [3]. In literature, there is some work which relates various measures such as ACPR or NPR to IP3 measured from two tone analysis and output IMD of a multitone excitation using Volterra analysis [12, 13].

## 2.4 Types and natures of signals

Signals can be classified as constant envelope and non-constant envelope. Constant envelope signals do not need linear amplifiers since information is carried by phase, not by amplitude and peak envelope is same as average envelope. Since input envelope is a constant it is not affected by AM/AM and AM/PM distortion. FM, GMSK, FSK can be included in this class. Non-constant envelope signals can result as a consequence of digitally modulated signals where information is carried by one of the parameters such as QPSK, linear modulation schemes where information is carried by amplitude and phase such as QAM or multicarrier signals with either constant or non-constant envelope modulation. For QPSK although information is carried by phase, signal level transitions occur while switching from one phase to another [2].

Peak-to-average envelope power ratio of multicarrier signals can be increased with the number of carriers. If all the carriers are assumed to be phase aligned, that is all the carriers have the same phase then mathematically it can be shown that peak envelopes occur periodically at short durations causing high peak to average envelope ratios. Although the average power is small, the amplifier has to handle these peak envelopes of short durations in order not to produce high IMD products. However if the phase and amplitude of the carriers are random, the resulting signal has a reduced peak to average envelope ratio. Hence, the amplifier has to be able to produce the peak power to handle peak envelope power while producing average power for the majority of time. In other words the amplifier has to operate at a certain dB output power back off (OPBO) which is determined by the peak to average ratio. This leads to complexity, cost and poor efficiency. Hence, it is important to know about the characteristic and statistics of the input modulation signal. Information about the distribution function or the probability density function of the input envelope is as important as peak to average ratio. Peak envelopes that have very low probability of existence may not need to be handled. When the number of carriers is large, carries can be considered as independent random variables with Gaussian probability distributions. The sum of Gaussian random

variables is itself a Gaussian random variable. As the number of carriers increase the envelope amplitude density function converges to Rayleigh distribution [2] which is:

$$f(v, \sigma) = \frac{v}{\sigma^2} e^{-\frac{v^2}{2\sigma^2}} \quad (2.16)$$

Hence the average power is:

$$P_{av} = \int_{-\infty}^{\infty} v^2 \cdot f(v) dv = 2 \cdot \sigma^2 \quad (2.17)$$

Stochastic analysis can be used to specify linearity parameters of an amplifier to meet the IMD requirements at a specified bandwidth. For instance spectrum of a CDMA signal is equivalent to that of a band limited white Gaussian stochastic process as long as the number of the spread spectrum signals involved in CDMA signal is large. Hence the CDMA signal can be expressed statistically. Using the Taylor series model of an amplifier the output of the amplifier can also be expressed statistically. The coefficients of the amplifier model can be related to its linear gain and IP3. Hence autocorrelation function and power spectral density of the output can be derived explicitly and IMD power at a specified bandwidth can be calculated and related to the IP3 of the amplifier. This gives us the flexibility of determining the linearity parameters of the amplifier that would meet the required IMD specifications. Once these parameters are determined the problem reduces to designing a conventional RF power amplifier [6, 14].

Using standard linear estimation theory and the amplifier model:

$$v_a(t) = G_0 v_m(t) + v_d(t) \quad (2.18)$$

where  $v_a(t)$  is the PA output,  $G_0$  is the linear gain,  $v_m(t)$  is the baseband complex envelope and  $v_d(t)$  is the IMD, the IMD power can be expressed in terms of complex gain of the amplifier and the probability density function (pdf) of the instantaneous power in the modulation. These expressions and power histograms of different types of digital modulated signals have been reported in [15].

## 2.5 Memory effects

Memory effects are defined as changes in the amplitude and phase of distortion components caused by changes in modulation frequency. Memory shows its effect under multitone test conditions. Even though linearization of a nonlinear amplifier improves AM/AM and AM/PM linearity performance for a single carrier, the same improvement may not be observed for multitone signal amplification if the amplifier has a considerable amount of memory [16]. Hence the effect of memory is something to do with the envelope frequency, in other words the frequency spacing between the tones. For different spacings, it is possible to obtain different AM/AM and AM/PM distortion characteristics. At a resonant frequency, maximum deviation from linearity can also be observed [16, 17]. For instance in a two tone analysis phase of the IMD products would be expected to have the same phase regardless what the tone difference is, if the amplifier were memoryless. However this is not true for an amplifier having memory and asymmetry between upper and lower IMD products occurs. This phenomenon exhibits an important problem especially for predistorters which usually introduce constant phase to compensate for the IMD products. Sources of memory effects can be classified as electrical and thermal [18].

In a practical nonlinear amplifier with memory, not only fundamental impedance but also second harmonic and envelope frequency impedances play an important role on the generation of third order nonlinearities. By keeping the impedances at the fundamental and harmonic frequencies constant within the modulation frequency, electrical memory effects due to variation of these impedances can greatly be eliminated. However the major source is envelope frequencies, which extends from DC to modulation frequencies. Within this range output impedances should be constant which is somewhat difficult to maintain because of the existence of the bias impedances and the requirement of large time constants in bias networks [18]. Especially bias circuits, which involve feedback like BJT bias circuitries involve large time constants. However in FET bias circuits this effect is relatively less due to its simple implementation. Short time memory effects caused by the parasitic of the chokes and resonance of the by-pass capacitors in the bias circuits can be degraded considerably by optimizing these components with proper grounding [16]. In [19] a two-tone set-up has been proposed to measure

electrical memory effects for high power LDMOS devices and the effect of bias and drive variations and both circuit and intrinsic device contributions on IMD asymmetries with respect to frequency spacing has been examined.

The second source of memory effects is thermal. Temperature of an amplifier changes by the ambient temperature, DC power consumption multiplied by the thermal resistance and the power dissipated at the envelope frequency multiplied by the thermal impedance at that frequency. In other words, temperature of the amplifier changes dynamically with the applied signal. If electrical properties of the amplifier such as gain, input and output impedances vary with the temperature then this variation may cause memory effects, which means that the amplifier response will be time dependent. This dynamical self-heating mechanism is called thermal power feedback [18]. Thermal model of an RF power amplifier has been developed and instantaneous junction temperature of a transistor die has been related to instantaneous power dissipation and thermal time constant in [20]. The model leads to the fact that electrical memory effects are more critical than thermal ones for power amplifiers under high varying amplitude and wideband (high speed) signals. Thermal memory effects become superior for narrow band signals.

In order to model phase distortion of a nonlinear system with memory Volterra series analysis can be used. A linear time-invariant system can be described by taking convolution:

$$y(t) = \int_{-\infty}^{\infty} h(\tau)x(t - \tau)d\tau \quad (2.19)$$

For nonlinear systems with memory (2.19) can be extended to Volterra series [21]:

$$y(t) = \sum_{n=1}^N w_n(t) \quad (2.20)$$

where

$$w_n(t) = \int_{-\infty}^{\infty} d\tau_1 \cdots \int_{-\infty}^{\infty} d\tau_n h_n(\tau_1, \dots, \tau_n) * \prod_{r=1}^n x(t - \tau_r) \quad (2.21)$$

The frequency domain form of the above response is:

$$w_n(t) = \frac{1}{2^n} \sum_{i_1=-M}^M \cdots \sum_{i_n=-M}^M V_{i_1} \cdots V_{i_n} \bullet H_n(\omega_{i_1}, \dots, \omega_{i_n}) \bullet e^{j(\omega_{i_1} + \dots + \omega_{i_n})t} \quad (2.22)$$

$H_n$  is called the Volterra Kernel and is usually very complicated to compute. There are several works published in literature, which try to estimate these kernels to analyze the nonlinear behavior of RF amplifiers. In [22], Volterra transfer functions are computed for an RF amplifier to be used for CDMA digital communications by representing the CDMA excitation as a zero mean white noise Gaussian process. In [23], third order Volterra transfer functions are found in terms of Kernels for a single tone and two tone excitation. Using Volterra analysis it is shown that AM/PM characteristic of an amplifier for a multitone input is the same as that of a single tone input assuming a third order nonlinearity. In [24], third order kernel of a single stage FET is computed using a Volterra simulator C/NL2. In [25], Volterra Series analysis has been done for a MESFET amplifier up to third order nonlinearity.

## 2.6 Methods of linearization

### 2.6.1 Cartesian Feedback

Cartesian Feedback was first proposed by Petrovic in 1983 and was originally used for SSB transmission. A block diagram for this method is seen in Figure 2.2. The generated I and Q signals are fed into the differential amplifiers which produce the error signals. The outputs of the differential amplifiers are then upconverted to RF using a quadrature local oscillator. The complex RF signal is amplified through a non-linear power amplifier. The output of the power amplifier is coupled and downconverted back to baseband I and Q signals. These signals are compared with the generated ones forming two closed loops. Since it involves feedback, its linearity performance is limited by the delay of the loop and the bandwidth over which the feedback can operate. Practically, the linearization bandwidth of such a system is on the order of kHzs. For narrowband channels (5-50 kHz) this technique can provide a good IMD correction (25-40 dB). Commercially it is used in DAMPS, TETRA,

GEONET. This system has advantages of being simple to implement, applicable to any modulation type whereas its being narrowband is the major drawback [26], [27], [28].

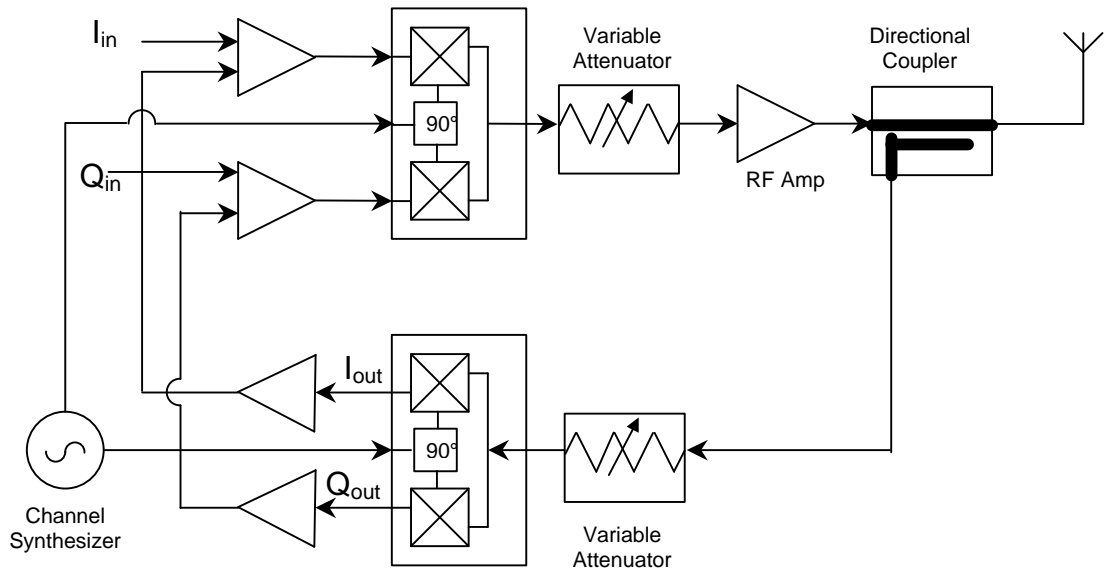


**Figure 2.2** Block diagram for Cartesian Feedback.

### 2.6.2 Envelope Elimination and Restoration (EER)

This technique was first introduced by Kahn in 1952. Originally it was used for the amplification of the high frequency SSB signals then it got involved in high power TV and radio broadcast operation and mobile radio applications due to its high efficiency and relative simplicity. A basic configuration is seen in Figure 2.3. A non constant envelope signal to be amplified is split into two. In the first branch the signal is amplitude limited using a limiter leading to a constant envelope signal. In the other branch the envelope of the input signal is detected utilizing an envelope detector resulting with amplitude varying baseband signal. This signal is amplified using a highly efficient audio frequency amplifier to modulate the power supply of the highly efficient and nonlinear (Class C, D, E, F) RF power amplifier which

amplifies the phase modulated constant envelope signal in the first branch. The output is the replica of the input signal with amplification. Amplifiers used in this technique can have 100 percent efficiency theoretically leading to a very efficient linearizer. However at high power applications this technique may require power regulators practically difficult to implement and at low envelope levels RF power transistors may cut-off causing distortion. This technique is good for reasonable levels of envelope variation [26], [28].

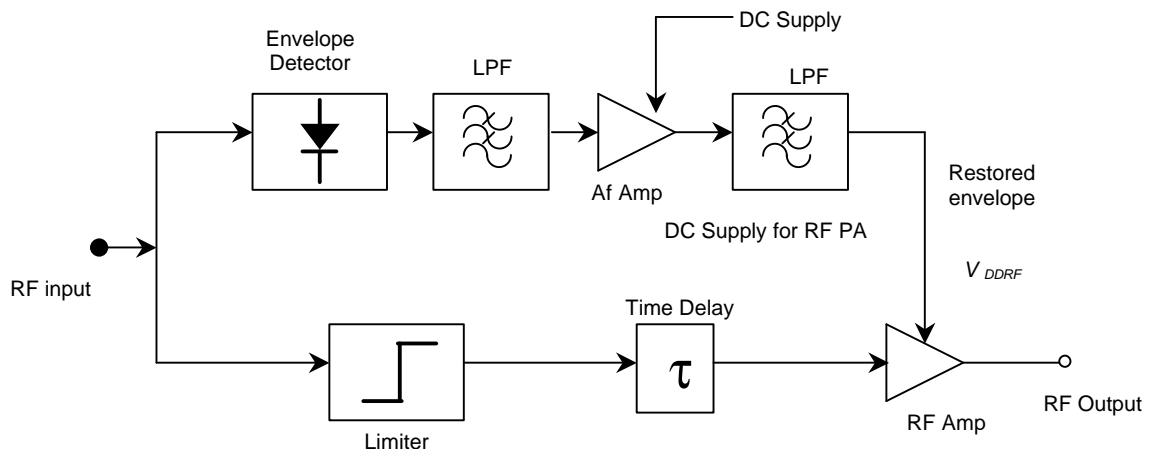


**Figure 2.3** Block diagram for EER.

### 2.6.3 Linear Amplification using Nonlinear Components (LINC)

This technique was first proposed by Donald Cox in 1974. The idea is to decompose the input RF signal into two phase modulated constant envelope signals so that the split signals can be amplified using highly nonlinear and efficient power amplifiers and recombined to form a linear amplification of the input signal as illustrated in Figure 2.4. Achievement of high efficiencies is the main attraction of this technique. The main problems with this technique are the strict cancellation requirements for the gain and phase matching of the two RF paths; loss of efficiency during the cancellation process and the thermal tracking problem which would be overcome by integrating both of the amplifier chains in the same module (for

transmitter application). Implementation of this technique carries financial risk and it is not practical. CALLUM (Combined Analogue-Locked Loop Universal Modulator) is used to generate the required signals for LINC and to attempt to overcome the problems mentioned above. No commercial designs have been produced so far but practical implementations are being developed nowadays [26], [28].

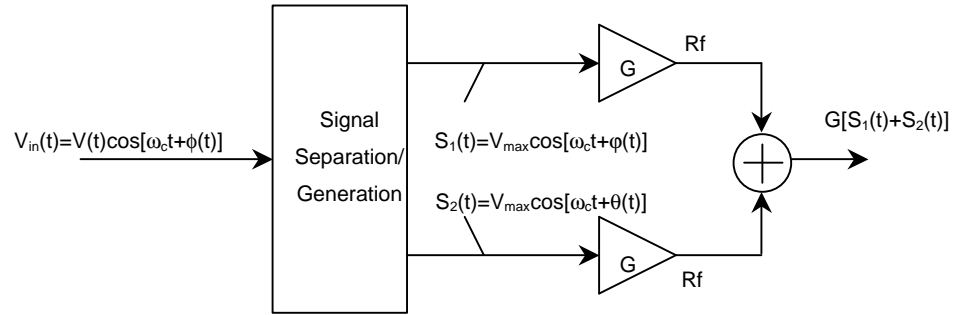


**Figure 2.4** Block diagram for LINC.

### 2.6.4 RF Predistortion

A predistorter is a nonlinear circuit which is placed in front of the RF power amplifier to be linearized. Its nonlinearity is such that it compensates for the amplitude and phase nonlinearities of the power amplifier so that the overall amplifier has linear characteristics until it gets to the SAT region without getting into compression (see Figure 2.5). The difficulties are to model the power amplifier exactly and to be able to generate the inverse characteristic. Usually to predistort only the third order characteristic is the most widely preferred approach. This can be accomplished by using cubic predistorters. Diode or transistor based predistorters can also be used but the performance is dependent on their nonlinearity characteristics. Transistors may need to be on a similar die type of the one used for the power amplifier. The principle of operation can be summarized as follows: Input signal is sampled using a coupler. The sampled signal is amplified using a transistor whose die structure and bias conditions are similar to the one used in the main amplifier but

at a smaller scale. The distorted output is cancelled from the sampled signal to obtain the pure IMD products. The phase and amplitude of the IMD products are adjusted

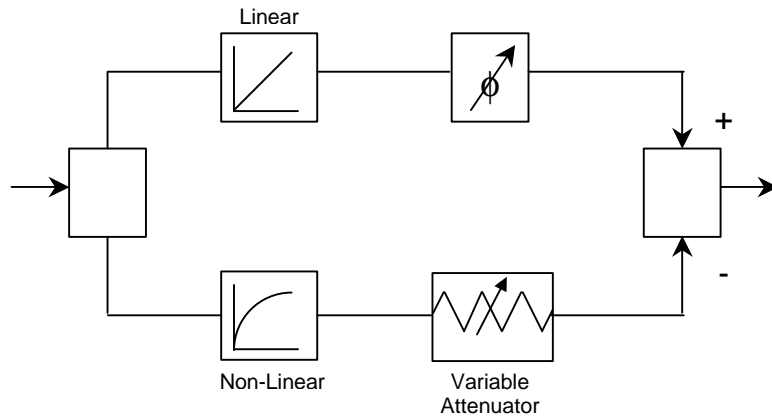


**Figure 2.5** Production of the inverse characteristic of an amplifier.

such that when they are combined with the original signal and amplified through the main amplifier the IMD products of the main amplifier are reduced. However it is usually difficult to give exact inverse characteristic and practically 10 dB of IMD cancellation can be achieved at most. Predistortion is more efficient than feedforward and can be used without changing the main amplifier configuration. In other words its flexibility is a major advantage but its bandwidth and linearity performance is not as good as feedforward. Nevertheless especially in base-station applications, predistorters are preferred to be used in conjunction with feedforward to relax the specifications of the error amplifier and increase the efficiency of the feedforward [3, 27].

### 2.6.5 Other linearization techniques

Adaptive baseband predistortion is a technique which combines Cartesian feedback and RF predistortion. Similar to the Cartesian feedback, power amplifier

output is sampled and downconverted to baseband I and Q s. The baseband signal is fed back to DSP unit where the input baseband to the amplifier is generated. DSP unit itself functions as a predistorter and consists of signal separation and complex weighting functions. These functions are mostly tabulated in the form of a look up table whose coefficients may vary adaptively due to the changing AM/AM, AM/PM characteristics of the amplifier. Although this technique is proposed for portable radio and handset applications, it is not very practical to implement since the DSP unit, A/D, D/A units have high power consumption relative to the output power of system and there is a limitation on memory issues. In addition to these facts, this technique is more narrowband compared to RF predistortion due to the feedback units [26, 27, 28].

Adaptive Parametric Linearization (APL) is another alternative to predistortion whose predistorter characteristic is mostly fixed by the diode or FET used and only minor modifications can be applied to change its characteristic. APL on the other hand allows generating the precorrector characteristic in a flexible way and adaptively. Hence its characteristic is controllable so as to adjust itself more accurately to linearize the main amplifier.

Another approach announced in literature - Interchange Second Harmonic Enhancement - involves extracting the second harmonic of the driver amplifier, amplifying it by a proper phase and gain adjustment and feedforwarding the output of the harmonic amplifier into the second amplifier together with the fundamental carrier output of the driver amplifier Hence, spectral regrowth can be reduced considerably [29].

## CHAPTER 3

### OVERVIEW ON FEEDFORWARD

In this chapter feedforward linearizer will be described in details. Principle of operation, functions of the major subcomponents and a brief literature survey will be presented. Feedforward linearizer consists of one main and one auxiliary amplifier building up two cancellation loops. Since there is a continuous forward signal flow, there is no feedback and consequently it is unconditionally stable theoretically over an infinite frequency bandwidth [2].

#### 3.1 Principle of operation

A schematic of feedforward is given in Figure 3.1. At the input the main signal (carrier) is sampled with a power splitter or usually with a coupler. While the main signal is amplified through the main amplifier, the sampled signal is passed through a delay element, which gives an equivalent delay that is introduced by the main amplifier. Some portion of the distorted output of the main amplifier is then compared with the sampled reference signal using a coupler and maybe an attenuator. Usually a phase shifter is put in front of the main amplifier to adjust the phase of the distorted output so that the reference signal and portion of the distorted output can be 180 degrees out of phase. If the two signals are also delay and amplitude matched then a perfect cancellation can be achieved and only the distortion component can be obtained. This distortion is the IMD product and it is referred as error signal. The first cancellation loop is called carrier cancellation loop.

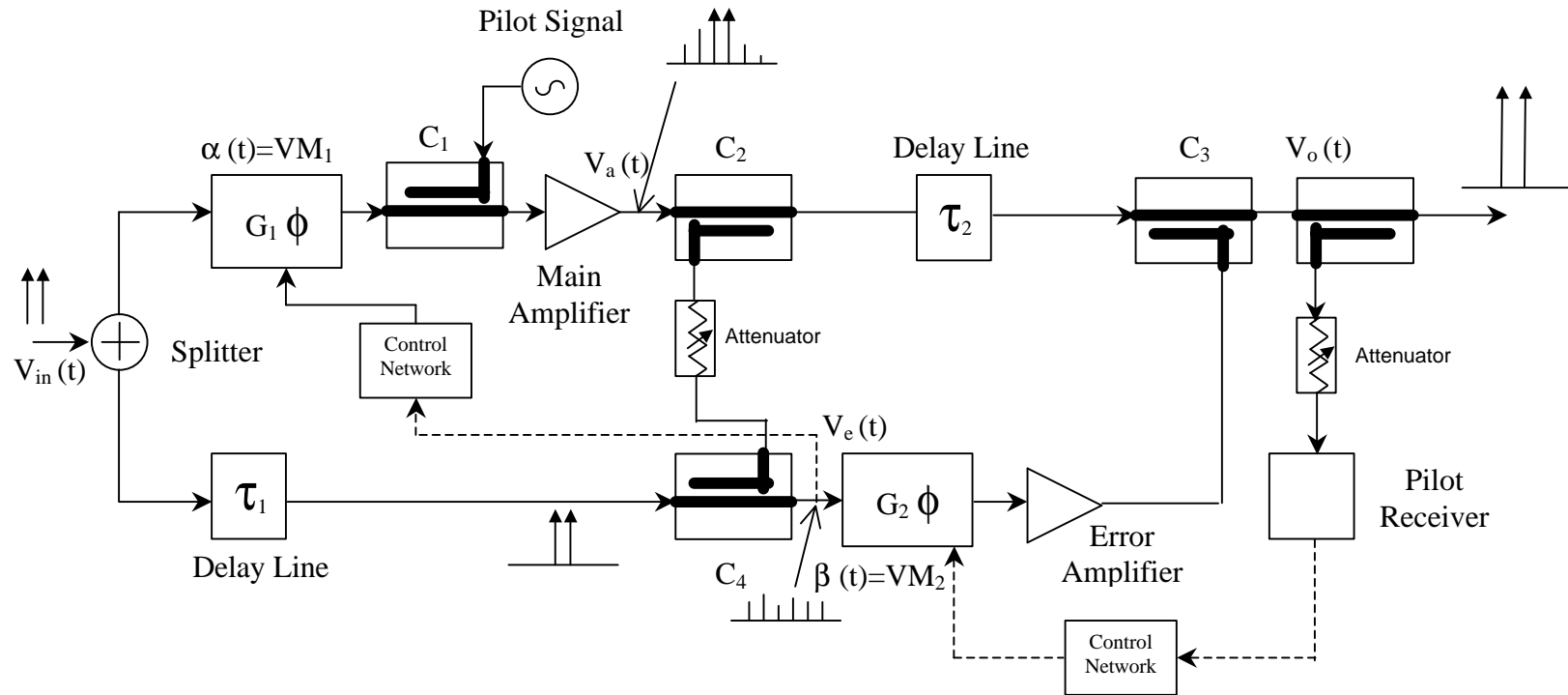


**Figure 3.1** Schematic of a feedforward circuit.

Once the error signal is obtained, it is amplified via an auxiliary amplifier, which is also called error amplifier. This amplifier should be highly linear in order not to introduce extra IMD to the system. Similar to the first loop, this time the distorted output of the main amplifier is passed through a delay element, which gives an equivalent delay introduced by the error amplifier. At the output of the delay element this signal is compared with the output of the error amplifier and when the conditions similar to the ones mentioned for the first loop are satisfied, distortion produced by the main amplifier can be cancelled and consequently the original signal can be recovered but this time amplified. This second loop is called error cancellation loop. Note that this technique involves time delay elements, phase shifters and couplers which mean that a considerable amount of loss is introduced. Of course this loss affects the overall efficiency. In addition to this, the linearity requirement of the error amplifier also reduces the efficiency. On the other hand this method can be used to linearly amplify both constant and nonconstant envelope signals and it allows ultra-linear operation over a wide bandwidth as long as a perfect broadband signal cancellation can be achieved within the loops. Broadband signal cancellation is possible when the two signals have equal amplitude and delay but are 180 degrees out of phase. The amounts of amplitude and phase mismatches affect the level of the suppressed signal. Hence, gain and phase adjustments are essential in both loops. In order to increase the bandwidth of the overall system automatic control schemes are used to adjust gain and phase for the best cancellation. In the first loop where carriers are cancelled, the loop cancellation bandwidth is equal to the transmitter bandwidth or maximum carrier spacing, while that of the second loop where distortion components are cancelled bandwidth is equal to the bandwidth over which significant distortion occurs. When the losses of couplers, delay lines, phase shifters and attenuators within each branch of the loop is equal to each other then the loops are balanced and feedforward gain is independent of any nonlinearities in the main and error amplifier and it behaves like a linear amplifier.

### **3.2 Delay matching**

Delay matching is one of the most important issues in broadband cancellation. Delay of an amplifier has two components: actual transmission delay (baseband phase shift) and phase shift introduced by poles and zeros in the transfer function (RF phase rotation). Delay is defined as the derivative of the phase with respect to frequency. Delay elements are lengthened or shortened until a delay match between the two paths is achieved. Once this unique value of delay is obtained, signal cancellation is independent of frequency because the phases of the two paths now have the same slope with respect to frequency and fine tuning can be done by using phase shifters. In some cases however delay mismatch can be introduced intentionally to reduce power dissipation in delay elements. Hence power efficiency can be increased with the penalty of reduction in bandwidth. Typical transmissive delays for high power RF amplifiers are at the order of nanoseconds. Due to their constant gain and linear phase characteristics, low pass structures such as coaxial cables are used as delay line elements. However they have to be lengthy and bulky because of the amount of delay to be compensated for. Because of their lossy nature, coaxial cables are preferred to be used in the lower path. For the main path delay line band pass filters are usually used. Although their loss is less compared to coaxial cables, their gain and phase flatness is not that good. Amplifiers can be characterized by a band-pass response. Delay is constant within the passband whereas deviation from linear phase occurs as amplitude rolls off at the band edges. The passband of an amplifier in a feedforward system should be wider than the cancellation bandwidth and have the gain and phase flatness over the bandwidth to ensure constant delay.

### **3.3 Gain and phase matching – Vector modulators**

Amplitude and phase mismatches determine the level of the cancellation. Better loop cancellation requires better amplitude and phase flatness. It is relatively simple to have a good cancellation for narrowband applications. Main factors that

affect amplitude flatness include amplitude ripple across the bandwidth of interest which arises from impedance mismatch, amplitude roll-off at the band edges, and gain degradation of the transistors due to frequency.

Phase flatness is a measure of deviation from linear phase hence deviation from constant delay. If the phase of a network is not linear, then each frequency component has different delay and there is a dispersive relation. If phase is linear then group velocity is equal to the phase velocity.

Phase linearity and gain and loss flatness of the subcircuits and impedance matching and isolation between subcircuits have considerable effect on amplitude and phase matching and consequently loop cancellation. Simulations have shown that imperfect isolation in couplers and power splitters is less critical than the return loss between the subcircuits for wideband loop cancellation. Narrowband cancellation on the other hand, is relatively less sensitive to impedance mismatches [30].

Phase and gain adjustments must be done to overcome temperature drifts, frequency and amplitude variations and component drifts. Conventional methods require the attenuation and phase circuits separately. Variable phase shift networks have a limitation in changing the phase and they do not allow random access for a specific phase shift. Hence long transition time may be required before reaching the final phase shift. Resistive attenuators experience group delay and phase changes as a function of attenuation change. Hence, this phase change should be taken into account together with phase shifters. Vector modulators perform the attenuation and phase change together. A specific phase shift can be accessed randomly. Thus there is a reduction in adjustment time in loops [31].

A typical vector modulator is seen in Figure 3.2 [31]. It is composed of two Wilkinson Power dividers, a 90 degree phase shifter and two branchline power dividers terminated with pin diodes. The input voltage  $V_{in}$  is decomposed to in-phase and quadrature components  $V_{ip}$  and  $V_q$  using the Wilkinson Power divider and a 90° phase shifter and then injected into the two branchline power dividers. The input voltages  $V_{ip}$  and  $V_q$  are multiplied by the reflection coefficients  $\Gamma_{ip}$  and  $\Gamma_q$  which can take values between  $-1$  and  $1$  depending on terminated resistance that is

adjusted by the pin diodes and the in phase and quadrature currents which are injected into the branchline power dividers. The output of branchline power dividers are then combined via Wilkinson Power divider. The output voltages and the phase shift are related as follows:

$$V_{out} = 0.5V_{in} \sqrt{|\Gamma_{ip}|^2 + |\Gamma_q|^2} \quad (3.1)$$

$$\phi = \tan^{-1} \left( \frac{\Gamma_{ip}}{\Gamma_q} \right) \quad (3.2)$$

In [32], a similar type of vector modulator has been utilized for a feedforward application at 5.7 GHz.

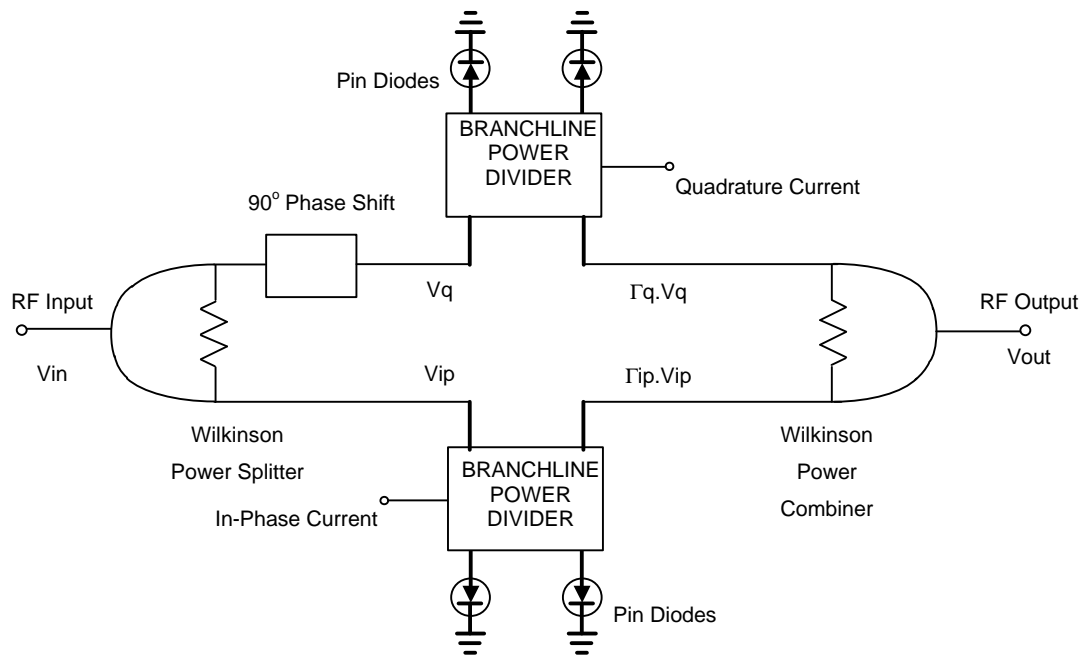


**Figure 3.2** Block diagram for a typical vector modulator.

### **3.4 Error amplifier**

One of the most important components of a feedforward circuitry is the error amplifier. Peak power requirement of the error amplifier is higher than the average power by an amount equal to peak to average ratio of the main amplifier and an additional margin, which is called back-off factor. This is necessary to ensure that the error amplifier contributes to distortion as little as possible. To minimize distortion due to signal clipping in the main amplifier, peak-to-average ratio of the main amplifier is designed to be equal to that of the feedforward input signal. Peak power of the error amplifier is a function of the peak power and intermodulation performance of the main amplifier, the level of the carrier suppression and coupler and delay line losses. Error amplifier has a major impact on the overall efficiency of a feedforward system.

### **3.5 Loop control**

In order to increase the operation bandwidth and compensate for changes in the phase and gain characteristics of the main and error amplifiers with respect to frequency, input signal level and temperature, control circuits should be utilized. There are various ways of controlling carrier cancellation loop [2].

One of the methods is loop control using look up tables. In this method, amplifier must be well characterized. Values of amplitude and phase which give good loop suppression are tabulated as a function of certain control parameters. Any knowledge of loop balance is not required but it takes time to fully characterize each amplifier, especially for mass production.

Another type of loop control is analog type where a sample of reference signal is correlated with the error signal (distortion + carrier). The alignment information is fed back via loop filters to the gain and phase control networks. Loop balance is obtained when the reference signal is uncorrelated with error signal. This method can compensate for rapid changes.

The third type of loop control is digital loop control where the sampled error signal (distortion carrier) is amplified and passed through a power detector which produces a DC voltage proportional to the input RF signal. Since the residual carrier level is dominant in the error signal output voltage level of power detector can be used to adjust the gain and phase control networks to decrease the residual carrier level. The control algorithm compares the current and previous values of detected power and then changes the amplitude or phase to see if the detected power decreases or increases. If the power decreases, then the direction of change is maintained, otherwise the direction reverses.

Another method reported in [33] generates error voltages to adaptively control the vector modulator by using a nulling combiner which is composed by cascading a quadrature branch-line hybrid and Wilkinson in-phase combiner for 1.7 GHz. A similar work has been reported in [34] for 1.9 GHz. Error voltages are generated by detecting the power at the output of the nulling combiner ports, which result from amplitude and phase mismatches between the output of the main amplifier and the sampled replica of the main amplifier input injected into the branch-line hybrid's ports.

There are several approaches to control the error cancellation loop. One of them involves using a spectrum analyzer circuit to locate the carrier and IMD products [2]. A microprocessor uses these measurements to balance the loop. However this method is highly complex to implement.

Another approach is the injection of a pilot signal to the input of the error cancellation loop. Since the loop is expected to cancel the signals at its input, the level of the residual pilot signal at the end of the loop is an indication of the performance of the loop. The disadvantage of this method is that it is narrowband. Since the IMD products are on both sides of the carrier, the cancellation bandwidth must be larger than the operating bandwidth. Use of pilot signal, on the other hand balances the loop at only the frequency of the pilot signal (see Figure 3.1). Since pilot receivers have to detect very small levels of power levels, isolation between the pilot receiver and other components of the circuit should be adequately high in order to avoid unwanted crosstalks [35]. To overcome the problem of bandwidth, the pilot

signal can be chosen to be broadband rather than a single tone. In [36] generation of a broadband pilot signal in the form of a band limited noise signal and adaptation of this signal in conjunction with correlation detectors to control the error cancellation loop has been described.

Finally some DSP adaptive algorithms are developed eliminating the requirement of pilot signals, to adapt the control parameters  $\alpha(t)$  and  $\beta(t)$  which belong to the vector modulators placed in carrier and error cancellation loops respectively [37]. This adaptation is based on linear estimation of the signal at the output of the main amplifier, which involves linearly amplified term and distortion. Using the linear estimation theory, a gradient signal can be defined to compute the control parameters in a compact form. A suitable gradient signal for the carrier cancellation loop would be:

$$D_{\alpha}(t) = v_e(t)v_m^*(t) \quad (3.3)$$

where,  $v_e(t)$  is the error signal at the input of the error amplifier and is the estimation error and  $v_m(t)$  is the main signal and is the basis for the estimation. When  $\alpha(t)$  is adjusted properly, the expected value of the gradient becomes zero since the error and the main signals are uncorrelated. This leads to following algorithm for the adaptation of  $\alpha(t)$ :

$$\alpha(t) = K_{\alpha} \int_0^t D_{\alpha}(\tau) d\tau \quad (3.4)$$

where  $K_{\alpha}$  is the time constant of the adaptation. A similar adaptation algorithm can be derived for  $\beta(t)$  also. This time, gradient signal would be:

$$D_{\beta}(t) = v_o(t)v_e^*(t) \quad (3.5)$$

where  $v_o(t)$  is the output signal and is the estimation error and  $v_e(t)$  is the basis of the estimate. The bandpass correlation of the RF signals would result in lowpass signals around DC. Hence DC offset and 1/f flickering noise of the mixers may cause poor convergence. Additionally, the implementation of (3.5) requires mixing of the error signal with the weak IM component in the output. Hence, much stronger components in the output of the main amplifier may behave like noise causing slow convergence.

These problems can be handled by making use of DSP techniques and filters to suppress the desired components in the output signal [38]. Adaptation in time delay matching can also be added to the control algorithm described above [39]. Perfect delay, phase and amplitude matching can be achieved at a single frequency. In order to increase the cancellation bandwidth use of multibranches in the reference path each having individual complex gain and time delay is proposed in [39].

### 3.6 Efficiency considerations

Although feedforward technique provides a better linearity performance compared to other techniques, power consumption in linear error amplifiers which are used for IMD cancellation and power loss in the delay elements and couplers used in the main path and peak-to-average ratio of the signal cause the system to be relatively inefficient. These effects can be formulated by the following relationship [2]:

$$\eta_{FF} = \frac{\alpha_1^2 l_2^2 \alpha_2^2}{\left( \frac{1}{\eta_M} + \frac{\Delta P_M}{\eta_E \cdot \Delta P_E} \right)} \quad (3.6)$$

where,

$\alpha_1$ =loss of the input coupler,

$\alpha_2$ =loss of the output coupler,

$l_2$ =loss of the delay line on the main path,

$\eta_{FF}$  = efficiency of the feedforward amplifier,

$\eta_M$  = efficiency of the main amplifier,

$\eta_E$  = efficiency of the error amplifier,

$\Delta P_M$  = peak-to-average ratio of the main amplifier,

$\Delta P_E$  = ratio of the peak power of the main amplifier to that of error amplifier.

Additionally, efficiency is also affected by power consumption of other circuit elements such as gain and phase adjustment circuits, detector circuits and loop control circuitry.

An alternative expression for overall efficiency can be given as follows [40]:

$$\epsilon = \frac{\epsilon_{PA} \epsilon_{LIN} C_2 (1 - C_2)}{\epsilon_{LIN} C_2 + \epsilon_{PA} f_{PA} (1 - C_2)} \quad (3.7)$$

where  $\epsilon_{PA}$  is efficiency of the main amplifier,  $\epsilon_{LIN}$  is efficiency of the linear error amplifier,  $C_2$  is coupling coefficient of the coupler at the end of the second loop,  $f_{PA}$  is  $10^{-C/I(PA)/10}$ ,  $C/I(PA)$  is main amplifier linearity – carrier to intermodulation ratio in dB. For the cases where efficiency is of primary importance rather than the linearity, an optimum value for  $C_2$  can be computed, by differentiating (3.7) with respect to  $C_2$  and equating to zero, to achieve an optimum overall efficiency. Optimum efficiency point is highly dependent on  $C_2$  for the case where the main and error amplifiers have high efficiency but poor linearity performance and the optimum efficiency is lower relatively to that of main amplifier but considerably higher than a classical class-A amplifier. As the linearities of the main and error amplifiers increase, the range of  $C_2$  for optimum efficiency becomes more broadband and efficiency is closed to the efficiency of the main amplifier, consequently coupling factor can be decreased to a certain value leading the advantage of lowering the output power of the error amplifier without affecting the overall efficiency [40].

In a practical feedforward system the output C/I is limited by the imperfect signal cancellation at the output of the first loop, imperfect intermodulation cancellation at the output of the second loop and extra intermodulation products produced by the error amplifier which is supposed to be linear. If the amplitude and phase matching in the second loop are not perfect then there is no point in overdesigning the error amplifier because no matter how linear the error amplifier is, overall distortion cancellation will be limited by the imperfect matching. In other words, the error amplifier linearity can be degraded according to the matching perfectness leading to a better efficiency [41]. In [42] a guideline is proposed to determine coupler values, error efficiency linearity and precision of the vector modulators for optimum feedforward linearizer design.

If the delay line on the main path is taken into consideration, then (3.7) is modified to the following:

$$\epsilon = \frac{\epsilon_{PA} \epsilon_{LIN} C_2 (1 - C_2)}{\epsilon_{LIN} L C_2 (1 + f_{PA}) + \epsilon_{PA} f_{PA} (1 - C_2)} \quad (3.8)$$

where, L is the fractional loss of the delay line. If we plot the overall efficiency with respect to the delay line loss, we observe that efficiency decreases rapidly as delay line loss is increased. In the case where C Class amplifiers are used for the main and error amplifiers, it can be observed that feedforward efficiency is not highly dependent on the error amplifier efficiency since error amplifier has considerably lower power than the main amplifier. This result becomes more obvious as the delay loss is increased. This is important because the input of the error amplifier consists of distortion whose peak-to-average ratio may be high reducing the efficiency of the error amplifier. By having the main and error amplifier class C type, a good Class A amplifier performance can be obtained with relatively high efficiency. To eliminate the extra distortion that will be introduced by the nonlinear error amplifier to some extent, the subtracted carrier level can be adjusted. This approach is valid if the system linearity requirement is at a moderate level [43].

As delay mismatch increases, cancellation gets poorer especially towards the edges of band. For wideband applications with moderate level of linearity requirement (satellite) and for narrowband applications with good linearity performance (cellular handsets) delay element can be reduced or eliminated allowing a certain amount of delay mismatch which would result with efficiency improvement since the loss due to the delay element decreases. With this delay mismatch feedforward will provide similar level of linearity to other techniques but it will still provide a better noise performance because noise will be cancelled to some extent by the error amplifier as if it is a distortion [44].

Theoretically efficiency can be doubled with around 15 dB IMD correction using predistortion. As a matter of fact, predistortion is more advantageous in the cases, where efficiency of the error amplifier is poor. In very high linearity demanding applications such as ETSI GSM 900, DCS1800 & 1900 Adaptive Parametric Linearisation (APL) can be used instead of predistortion and even more

efficiency improvement can be achieved. [45]. In [46] a research on optimizing efficiency of a feedforward amplifier using input power statistics has been reported. In [47] a highly efficient feedforward amplifier is proposed for PDS base station applications. The idea is to increase the feedforward efficiency by increasing the main amplifier efficiency and reducing required back-off at the output of the main amplifier (see (3.6)). These requirements are met by replacing the main amplifier by a Doherty amplifier operated at class F.

In Chapter 4, we have developed an analytical tool that formulates feedforward output in terms of feedforward parameters for CDMA applications. Such a tool provides the designer the flexibility of observing the impact of each parameter on the performance of the linearizer and adjusting the circuit parameters for optimum efficiency and linearity. Results presented in Chapter 5 clearly demonstrate the facts that, varying the coupling of the input coupler can improve the linearity performance with the cost of decrement in the output power; adjusting the coupling of the output coupler can improve the linearity considerably at a given efficiency; performance of the linearizer is sensitive to the delay mismatch in the second loop much more than that of in the first loop and depending on amplitude and delay matchings increasing the linearity of the error amplifier may have no impact on the improvement of the feedforward linearizer. In the same chapter, an application of the model on the design of a wideband linearizer with the motivation towards increasing efficiency for a given linearity performance is presented as well. In Chapter 6 an alternative model is proposed to handle arbitrary time domain signals for optimizing feedforward parameters.

### **3.7 Nested feedforward system**

The nonideal gain and phase variation with respect to frequency is called linear distortion. Amplitude and phase ripple across the bandwidth of the main amplifier and roll-offs at the band edges are the main causes of linear distortion. Since linear distortion does not produce inband spurious, it is more acceptable compared to nonlinear distortions such as intermodulation. For very broadband

applications a nested feedforward system (two feedforward loops together) can be used. The first feedforward loop is used to stabilize the gain and phase flatness. After maintaining a good flatness it is more relaxing to design the second feedforward loop which is used to achieve high degree of IMD correction. Simulations have shown that this technique can also be used to flatten the amplitude and phase characteristics of a practical nonideal amplifier at roll-off edges. In some cases a powerful error amplifier may be required to regenerate the missing power during the low points of the frequency response [48].

### **3.8 Research topics**

Feedforward is the best technique in power amplifier linearization that has been introduced so far, in terms of IMD correction and operation bandwidth. However the performance of the technique is highly dependent upon the gain and phase flatness of its passive and active components at the specified bandwidth. Since it involves cancellation of signals whose amplitude levels are closed to each other, IMD correction performance is very sensitive to phase, gain and delay mismatches within the cancellation loops. The major drawback of feedforward is its poor efficiency due to the requirement of an additional linear amplifier and as a consequence of this fact its complexity and cost. Hence research activities that would take part should provide solutions to bandwidth and efficiency problems. In this thesis we constructed a mathematical model for the overall feedforward circuitry for a stochastically well defined input wave form; developed a tool towards optimizing the specifications of the active and passive components for linearity performance, bandwidth and efficiency and proposed an alternative model to characterize feedforward systems for arbitrary waveforms by defining an effective peak to average ratio. However, additional research activities need to be carried on particularly in component and system point of view.

### 3.8.1 Component approach

The most important components in a feedforward circuit that limit the bandwidth and IMD correction performance are vector modulators and time delay components.

As described above vector modulators involve pin diodes (or similar structures) which can produce distortion products when they are subject to high RF power. Hence use of vector modulators enables the adjustment of amplitude and phase of the input of the amplifiers with a drawback of limitation on the input RF level. This raises the requirement of increase in the gain stages of the amplifiers to compensate for the RF level degradation. Increasing the number of the gain stages is something undesirable since time delay and gain ripples increase within the bandwidth. Hence increasing the IP3 of the vector modulators and if possible building them without using any kind of distortion producing elements is a challenging research area in implementation of feedforward. 90 degrees phase shifters are used in vector modulators to produce I and Q components. Thus, broadband operation of a vector modulator is highly dependent on how well this phase shifter works broadband. To overcome this problem within reasonable physical dimensions is a contribution in particularly for nearly octave operation bandwidths.

Delay matching is another important issue in bandwidth considerations and time delay components are the major sources of poor efficiencies in feedforward applications because of the loss they introduce in the main signal path. Particularly for broadband applications, it is very difficult to maintain a good delay matching since it is not easy to provide a flat amplifier gain and phase characteristic. The ripple in the gain and phase with respect to frequency also causes the delay to vary. For relaxed IMD specifications, tight delay matchings can be sacrificed resulting with less loss and consequently higher efficiencies. However very high IMD corrections are possible as far as a good delay matching is achieved within the cancellation loops. Electronically or even mechanically adjustable time delay components to be used in low power path would serve a lot for the broadband performance of this technique. Compensation for delay mismatches opens a good

research area in which MEMS (Micro Electro Mechanical System) technology can play an important role. For instance, effective dielectric constant and thus time delay of a microstrip line can be varied by electronically adjusting the position of the conductor of the strip with respect to ground plane. Even a mechanically trimmable component would be very useful in this sense, by letting the manufacturer to produce his own delay component at a specific length of coaxial cable or a specific delay line filter and make the fine tuning that would vary from system to system using the adjustable delay components. Actually time delay response of low pass type harmonic filters are also worth making research because harmonic filters constitute an essential role in most of the communication systems and if they can be designed such that their delays are comparable to those of the error amplifiers then they can be used as a delay matching component in the main path. Of course this would help with the overall efficiency of the system since there will be no filter redundancy. This approach is also valid for the couplers used at the end of the power amplifiers for power sampling.

### **3.8.2 System Approach**

The system approach considers the contributions to the feedforward technique in terms of efficiency and bandwidth in system level. Statistics of the input signal plays an important role in determining the linearity and efficiency requirement of an RF power amplifier. To characterize the input signal not only its peak to average ratio but also its probabilistic distribution is required. For an arbitrary modulated signal a maximum peak to average ratio can be obtained. For a given output linearity requirement, efficiency of a feedforward amplifier is a function of this peak to average ratio. If the amplifier is designed for the maximum peak to average ratio then the amplifier would meet the linearity requirement for all the times with the cost of low efficiency. However the system designer can define some thresholds for the expected IMD power with a probabilistic distribution. Using the stochastic characterization of the input signal together with this threshold an effective peak to average ratio can be defined. This is a useful parameter to optimize for efficiency and

relax the specifications of the active and passive components of the feedforward amplifier. Hence overdesign can be avoided and efficiency can be improved.

Another essential point in specifying the linearity requirements is to have accurate mathematical model of the IMD products. Hence nonlinear behavior of the amplifier needs to be analyzed explicitly. Most of the analyses have assumed the memoryless weakly nonlinear models for the amplifiers and IMD products have been modeled accordingly. These models need to be improved to include memory effects. As described in Chapter 2, memory effect is defined as the time dependency of the nonlinear amplifier and it may be both electrically and thermally originated. Hence, Pout Pin characteristic is within a bound rather than a single deterministic line. This effect needs to be analyzed and by taking this effect into account, the nonlinear behavior of a power amplifier needs to be remodeled. This model would form a more realistic and accurate base in the mathematical analysis of the IMD products and the overall feedforward circuitry. Actually a precise model which takes the memory effects into account would help not only feedforward but also other linearization techniques such as predistortion. Note that the main limitation on predistortion is the lack of accurate modeling of amplifier characteristic and thus the inverse amplifier characteristic.

Some methodologies need to be developed to explain this memory effect or time variance property. Remember that an amplifier can be modeled using power series expansion in the immediate vicinity of a particular DC bias point. Bias conditions may change with respect to input frequency and input and output matching conditions. Suppose we apply a multitone signal to the amplifier. Even order products will fall in a low frequency band within DC. These products can be expected to change the DC bias conditions of the amplifier and consequently the power expansion coefficients. This phenomenon would result with a change in gain and IMD products. Varying the frequency spacing of the multitone signal will also vary the operating bias conditions. Similar observations have been reported in [3]. Hence the change in bias and thus change in power expansion coefficients can also be expressed in terms of the frequency spacing of the multitone signal or the input digital modulated signal with a specified channel bandwidth.

Adaptive control algorithms play an important role in compensating for the component drifts, temperature effects and changing frequency effects. The advantage of using them is to eliminate the use of pilot signal and to achieve a faster adaptation with varying conditions. The algorithms used in these adaptive control schemes are based on a memoryless amplifier model. To include the memory effect would also serve for a more advanced, accurate and broadband adaptive algorithm.

## CHAPTER 4

### FEEDFORWARD CHARACTERIZATION FOR CDMA SYSTEMS

#### 4.1 Overview

Today most of the modern communication systems use digital modulation such as QPSK, QAM etc. Hence it is possible to transmit more data at high data rates and preserve the quality of the signal without loss of information. In cellular communication systems digital modulations where the information is carried, are accessed by various schemes such as TDMA (Time Division Multiple Access) and CDMA (Code Division Multiple Access). In CDMA systems a certain number of users can communicate at the same time and frequency as long as each user uses a unique code. This makes CDMA spectrally efficient and popular in modern communication systems. However, the resulting signal has a high envelope peak-to-average ratio (crest factor) and linear power amplifiers with high back-off are required in order not to degrade the quality of the signal.

There are various CDMA standards used in communication systems. One of the most important standards is IS-95. The user data is modulated in the base-band with 1.2288 Mbit/sec pn-sequence codes in I and Q channels before base-band filtering and QPSK is used for RF carrier modulation [49]. The highest power peak-to-average ratio (crest factor) for an individual CDMA channel is around 6.5 dB with a probability of occurrence of less than 0.1%. The crest factor increases with the number of superimposed channels although the spectrum does not change. Although

an Additive White Gaussian Noise (AWGN) is usually recommended for representing a typical CDMA signal, in [49] it is stated that AWGN can replace a CDMA signal with 2 channels, whereas for instance for 9 channels the probabilistic distributions of the peaks of a typical CDMA deviate from that of AWGN. Therefore to simulate a 9-channel system, AWGN test level of 1 dB higher needs to be used.

In literature there has been various work which characterize spectral regrowth caused by nonlinear transformation of complex Gaussian processes representing digitally modulated complex enveloped signals. One of them is presented in [50] where an RF nonlinear amplifier is modeled using Taylor series whose coefficients are complex representing AM/AM and AM/PM nonlinearities which are obtained using a single tone test. Spectral regrowth is analyzed by characterizing the complex base-band signal by its autocorrelation functions (AF) and nonlinearly transformed RF amplifier output in terms of input autocorrelation. Power spectra are calculated by taking Fourier transforms of corresponding AF. A general band-pass signal can be represented as follows:

$$w(t) = x(t) \cos(2\pi f_c t) + y(t) \sin(2\pi f_c t) \quad (4.1)$$

which can be rewritten as follows:

$$w(t) = A(t) \cos(2\pi f_c t + \theta(t)) \quad (4.2)$$

where

$$A(t) = \sqrt{x^2(t) + y^2(t)} \quad (4.3)$$

and

$$\theta(t) = \tan^{-1} \left( \frac{y(t)}{x(t)} \right) \quad (4.4)$$

or

$$w(t) = \frac{1}{2} \left[ z(t) e^{j2\pi f_c t} + z^*(t) e^{-j2\pi f_c t} \right] \quad (4.5)$$

where  $z(t) = A(t) e^{j\theta(t)}$  is the input phasor. In [50] an expression is derived which relates the phasor at the output of a nonlinear system to the corresponding input phasor. Fitting this expression to complex polynomial obtained from the AM/AM and AM/PM characterization of the amplifier for a single tone, complex power series coefficients are found out. These coefficients are then transformed to base-band behavioral model coefficients to be used in autocorrelation calculations. An

application of this analysis is used in [51] to determine the effect of the cross-modulation of a transmitted leakage CDMA signal and a single tone jammer to a received CDMA signal.

In [6] closed form expressions for the linearity performance of a memoryless CDMA RF power amplifier whose third and fifth order nonlinearities are specified by IP3 and IP5 parameters have been derived. Such an expression gives the designer a tool to determine the necessary IP3 of the power amplifier for a given linearity requirement. In this work the third and fifth order Taylor series coefficients are real and are directly related to measured IP3 and IP5. CDMA signal has been represented as a Bandlimited White Gaussian Noise (BWGN). A similar approach has also been applied in [52], however the effect of the AM/PM distortion on the spectrum of the output of a CDMA RF amplifier is brought into consideration as well. In this work, the amplifier nonlinearity has been represented by complex Taylor series and the RF amplifier output spectrum has been computed in terms of input complex coefficients. The magnitudes of the coefficients have been determined using two tone analysis and measuring the power of the IMD products. Although phase terms of the coefficients have not been determined explicitly, a case study has been done and best and worst cases for output spectrum have been computed. Hence the effect of AM/PM distortion has been observed. Thus, CDMA output spectrum has been predicted using a two tone test.

In literature so far, modeling issue of RF power amplifiers for CDMA and complex Gaussian processes has been examined in details. However autocorrelation analysis of a feedforward linearizer has not been studied before. The difficulty with feedforward modeling is that, the analysis involves two nonlinear amplifiers which are coupled to each other. Hence even if the amplifiers are modeled with third order nonlinearities, the order of the nonlinearity of the overall system jumps to ninth order. This makes the computations very tedious and complex. Since a feedforward circuit includes delay elements the autocorrelation formulations need to be improved which makes this analysis distinguished from the previous ones.

In this chapter, the approach used in [6], is extended to a simple feedforward system for a typical CDMA application where two nonlinear power amplifiers, couplers and delay units participate. Hence a mathematical model has been proposed

leading closed form expressions, which relate the linearity performance of the system to the parameters of the whole linearizer. Using such a tool, system parameters can be optimized for optimum efficiency and given linearity performance. We used CDMA signal for our analysis because it is a popular modulation scheme used in modern communication system for many advantages such as reduced spectral density, high communications security and protection against co-channel interference. In addition to this, its stochastic functions are in a relatively simple form which would make our derivations handier. However we will also see that, even though the input signal characterization is simple, the derived closed form expressions for the output of the feedforward circuit are still complicated and require messy calculations.

For the sake of simplicity, in the beginning no delay and phase mismatch is assumed, and the main and error amplifiers used in the system are considered to have a third order AM/AM nonlinearity only. First, the transfer function of the feedforward circuit shown in Figure 4.1 will be derived. Then using this transfer function, closed form expressions, which characterize main amplifier and feedforward output will be derived by making use of the stochastic characterization of the input CDMA signal. The derived closed form expressions are then verified through simulations. As a consequence of these derivations, closed form expressions, which provide a tool to control circuit parameters for optimum efficiency and linearity and to compute main and adjacent channel powers easily, are obtained. The conditions for the validity of these expressions are brought into consideration. Then for a special case, we end up with a compact relationship, which clearly demonstrates the trade off between main and error amplifier nonlinearities. Later the derived closed form expressions are modified to demonstrate the effect of the delay mismatch in the second loop. Finally the analysis will further be developed to include delay mismatches in the first loop. Verification of the model with MATLAB and DSP simulations will also be performed. The verification with RF simulations will be demonstrated in the next chapter.

## 4.2 Model Analysis

### 4.2.1 Transfer function of a feedforward circuit without delay mismatches

A simplified feedforward circuit is illustrated in Figure 4.1. While formulating the transfer function of the feedforward circuit, it is assumed that the main and the error amplifiers are memoryless in other words their nonlinearity are limited to AM/AM distortion only and the nonlinearity can be expressed by power series.

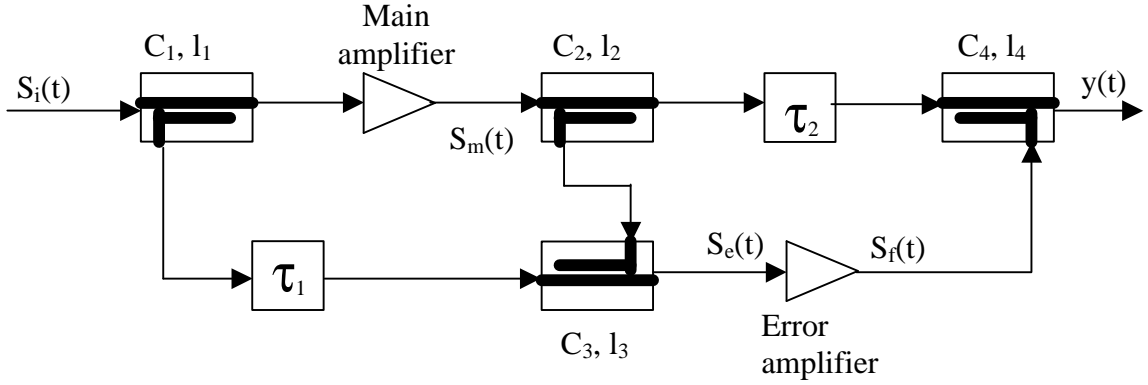


**Figure 4.1** A simplified form of a feedforward circuit.

For the sake of simplicity the amplifiers are assumed to have a third order nonlinearity only and there is no delay and phase mismatch. A general signal input to the feedforward circuit can be expressed as following:

$$s(t) = s_i(t) \cos(2\pi f_c t + \theta(t)) \quad (4.6)$$

where  $s_i(t)$  is the envelope of the input signal and  $f_c$  is the carrier frequency. Then the output of the main amplifier is:

$$s'_{mo}(t) = l_1 a'_1 s(t) + l_1^3 a'_3 s^3(t) \quad (4.7)$$

where  $l_1$  is the loss of the coupler C1;  $a'_1$  and  $a'_3$  are the power series coefficients which characterize the third order nonlinearity of the main amplifier and they can be

written in terms of the main amplifier linear gain,  $G_m$  (dB) and main amplifier third order intercept point,  $IP_3^m$  (dBW) [53]:

$$\begin{aligned} a'_1 &= 10^{G_m/20} \\ a'_3 &= \frac{-2}{3R} 10^{\left(\frac{-IP_3^m}{10} + \frac{3G_m}{20}\right)} \end{aligned} \quad (4.8)$$

Note that  $R$  is the reference impedance of the circuit, which is usually  $50 \Omega$ . Substituting (4.6) and neglecting third order harmonics, (4.7) can be expressed as follows:

$$s_{mo}(t) = s_m(t) \cos(2\pi f_c t + \theta(t)) \quad (4.9)$$

where

$$s_m(t) = l_1 a_1 s_i(t) + l_1^3 a_3 s_i^3(t) \quad (4.10)$$

$$\begin{aligned} a_1 &= a'_1 \\ a_3 &= \frac{3}{4} a'_3 \end{aligned} \quad (4.11)$$

since

$$\cos^3(\theta) = \frac{3}{4} \cos(\theta) + \frac{1}{4} \cos(3\theta) \quad (4.12)$$

Similarly the envelope of the signal at the input of the error amplifier, in other words output of the carrier cancellation loop, can be expressed as follows assuming there is no phase mismatch:

$$s_e(t) = \frac{s_m(t)}{C_2 C_3} - \frac{l_3 s_i(t)}{C_1} \quad (4.13)$$

where  $C_1$ ,  $C_2$  and  $C_3$  are the coupling coefficients of the couplers  $C1$ ,  $C2$  and  $C3$  respectively and  $l_3$  is the loss factor of  $C3$ . Envelope of the output of the error amplifier, ignoring the third order harmonics is:

$$s_f(t) = b_1 s_e(t) + b_3 s_e^3(t) \quad (4.14)$$

where

$$\begin{aligned}
b_1 &= b'_1 \\
b_3 &= \frac{3}{4}b'_3
\end{aligned}
\tag{4.15}$$

Note that  $b'_1$  and  $b'_3$  are Taylor series coefficients of the error amplifier which has a third order nonlinearity and (4.8) is valid for these coefficients. However  $G_m$  and  $IP3^m$  are now replaced with  $G_e$  and  $IP3^e$  respectively. Finally envelope of the error cancellation loop output can be written as:

$$y(t) = l_2 l_4 s_m(t) - \frac{s_f(t)}{C_4}
\tag{4.16}$$

where  $l_4$  and  $C_4$  are the loss factor and coupling coefficient of the coupler C4 respectively. If we combine the above equations and rearrange terms we obtain the following simplified result:

$$y(t) = D_1 s_i(t) + D_3 s_i^3(t) + D_5 s_i^5(t) + D_7 s_i^7(t) + D_9 s_i^9(t)
\tag{4.17}$$

where, D coefficients can be found in Appendix A. To show the utility of (4.17)  $y(t)$  versus  $s_i(t)$  has been plotted for various  $IP3^e$  (error amplifier IP3 which is related with  $b_1$  and  $b_3$ ) and  $C_2$  values in Figure 4.2. It should be noted that  $s_i(t)$  and  $y(t)$  correspond to instantaneous feedforward input and output envelope voltages at the fundamental frequency respectively.

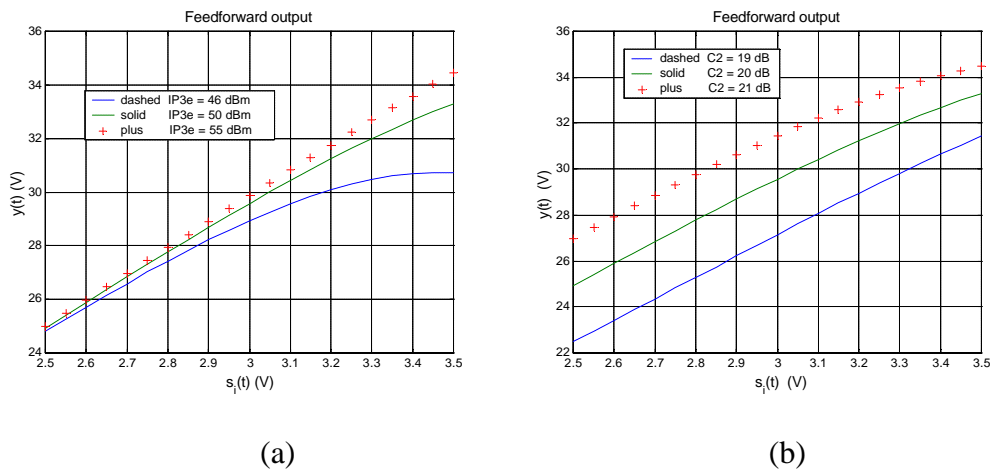


**Figure 4.2 a)** Response of (4.17) for various  $IP3^e$  values ( $IP3^m=45.5$  dBm,  $G_m=20$  dB,  $G_e=40$  dB,  $C_1=C_3=C_4=10$  dB,  $C_2=20$  dB) **b)** Response of (4.17) for various  $C_2$  values ( $IP3^m=45.5$  dBm,  $G_m=20$  dB,  $IP3^e=50$  dBm,  $G_e=40$  dB,  $C_1=C_3=C_4=10$  dB).

#### 4.2.2 Main amplifier and feedforward output characterization

In order to derive a closed form expression for power spectrum of the signal at the output of the feedforward circuit using the transfer function derived above, we have to characterize the input signal first. If we can define the stochastic characterization of the input signal such as its probability density function (PDF), power histogram, autocorrelation function (AF) or power spectral density (PSD) explicitly, we can find out the autocorrelation function and power spectral density at any point in the feedforward circuit. Hence we can derive a closed form relationship between the adjacent channel distortion power and the circuit parameters such as coupling coefficients, main and error amplifier gain and IP3s. The closed form expression will give us the flexibility of adjusting the circuit parameters for optimum linearity and efficiency. In our analysis we used a CDMA signal with  $n$  spread spectrum signals as the input signal. A general CDMA signal can be expressed as follows [6, 22]:

$$s(t) = \sum_{i=1}^n m_i(t)c_i(t) \cos[2\pi f_c t + \theta_i(t)] \quad (4.18)$$

where  $m_i(t)$  is the  $i^{\text{th}}$  baseband modulated signal,  $c_i(t)$  is the  $i^{\text{th}}$  pseudonoise binary code whose bandwidth is  $B$  which determines the base-bandwidth of the main channel and  $f_c$  is the carrier frequency. According to the law of large numbers and central limit theorem, as the number of spread spectrum signals,  $n$ , becomes larger (practically between 9 and 64) the overall signal  $s(t)$  will converge to a bandlimited white Gaussian noise (BWGN) with zero mean [6, 22, 52]. Such a signal has a well-known AF and PSD. Hence (4.18) can be written as:

$$s(t) = s_i(t) \cos[2\pi f_c t + \theta(t)] \quad (4.19)$$

where  $s_i(t)$  is a Gaussian wide-sense stationary process with PSD

$$P_s(f) = \begin{cases} \frac{N_0}{2}, & |f| \leq B \\ 0, & \text{else} \end{cases} \quad (4.20)$$

and with AF:

$$R_{s_i}(\tau) = E\{s_i(t)s_i(t+\tau)\} = \frac{N_0 \sin(2\pi B\tau)}{2\pi\tau} \quad (4.21)$$

where  $E\{\bullet\}$  denotes expected value.  $N_0$  is a constant which determines the input power and is equal to  $kT_e$  where  $k$  is the Boltzmann's constant and  $T_e$  is the equivalent noise temperature [54]. Once AF of the input signal envelope is determined, one can find out the corresponding envelope AF at any point in the feedforward system. Hence AF at the output of the main amplifier, carrier cancellation loop and feedforward system can be computed using (4.10), (4.13) and (4.17) respectively, without taking phase and delay mismatches into account. Hence:

$$R_{s_m}(\tau) = E\{s_m(t)s_m(t+\tau)\} = E\left\{[E_1 s_i(t) + E_3 s_i^3(t)][E_1 s_i(t+\tau) + E_3 s_i^3(t+\tau)]\right\} \quad (4.22)$$

where

$$\begin{aligned} E_1 &= a_1 l_1 \\ E_3 &= a_3 l_1^3 \end{aligned} \quad (4.23)$$

$$R_{s_e}(\tau) = E\{s_e(t)s_e(t+\tau)\} = E\left\{[F_1 s_i(t) + F_3 s_i^3(t)][F_1 s_i(t+\tau) + F_3 s_i^3(t+\tau)]\right\} \quad (4.24)$$

where

$$\begin{aligned} F_1 &= \frac{a_1 l_1}{C_2 C_3} - \frac{l_3}{C_1} \\ F_3 &= \frac{a_3 l_1^3}{C_2 C_3} \end{aligned} \quad (4.25)$$

$$R_y(\tau) = E\{y(t)y(t+\tau)\} = E\left\{\left(\sum_{m=1,3}^9 D_m s_i^m(t)\right)\left(\sum_{m=1,3}^9 D_m s_i^m(t+\tau)\right)\right\} \quad (4.26)$$

Equations (4.22), (4.24) and (4.26) involve computation of expected values of expressions in the form  $s_1^m s_2^n$  where,  $s_1 = s_i(t)$ ,  $s_2 = s_i(t + \tau)$  and both  $s_1$  and  $s_2$  are zero mean Gaussian random processes. The computation can be performed via following equation [55]:

$$E\{s_1^m s_2^n\} = \left. \frac{\partial^m \partial^n}{\partial s_1^m \partial s_2^n} \phi(s_1, s_2) \right|_{(s_1, s_2) = (0, 0)} \quad (4.27)$$

where  $\phi(s_1, s_2)$  is the joint characteristic function of two jointly Gaussian random variables and is defined as follows for zero mean processes:

$$\phi(s_1, s_2) = \exp\left[\frac{1}{2}(C_{1,1}s_1^2 + 2C_{1,2}s_1s_2 + C_{2,2}s_2^2)\right] \quad (4.28)$$

where C is the covariance function and is defined as follows:

$$C_{m,n} = E\{s_m s_n\} \quad (4.29)$$

which reduces to power of the signal for  $m=n$  and AF defined in (4.21) for  $m$  different from  $n$ . Computation of (4.27) may require lengthy calculations and some auxiliary software for taking derivatives. However the following expression has been derived to compute the AF represented in (4.27) in a much faster and easier way:

$$E\{s^m(t) s^n(t + \tau)\} = 1 \cdot 3 \cdots n \cdot \sum_{k=1,3,5}^m R_s^k(t) K^{\frac{m+n-k}{2}} \cdot \prod_{j=1,3}^{m-k-1} j \cdot \prod_{j=1,3}^{k-2} (n-j) \cdot \binom{m}{k} \quad (4.30)$$

for  $m \leq n$ ,  $m, n$  odd

Using (4.30), (4.22) can be expanded and simplified as following:

$$R_{sm}(\tau) = N_1 R_{si}(\tau) + N_3 R_{si}^3(\tau) \quad (4.31)$$

where

$$N_1 = E_1^2 + 9E_3^2 K^2 + 6E_1 E_3 K \quad (4.32)$$

$$N_3 = 6E_3^2 \quad (4.33)$$

$$K = N_0 B \quad (4.34)$$

Similarly carrier cancellation output AF can be derived as follows:

$$R_{se}(\tau) = P_1 R_{si}(\tau) + P_3 R_{si}^3(\tau) \quad (4.35)$$

where

$$P_1 = F_1^2 + 9F_3^2 K^2 + 6F_1 F_3 K \quad (4.36)$$

$$P_3 = 6F_3^2 \quad (4.37)$$

and feedforward output AF can be derived as follows:

$$R_y(t) = E\{y(t)y(t+t)\} = \sum_{n=1,3}^9 M_n R_{si}^n(\tau) \quad (4.38)$$

where  $M$  coefficients indicated in (4.38) are explicitly found in Appendix A.

Once AF of the envelopes of the main amplifier and feedforward output are determined, PSD functions can be found by taking Fourier Transform of AFs. PSD of the signals at the output of the main amplifier and feedforward output are given by,

$$P_m(f) = N_1 P_s(f) + N_3 P_s(f) \otimes P_s(f) \otimes P_s(f) \quad (4.39)$$

$$P_e(f) = P_1 P_s(f) + P_3 P_s(f) \otimes P_s(f) \otimes P_s(f) \quad (4.40)$$

$$P_y(f) = M_1 P_s(f) + M_3 P_s(f) \otimes P_s(f) \otimes P_s(f) + M_5 P_s(f) \otimes P_s(f) \otimes P_s(f) \otimes P_s(f) \otimes P_s(f) + M_7 P_s(f) \otimes \dots \otimes P_s(f) \quad (4.41)$$

where  $\otimes$  denotes convolution. Note that up to seventh order coefficients are taken into consideration while computing the third order distortion products. Ninth order has been observed to be negligible. In our analysis the parameter  $K=N_0B$  is replaced by the following expression:

$$K = \frac{2P_m}{a_1^2 l_1^2} \quad (4.42)$$

where  $K/2$  is the main channel input power and  $P_m$  is the linear output power of the main amplifier if there were no in-band distortion. After expanding (4.39) - (4.41), closed form expressions for PSDs have been derived as follows:

$$P_m(f) = \begin{cases} N_3 \left( \frac{N_0}{2} \right)^3 \left[ \frac{f^2}{2} + 3Bf + \frac{9}{2} B^2 \right], & -3B < f < -B \\ N_1 \frac{N_0}{2} + N_3 \left( \frac{N_0}{2} \right)^3 \left[ -f^2 + 3B^2 \right], & -B < f < B \\ N_3 \left( \frac{N_0}{2} \right)^3 \left[ \frac{f^2}{2} - 3Bf + \frac{9}{2} B^2 \right], & B < f < 3B \end{cases} \quad (4.43)$$

$$P_e(f) = \begin{cases} P_3 \left( \frac{N_0}{2} \right)^3 \left[ \frac{f^2}{2} + 3Bf + \frac{9}{2} B^2 \right], & -3B < f < -B \\ P_1 \frac{N_0}{2} + P_3 \left( \frac{N_0}{2} \right)^3 \left[ -f^2 + 3B^2 \right], & -B < f < B \\ P_3 \left( \frac{N_0}{2} \right)^3 \left[ \frac{f^2}{2} - 3Bf + \frac{9}{2} B^2 \right], & B < f < 3B \end{cases} \quad (4.44)$$

$$P_y(f) = \begin{cases} M_3 \left( \frac{N_0}{2} \right)^3 \left[ \frac{f^2}{2} + 3Bf + \frac{9}{2} B^2 \right] + M_5 \left( \frac{N_0}{2} \right)^5 \left[ \frac{-f^4}{6} - \frac{5}{3} Bf^3 - 5B^2 f^2 - \frac{5}{3} B^3 f + \frac{55}{6} B^4 \right] + \\ M_7 \left( \frac{N_0}{2} \right)^7 \left[ \frac{15}{720} f^6 + \frac{35}{120} Bf^5 + \frac{63}{48} B^2 f^4 + \frac{35}{36} B^3 f^3 - \frac{273}{48} B^4 f^2 + \frac{35}{120} B^5 f + \frac{23583}{720} B^6 \right], & -3B < f < -B \\ M_1 \frac{N_0}{2} + M_3 \left( \frac{N_0}{2} \right)^3 \left[ \frac{-f^2}{2} + 3B^2 \right] + M_5 \left( \frac{N_0}{2} \right)^5 \left[ \frac{f^4}{4} - \frac{5}{2} B^2 f^2 + \frac{230}{24} B^4 \right] + \\ M_7 \left( \frac{N_0}{2} \right)^7 \left[ \frac{-20}{720} f^6 + \frac{28}{48} B^2 f^4 - \frac{308}{48} B^4 f^2 + \frac{23548}{720} B^6 \right], & -B < f < B \\ M_3 \left( \frac{N_0}{2} \right)^3 \left[ \frac{f^2}{2} - 3Bf + \frac{9}{2} B^2 \right] + M_5 \left( \frac{N_0}{2} \right)^5 \left[ \frac{-f^4}{6} + \frac{5}{3} Bf^3 - 5B^2 f^2 + \frac{5}{3} B^3 f + \frac{55}{6} B^4 \right] + \\ M_7 \left( \frac{N_0}{2} \right)^7 \left[ \frac{15}{720} f^6 - \frac{35}{120} Bf^5 + \frac{63}{48} B^2 f^4 - \frac{35}{36} B^3 f^3 - \frac{273}{48} B^4 f^2 - \frac{35}{120} B^5 f + \frac{23583}{720} B^6 \right], & B < f < 3B \end{cases} \quad (4.45)$$

Using PSD functions of the main amplifier and feedforward output we can also find out the total power at the main and adjacent channels in closed form by integrating the above expressions over the specified bandwidths:

$$P_{main} = \frac{1}{2} \int_{-B}^B P_m(f) df = N_1 \frac{K}{2} + \frac{8}{3} N_3 \left( \frac{K}{2} \right)^3 \quad (4.46)$$

$$P_{mainacp} = \int_B^{3B} P_m(f) df = \frac{4}{3} N_3 \left( \frac{K}{2} \right)^3 \quad (4.47)$$

$$P_{err} = \frac{1}{2} \int_{-B}^B P_e(f) df = P_1 \frac{K}{2} + \frac{8}{3} P_3 \left( \frac{K}{2} \right)^3 \quad (4.48)$$

$$P_{erracp} = \int_B^{3B} P_e(f) df = \frac{4}{3} P_3 \left( \frac{K}{2} \right)^3 \quad (4.49)$$

$$P_{out} = \frac{1}{2} \int_{-B}^B P_y(f) df = M_1 \frac{K}{2} + \frac{8}{3} M_3 \left( \frac{K}{2} \right)^3 + \frac{44}{5} M_5 \left( \frac{K}{2} \right)^5 \quad (4.50)$$

$$P_{outacp} = \int_B^{3B} P_y(f) df = \frac{4}{3} M_3 \left( \frac{K}{2} \right)^3 + \frac{104}{15} M_5 \left( \frac{K}{2} \right)^5 + \frac{3176}{105} M_7 \left( \frac{K}{2} \right)^7 \quad (4.51)$$

where

$P_{main}$  is the total power at the output of the main amplifier,

$P_{mainacp}$  is the total ACP at the output of the main amplifier,

$P_{err}$  is the total power at the output of the carrier cancellation loop,

$P_{erracp}$  is the total ACP at the output of the cancellation loop,

$P_{out}$  is the total power at the output of the feedforward,

$P_{outacp}$  is the total ACP at the output of the feedforward.

### 4.2.3 Feedforward output characterization with delay mismatches in the second loop

The analysis explained above assumes that there is no delay mismatch. Addition of the delay mismatches, especially the one in the first loop would make the closed form formulations very complex due to the transformation of delay mismatches through the error amplifier, even though the model is based upon third order nonlinearities. In the following sections delay mismatch in the first (carrier cancellation) loop will be analyzed in details. However delay mismatch in the second (error cancellation) loop,  $\tau_2$ , is relatively simple to analyze. Taking  $\tau_2$  into consideration would cause  $s_m(t)$  in (4.10) to shift  $\tau_2$  in time domain resulting the following

$$s_m(t) = l_1 a_1 s_i(t - \tau_2) + l_1^3 a_3 s_i^3(t - \tau_2) \quad (4.52)$$

Injecting (4.52) into (4.16) would modify (4.17) into following:

$$y(t) = \sum_{n=1,3}^9 D_n' s_i^n(t) + \sum_{n=1}^3 D_n'' s_i^n(t - \tau_2) \quad (4.53)$$

where  $D'$ ,  $D''$  coefficients can be found in Appendix A. After taking AF of (4.53), we obtain a modified form of (4.38):

$$R_y(t) = E\{y(t)y(t+t)\} = M_1' R_{si}(t) + M_3' R_{si}^3(t) + M_5' R_{si}^5(t) + M_7' R_{si}^7(t) + M_9' R_{si}^9(t) + M_1'' [R_{si}(t - \tau_2) + R_{si}(t + \tau_2)] + M_3'' [R_{si}^3(t - \tau_2) + R_{si}^3(t + \tau_2)] \quad (4.54)$$

where  $M'$ ,  $M''$  coefficients can be found in Appendix A. PSD at the output of the feedforward can be computed by taking Fourier transform of (4.54):

$$P_y(f) = \left[ M_1' + 2M_1'' \cos(2\pi f t_2) \right] P_s(f) + \left[ M_3' + 2M_3'' \cos(2\pi f t_2) \right] * P_s(f) \otimes P_s(f) \otimes P_s(f) + M_5' P_s(f) \otimes \dots \otimes P_s(f) + M_7' P_s(f) \otimes \dots \otimes P_s(f) \quad (4.55)$$

PSD expression for the feedforward output is similar to the one in (4.45), except  $M_1$ ,  $M_3$ ,  $M_5$  and  $M_7$  are replaced with  $\left[ M_1' + 2M_1'' \cos(2\pi ft_2) \right]$ ,  $\left[ M_3' + 2M_3'' \cos(2\pi ft_2) \right]$ ,  $M_5'$  and  $M_7'$ , respectively. Integrating the expressions in (4.45) over the main channel and adjacent channel limits, yield the following equations for the total power at the main and adjacent channels:

$$P_{out} = \frac{N_0}{2} \frac{\left[ M_1' A + M_1'' \sin(2A) \right]}{\pi \tau_2} + \left( \frac{N_0}{2} \right)^3 \frac{\left[ 16M_3' A^3 - 6M_3'' A \cos(2A) + 12M_3'' A^2 \sin(2A) + 3M_3'' \sin(2A) \right]}{6(\pi \tau_2)^3} + \frac{44}{5} M_5 \left( \frac{K}{2} \right)^5 \quad (4.56)$$

$$P_{outacp} = \left( \frac{N_0}{2} \right)^3 \frac{\left[ 16M_3' A^3 + 12M_3'' A \cos(2A) + (3 - 24A^2) M_3'' \sin(2A) - 3M_3'' \sin(6A) \right]}{12(\pi \tau_2)^3} + \frac{104}{15} M_5' \left( \frac{K}{2} \right)^5 + \frac{3176}{105} M_7' \left( \frac{K}{2} \right)^7 \quad (4.57)$$

where  $A = \pi B \tau_2$ .

#### 4.2.4 Feedforward output characterization with delay mismatches in both loops

To include delay mismatches in the analysis of the feedforward circuit we need to modify the envelope expressions at the input and output of the error cancellation loops such that the signal at the input of the error amplifier is the difference of the sampled main amplifier output and sampled input signal with a time shift,  $\tau_1$  and feedforward output is the difference of the sampled error amplifier output and the main amplifier output with a time shift,  $\tau_2$ . Hence (4.13) and (4.16) are modified as follows:

$$s_e(t) = \frac{s_m(t)}{C_2 C_3} - \frac{l_3 s_i(t - \tau_1)}{C_1} \quad (4.58)$$

$$y(t) = l_2 l_4 s_m(t - \tau_2) - \frac{s_f(t)}{C_4} \quad (4.59)$$

Correspondingly feedforward output can be expressed as following:

$$\begin{aligned} y(t) = & D_9 s_i^9(t) + D_7 s_i^7(t) + D_5 s_i^5(t) + D_3 s_i^3(t) + D_1 s_i(t) + D_8 s_i^6(t) s_i(t - \tau_1) + \\ & D_6 s_i^4(t) s_i(t - \tau_1) + D_{14} s_i^3(t) s_i^2(t - \tau_1) + D_4 s_i^2(t) s_i(t - \tau_1) + D_2 s_i(t) s_i^2(t - \tau_1) + \\ & D_{10} s_i(t - \tau_2) + D_{11} s_i^3(t - \tau_2) + D_{12} s_i^3(t - \tau_1) + D_{13} s_i(t - \tau_1) \end{aligned} \quad (4.60)$$

where the modified  $D$  coefficients are found in Appendix A. In order to compute the PSD at the output of the feedforward linearizer the AF at the output –  $R_y(\tau) = E\{y(t)y(t+\tau)\}$  – needs to be computed. Different from the derivations explained in previous sections, this time we face with computation of expected values of up-to 4 different zero mean Gaussian random processes. For  $n$  different zero mean Gaussian random variables the expected value expression given in (4.27) can be extended as following:

$$E\{s_1^{m_1} \dots s_n^{m_n}\} = \frac{\partial^{m_1}}{\partial s_1^{m_1}} \dots \frac{\partial^{m_n}}{\partial s_n^{m_n}} \phi(s_1, \dots, s_n) \Big|_{(s_1, \dots, s_n)=0} \quad (4.61)$$

where the function  $\phi$  is the joint characteristic function of  $n$  jointly Gaussian random variables and can be expressed as follows:

$$\phi(s_1, \dots, s_n) = \exp\left(\sum_{p=1}^n \sum_{r=1}^n C_{p,r} s_p s_r\right) \quad (4.62)$$

where  $C$  is the covariance function and can be represented as:

$$C_{p,r} = \begin{cases} E\{s_p s_r\} = R_{pr}(\tau), & p \neq r \\ \frac{1}{2} E\{s^2(t)\} = \frac{K}{2}, & p = r \end{cases} \quad (4.63)$$

Expansion of  $R_y(\tau)$  results with lots of terms which involve expected value of different combinations of random variables whose number of them ( $n$ ) vary from 2 to 4. These expressions have been derived explicitly and are listed in Appendix B. Fourier transform of most of these terms can be taken in closed form. However some

of them are not simple enough and they need to be taken computationally. The autocorrelation function below includes terms whose Fourier transform can be taken in closed form:

$$\begin{aligned}
R_{closed}(\tau) = & M_1 R_{si}(\tau) + M_3 R_{si}^3(\tau) + M_5 R_{si}^5(\tau) + M_7 R_{si}^7(\tau) + M_9 R_{si}^9(\tau) + M_2 [R_{si}(\tau - \tau_1) + R_{si}(\tau + \tau_1)] + \\
& M_4 [R_{si}^3(\tau - \tau_1) + R_{si}^3(\tau + \tau_1)] + M_2' [R_{si}(\tau - \tau_2) + R_{si}(\tau + \tau_2)] + M_4' [R_{si}^3(\tau - \tau_2) + R_{si}^3(\tau + \tau_2)] + \\
& M_6 [R_{si}(\tau - \tau_1 + \tau_2) + R_{si}(\tau - \tau_2 + \tau_1)] + M_6' [R_{si}^3(\tau - \tau_1 + \tau_2) + R_{si}^3(\tau - \tau_2 + \tau_1)]
\end{aligned} \tag{4.64}$$

where the modified  $M'$ ,  $M''$  coefficients can be found in the Appendix B. The other elements of  $R_y(\tau)$  are tabulated in a matrix and the overall  $R_y(\tau)$  is computed using the following relationship:

$$R_y(\tau) = R_{closed}(\tau) + R_{comp}(\tau) \tag{4.65}$$

where

$$\begin{aligned}
R_{comp} = & \sum_{i=1}^n D(A(i,1)) * D(A(i,2)) * A(i,3) * K^{A(i,4)} * R^{A(i,5)} * \left( \prod_{j=1}^7 R_j^{A(i,j+5)} + \prod_{j=1}^7 R_j^{A(i,j+5)} \right) \\
& \text{for } D(A(i,1)) \neq D(A(i,2)) \\
R_{comp} = & \sum_{i=1}^n D(A(i,1)) * D(A(i,2)) * A(i,3) * K^{A(i,4)} * R^{A(i,5)} * \left( \prod_{j=1}^7 R_j^{A(i,j+5)} \right) \\
& \text{for } D(A(i,1)) = D(A(i,2))
\end{aligned} \tag{4.66}$$

$$\begin{aligned}
R_1 = R_s(\tau_1), R_2 = R(n + n_1), R_3 = R(n - n_1), R_4 = R(n - n_2), R_5 = R(n + n_2), \\
R_6 = R(n + n_1 - n_2), R_7 = R(n + n_2 - n_1)
\end{aligned} \tag{4.67}$$

$$R'_1 = R_1, R'_2 = R_3, R'_3 = R_2, R'_4 = R_5, R'_5 = R_4, R'_6 = R_7, R'_7 = R_6 \tag{4.68}$$

$n_1 = t_1/T_s$ ,  $n_2 = t_2/T_s$ ,  $A$  is the generated matrix which can be found in Appendix B. The array,  $R(n)$ , is computed using inverse fast Fourier Transform of the rectangular function  $P(n)$  which represents the PSD of a BWGN in MATLAB:

$$R(n) = \text{ifft}(P(n), N) / T_s \quad (4.69)$$

where  $N$  (8192) is the length of the array (same as the original stimulus),  $T_s$  is the operating sampling period which is determined by the resolution of the delay mismatch to be analyzed and the sequence  $P(n)$  is:

$$P(n) = \begin{cases} N_0 / 2, & N1 < n < N2 \\ 0, & \text{else} \end{cases} \quad (4.70)$$

$N1 = N/2 - B*(N*T_s)$  and  $N2 = N/2 + B*(N*T_s)$ ,  $B$  is the bandwidth of the CDMA baseband signal (615 kHz). The PSD at the output is computed by taking the Fourier transform of (4.65):

$$P_y(f) = P_{\text{closed}}(f) + P_{\text{comp}}(f) \quad (4.71)$$

where

$$P_{\text{comp}}(f) = T_s * \text{fft}(R_{\text{comp}}(n), N) \quad (4.72)$$

Expression for  $P_{\text{closed}}(f)$  is same as (4.45) except  $M_1$  and  $M_3$  are replaced by  $M_1'$  and  $M_3'$  which are expressed as follows:

$$M_1' = M_1 + 2M_2 \cos(2\pi f \tau_1) + 2M_2' \cos(2\pi f \tau_2) + 2M_6 \cos(2\pi f (\tau_1 - \tau_2)) \quad (4.73)$$

$$M_3' = M_3 + 2M_4 \cos(2\pi f \tau_1) + 2M_4' \cos(2\pi f \tau_2) + 2M_6' \cos(2\pi f (\tau_1 - \tau_2)) \quad (4.74)$$

#### 4.2.5 Error amplifier input characterization with delay mismatch in the first loop

At the output of the carrier cancellation loop, i.e. at the input of the error amplifier, the envelope of the error signal can be expressed as following:

$$s_e(t) = F_1 s_i(t) + F_1' s_i(t - \tau_1) + F_3 s_i^3(t) \quad (4.75)$$

where

$$\begin{aligned}
F_1 &= \frac{l_1 a_1}{C_2 C_3} \\
F_1' &= \frac{-l_3}{C_1} \\
F_3 &= \frac{l_1^3 a_3}{C_2 C_3}
\end{aligned} \tag{4.76}$$

The AF of (4.75) –  $R_{se}(t) = E\{s_e(t)s_e(t+t)\}$  – can be expressed as following:

$$R_{se}(\tau) = P_1 R_{si}(\tau) + P_3 R_{si}^3(\tau) + P_1' [R_{si}(\tau - \tau_1) + R_{si}(\tau + \tau_1)] \tag{4.77}$$

where

$$\begin{aligned}
P_1 &= F_1^2 + F_1'^2 + 6F_1 F_3 K + 9F_3^2 K^2 \\
P_1' &= F_1 F_1' + 3F_1' F_3 K \\
P_3 &= 6F_3^2
\end{aligned} \tag{4.78}$$

PSD at the output of the carrier cancellation loop - $P_e(f)$ - can be computed by taking Fourier Transform of (4.77):

$$P_e(f) = \begin{cases} P_3 \left( \frac{N_0}{2} \right)^3 \left[ \frac{f^2}{2} + 3Bf + \frac{9}{2} B^2 \right], & -3B < f < -B \\ \frac{N_0}{2} [P_1 + 2P_1' \cos(2\pi f \tau_1)] + P_3 \left( \frac{N_0}{2} \right)^3 [-f^2 + 3B^2], & -B < f < B \\ P_3 \left( \frac{N_0}{2} \right)^3 \left[ \frac{f^2}{2} - 3Bf + \frac{9}{2} B^2 \right], & B < f < 3B \end{cases} \tag{4.79}$$

The total error power - $P_e$ - is computed by integrating (4.79) and can be represented by the following relationship:

$$P_e = \frac{K}{2} \frac{[P_1 A' + P_1' \sin(2A')]}{A'} + \frac{8}{3} \left( \frac{K}{2} \right)^3 P_3 \tag{4.80}$$

where  $A' = \pi B \tau_1$ .

### 4.3 Verification of the model with simulations

In order to verify the expressions derived, we simulated the system using Advanced Design Suit (ADS) 2002C simulation program, which has been developed by Agilent Technologies. The zero mean BWGN input, which represents n-coded CDMA signal has been generated using the component palette AWGC (Additive White Gaussian Channel) in DSP environment with a sampling period of 0.27 usec and number of samples of 8192. This signal is then passed through a lowpass Chebyshev filter whose pass-band frequency is 615 kHz, to achieve a BWGN whose bandwidth is compatible to standard CDMA (1.23 MHz). The generation of the input data is illustrated in Figure 4.3. A BWGN has been used as the stimulus instead of real CDMA data because the essential point regarding to this analysis is the nature of the source and the analysis applies to any CDMA data as long as it obeys the Gaussian noise nature. The schematic of the feedforward system in DSP environment is illustrated in Figure 5.1 in the next chapter. The power spectrum at each node of the system is monitored using FFT analyzers whose window types are chosen to be rectangular. The number of FFT points ( $N_{points}$ ) should be power of 2, if not the closest power of 2 is chosen. In our case  $N_{points}$  is chosen as 8192. The Resolution

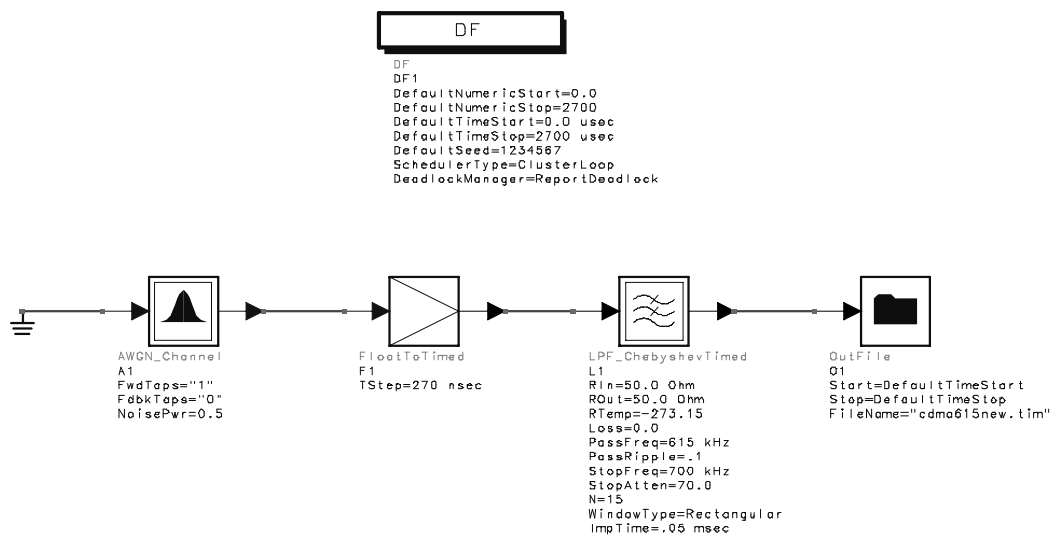


**Figure 4.3** Generation of the input data.

Bandwidth (RBW) of the power spectrum is  $1/(N_{points} \times T_s)$  which is equal to 451.8 Hz ( $1/(8192 \times 0.27 \text{ usec})$ ) in our simulation. In order to decrease the RBW time duration must be increased. The monitored spectra can be smoothed by adjusting the parameter *Naverage*. The nonlinear main and error amplifiers are represented using RFGain blocks whose IP3 (*output IP3*) and voltage gains can be specified. The coupling coefficients of the couplers ( $C_i$ ) are represented using linear gain blocks whose voltage gains ( $G_i$ ) are specified as follows:

$$G_i = 1/10^{(C_i/20)} \quad (4.81)$$

In order to achieve a better understanding about the signal processing and power spectrum analysis we adapted the same feedforward system to MATLAB environment. We formulated the system using equations used to derive the transfer function of the system. Then we compared the MATLAB and DSP simulation results and verified the equations used to derive closed form formulations. After discussing the validity of the formulations we extended the analysis to actual RF simulations performed in both DSP and Analog/RF environment supported by ADS. In the following sections these aspects will be discussed in details.

#### 4.3.1 Verification of the model in MATLAB environment

The time domain envelope data at the output of the main amplifier, input of the error amplifier and output of the feedforward are computed using the transfer function equations outlined in previous sections. The power spectra of these time domain envelope data have been computed by MATLAB and compared with ADS results to verify the formulation of the feedforward system. Thus, our simulation has been intended to be flexible to any arbitrary time data input. In order to estimate the PSD for a wide sense stationary discrete time data the following relation can be used [56]:

$$P_{xx}(f) = \frac{|X_N(f)|^2}{NT_s} \quad (4.82)$$

where,  $T_s$  is the sampling period (0.27 usec). In MATLAB simulation we made use of the FFT function for the rapid computation of the discrete Fourier series. Hence, PSD estimate has been computed using the following formula:

$$P_{xx}(f) = \frac{T_s^2 * |FFT(x, N)|^2}{(NT_s)} \quad (4.83)$$

where N is chosen to be power of 2 (8192) closest to the number of data points. Note that, for a  $50 \Omega$  system the expression above must be divided by 50.

The results of ADS and MATLAB simulation for the power spectra of the main amplifier and feedforward output are shown and compared in Figure 4.4 and Figure 4.5 for the given parameters ( $C_1 = 10$  dB,  $C_2 = 20$  dB,  $C_3 = 10$  dB,  $C_4 = 10$  dB,  $G_m = 20$  dB,  $IP3^m = 46$  dBm,  $G_e = 40$  dB,  $IP3^e = 50$  dBm). Close observation of the figures shows that ADS and MATLAB simulation results agree with each other. It should be noted that, MATLAB results are added by 26.5 dB ( $10 \times \log_{10}(451.8 \text{ Hz})$ ) to be equivalent to ADS results. Both ADS and MATLAB results are around 900 MHz carrier frequency. These results are a good validation for the expressions derived and used in the MATLAB simulation. Note that these expressions are also used for closed form derivations.

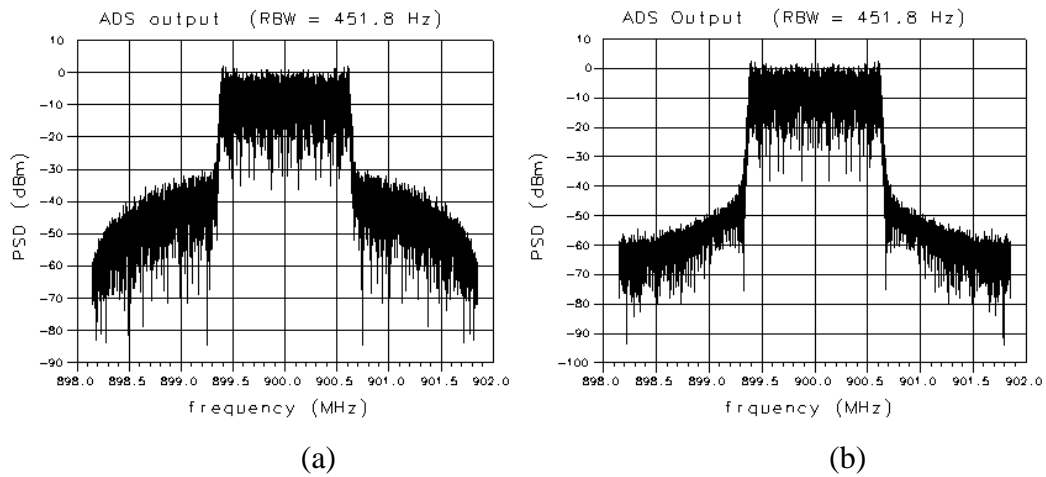


**Figure 4.4 a)** ADS simulation for main amplifier output. **b)** ADS simulation for feedforward output ( $C_1 = 10$  dB,  $C_2 = 20$  dB,  $C_3 = 10$  dB,  $C_4 = 10$  dB,  $G_m = 20$  dB,  $IP3^m = 46$  dBm,  $G_e = 40$  dB,  $IP3^e = 50$  dBm).

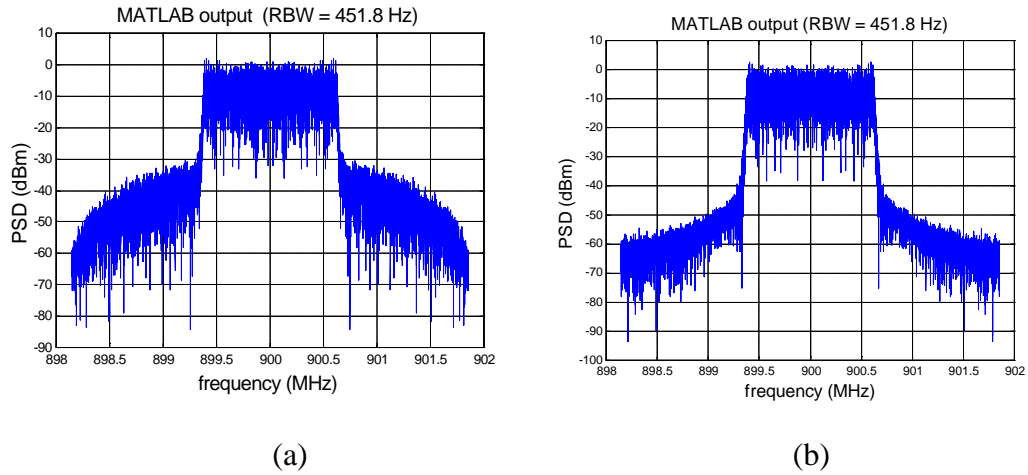


**Figure 4.5** a) MATLAB simulation for main amplifier output. b) MATLAB simulation for feedforward output ( $C_1 = 10$  dB,  $C_2 = 20$  dB,  $C_3 = 10$  dB,  $C_4 = 10$  dB,  $G_m = 20$  dB,  $IP3^m = 46$  dBm,  $G_e = 40$  dB,  $IP3^e = 50$  dBm).

Since MATLAB simulations are verified with ADS results, the derived closed form expressions can now be validated using the MATLAB environment which is a more convenient and faster simulation environment and the input data can be processed so that its characteristic is similar to the one used for the closed form derivations. Since the input data used for closed form expression is a perfect band limited white Gaussian noise with zero mean, power spectrum is concentrated in the main channel and adjacent channel power does not exist. In order to create a similar input data in MATLAB environment, the adjacent channels of the generated ADS data has been filtered out ideally. The closed form expressions and MATLAB simulations for the main amplifier and feedforward output are compared in Figure 4.6 for  $C_1 = 10$  dB,  $C_2 = 20$  dB,  $C_3 = 10$  dB,  $C_4 = 10$  dB,  $G_m = 20$  dB,  $IP3^m = 46$  dBm,  $G_e = 40$  dB,  $IP3^e = 50$  dBm,  $P_{out} = 28.5$  dBm.

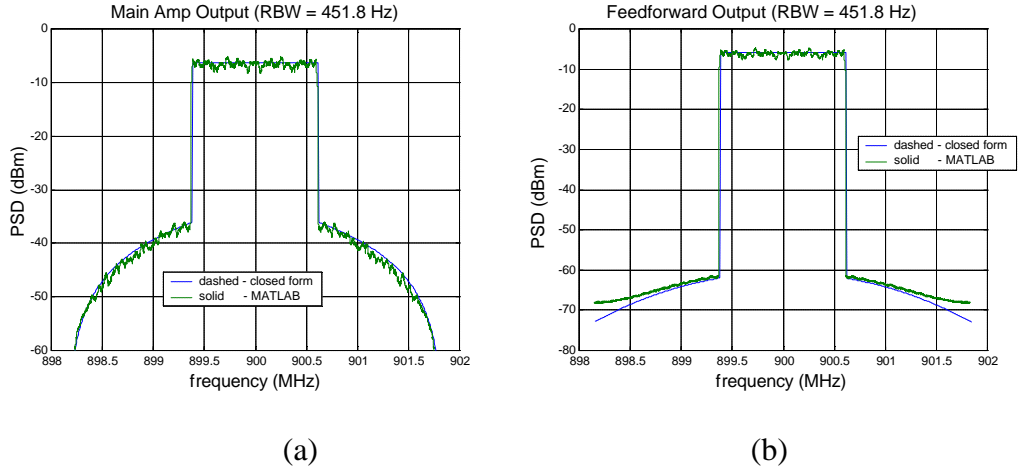


**Figure 4.6** Comparison of MATLAB simulation and closed form expressions for **a)** main amplifier output **b)** feedforward output ( $C_1 = 10$  dB,  $C_2 = 20$  dB,  $C_3 = 10$  dB,  $C_4 = 10$  dB,  $G_m = 20$  dB,  $IP3^m = 46$  dBm,  $G_e = 40$  dB,  $IP3^e = 50$  dBm,  $P_{out} = 28.5$  dBm).

Note that, closed form results coincide with MATLAB simulations. The small deviations are possibly due to the techniques used for averaging MATLAB simulation results and deviation of the generated noise data from the BWGN. After validating the closed form expressions we can use equations (4.46) – (4.51) in order to compute main channel power and ACP of the main amplifier and feedforward outputs. For our case these quantities are computed and compared with simulation results in Table 4.1. Note that main amplifier output power is approximately 0.5 dB lower than it should be because of the existence of inband distortion. The amount of inband distortion can be computed as 4.3 dBm using (4.46) and setting  $E_1$  in (4.32) to zero. After the carrier cancellation, the error cancellation loop cancels the inband distortion and the feedforward compensates for this loss. To show the utility of the closed form results a similar comparison has been made for different coupling values in Table 4.2 to take loop mismatches and losses into consideration.

**Table 4.1** Quantitative comparison of the closed form and simulation results ( $C_1 = 10$  dB,  $C_2 = 20$  dB,  $C_3 = 10$  dB,  $C_4 = 10$  dB,  $G_m = 20$  dB,  $IP3^m = 46$  dBm,  $G_e = 40$  dB,  $IP3^e = 50$  dBm,  $P_{out} = 28.5$  dBm).

	<b>Closed Form</b>	<b>Simulation</b>
<b>Pmain (dBm)</b>	28.0	28.0
<b>Pmainacp(dBm)</b>	-3.5	-4.0
<b>Pout (dBm)</b>	28.5	28.5
<b>Poutacp (dBm)</b>	-28.1	-27.2

**Table 4.2** Quantitative comparison of the closed form and simulation results for different loop mismatches ( $l_1=l_2=l_3=l_4=0.3$  dB,  $C_1 = 10$  dB,  $C_2 = 20$  dB,  $C_3 = 10$  dB,  $C_4=10$  dB,  $G_m = 20$  dB,  $IP3^m = 46$  dBm,  $G_e = 40$  dB,  $IP3^e = 50$  dBm,  $P_{out} = 28.5$  dBm).

	<b>C<sub>1</sub> = 9 dB</b>		<b>C<sub>2</sub> = 19 dB</b>		<b>C<sub>4</sub> = 9 dB</b>	
	<b>Closed Form</b>	<b>Simulation</b>	<b>Closed Form</b>	<b>Simulation</b>	<b>Closed Form</b>	<b>Simulation</b>
<b>Pout(dBm)</b>	28.7	28.7	26.5	26.5	27.7	27.7
<b>Poutacp(dBm)</b>	-23.8	-22.5	-19.1	-19.7	-19.8	-20.7

Since the nonlinearities of the main and error amplifiers are limited by third order power series expansion, there is a critical input voltage up-to where the third order model represents the nonlinearity correctly. As the input voltage increases the output begins to compress and at the critical point the output is just at the saturation. In MATLAB simulation the output is allowed to be constant at the saturation value beyond this critical point. However for closed form expressions we cannot make a similar adjustment and beyond this critical point the output voltage value deviates from the saturation point which makes the results incorrect. Range of the input voltage value can be increased with the order of nonlinearities. As a consequence of this observation, it can be deduced that there exists a minimum  $IP3$  for the main and error amplifiers where the closed form expressions give compatible results with simulation. The critical input voltage value for the main and error amplifiers can be determined by differentiating the power series expansions (4.10) and (4.14) with respect to input voltage and equating them to zero. Hence we get:

$$V_{si\_crit} = \sqrt{\frac{-a_1}{3a_3l_1^2}} \quad (4.84)$$

$$V_{se\_crit} = \sqrt{\frac{-b_1}{3b_3}} \quad (4.85)$$

If the maximum input voltage value to the system is known then the minimum IP3 value of the main amplifier with which closed form expressions can be used for 50 Ohm system, can be calculated using (4.8), (4.11) and (4.84)

$$IP_3^m = G_m + 20\log(V_{si\_max}) + 20\log l_1 + 14.77 \quad (4.86)$$

noting that  $V_{si\_max}$  is the absolute maximum voltage level at the input of the main amplifier and now is the critical voltage  $V_{si\_crit}$  for the worst case. Absolute maximum voltage level at the input of the error amplifier ( $V_{se\_max}$ ) and the required minimum IP3 can be computed using the following equations assuming that there is no phase or delay mismatch:

$$V_{se\_max} = \left| V_{si\_max} \left( \frac{a_1 l_1}{C_2 C_3} - \frac{l_3}{C_1} \right) + V_{si\_max}^3 \left( \frac{a_3 l_1^3}{C_2 C_3} \right) \right| \quad (4.87)$$

$$IP_3^e = G_e + 20\log(V_{se\_max}) + 14.77 \quad (4.88)$$

In our case time domain data of main amplifier and error amplifier inputs are seen in Figure 4.7. Note that absolute maximum voltage value at the main amplifier input is 3.55 V. Hence using (4.86) minimum required IP3 for the main amplifier can be computed as 45.8 dBm. For this main amplifier IP3, the absolute maximum at the input of the error amplifier is computed as 0.37 V using (4.87) which can also be verified in Figure 4.7. Finally by using (4.88) the minimum required error amplifier IP3 is found as 46.2 dBm. These values are the minimum required IP3 parameters for the coincidence of the simulation and closed form results.

The envelope peak-to-average ratio of the main amplifier input is approximately 13 dB. Envelope peak-to-average ratio for the error amplifier input increases up-to 26 dB. The average power at the input of the error amplifier can be

computed as  $-25.5$  dBm. Hence the average power at the output of the 40 dB gain error amplifier is approximately 14.5 dBm. Considering the crest factor and 10 dB extra for IP3 we end up with at least 50.5 dBm for IP3 of the error amplifier. Although the required average power at the output of the error amplifier is not that high, because of the high peak to average ratio at the input of the error amplifier, IP3 of the amplifier needs to be quite high not to introduce additional distortion products. Unfortunately among other factors, this requirement makes the feedforward technique inefficient. The derived closed form expressions are believed to be a convenient and fast tool to make these trade-offs for a given output linearity.

For the lossless case where perfect matching within the loops exists, the coefficients  $D_3$ ,  $D_5$  and  $D_7$  in (4.17) tend to vanish and the expression derived for the ACP of the feedforward output (4.51) reduces to the following:

$$P_{outacp} = 6,846,120 D_9^2 K^9 \quad (4.89)$$

If we substitute the expression for  $D_9$  and (4.42) in the above expression we get:

$$P_{outacp} = 6,846,120 \frac{b_3^2 a_3^6}{C_2^6 C_3^6 C_4^2} \frac{2^9 P_m^9}{a_1^{18}} \quad (4.90)$$

By making use of (4.8), (4.11), and (4.15), (4.90) can be reduced to the following compact relationship:

$$IP_3^e + 3IP_3^m = 35.68 + \frac{9}{2} P_m - \frac{1}{2} P_{outacp} + C_4 \quad (4.91)$$

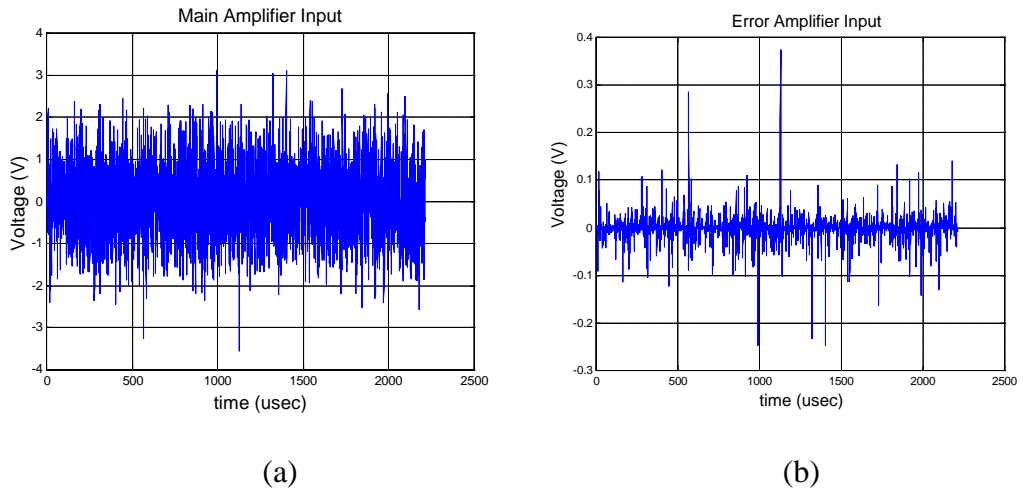


**Figure 4.7** (a) Time domain data at the input of the main amplifier for  $IP_3^m = 45.8$  dBm. (b) Time domain data at the input of the error amplifier for  $IP_3^m = 45.8$  dBm.

Hence, (4.91) relates the desired output ACP to the nonlinearities of the main and error amplifiers, the proposed output power and the coupling coefficient of  $C_4$  for a lossless feedforward circuit with perfect matching. This relationship is verified in our example ( $IP_3^e = 50$  dBm,  $IP_3^m = 46$  dBm,  $P_m = 28.5$  dBm,  $P_{outacp} = -28.1$  dBm,  $C_4 = 10$  dB). For a fixed output power, ACP and  $C_4$ , third order nonlinearities of the main and error amplifiers can be adjusted for optimum overall efficiency.

Graphical and quantitative comparisons of the closed form formulations and simulation results for  $\tau_2=270$  nsec are shown in Figure 4.8 and Table 4.3 respectively. Note that results are quite closed to each other. Comparison of Table 4.1 and Table 4.3 emphasizes the drastic effect of delay mismatch on the linearization performance of the system. The comparison of the closed form and the simulation results for different delay mismatches in both loops and for the case  $P_{out}=28.2$  dBm,  $G_m=20$  dB,  $IP_3^m=46$  dBm,  $IP_3^e=50$  dBm,  $G_e=40$  dBm,  $C_1=C_3=C_4=10$  dB,  $C_2=20$  dB are illustrated in Figure 4.9.

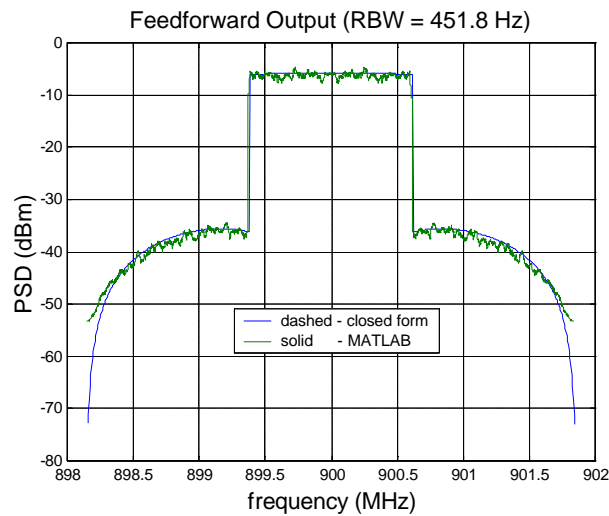


**Figure 4.8** Comparison of MATLAB simulation and closed form expressions for feedforward output ( $C_1 = 10$  dB,  $C_2 = 20$  dB,  $C_3 = 10$  dB,  $C_4 = 10$  dB,  $G_m = 20$  dB,  $IP_3^m = 46$  dBm,  $G_e = 40$  dB,  $IP_3^e = 50$  dBm,  $P_{out} = 28.5$  dBm,  $\tau_2=270$  nsec)

**Table 4.3** Quantitative comparison of the closed form and simulation results for  $\tau_2=270$  nsec ( $C_1 = 10$  dB,  $C_2 = 20$  dB,  $C_3 = 10$  dB,  $C_4 = 10$  dB,  $G_m = 20$  dB,  $IP3^m = 46$  dBm,  $G_e = 40$  dB,  $IP3^e = 50$  dBm,  $P_{out} = 28.5$  dBm).

	Closed Form	Simulation
<b>Pout (dBm)</b>	28.4	28.4
<b>Poutacp (dBm)</b>	0.1	-1.1

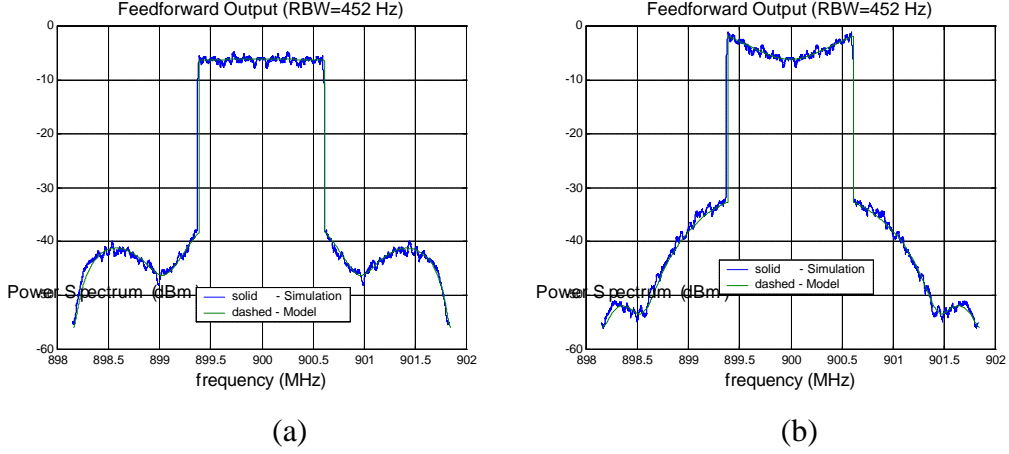


**Figure 4.9** Comparison of the closed form and simulation results a)  $\tau_1=1, \tau_2=0$   
b)  $\tau_1=1, \tau_2=1$  samples.

In our model the main and error amplifiers are based on third order nonlinearities only. Equations that have been derived and the analysis show that even third order approximations lead to tedious and complex closed form expressions for the whole system since the system involves two nonlinear amplifiers together. Table 4.4 demonstrates the effect of additional fifth order nonlinearity for the main amplifier on the output distortion products of the main amplifier and the feedforward system. Hence (4.10) expands to following form:

$$s_m(t) = l_1 a_1 s_i(t) + l_1^3 a_3 s_i^3(t) + l_1^5 a_5 s_i^5(t) \quad (4.92)$$

Note that for our example ( $G_m=10$  dB,  $IP3^m = 46$  dBm)  $a_1 = 10$  and  $a_3 = -0.25$ . For  $a_5 > -0.002$  which corresponds to the case  $IP5 < 48$  dBm simulation results begin to deviate from third order model. However Table 4.5 shows that there exists an

approximately equivalent third order model for the main amplifier that would fit the fifth order one to give similar quantities of distortion products at the output of the main amplifier and the feedforward system. Table 4.5 demonstrates the equivalent  $a_3$  values for various fifth order nonlinearities in Table 4.4. Comparison of these two tables shows that distortion products at the output are closed to each other within 1 dB.

**Table 4.4** Main amplifier and feedforward outputs for various fifth order nonlinearities –  $a_5$  values ( $C_1 = 10$  dB,  $C_2 = 20$  dB,  $C_3 = 10$  dB,  $C_4 = 10$  dB,  $G_m = 20$  dB,  $IP3^m = 46$  dBm,  $G_e = 40$  dB,  $IP3^e = 50$  dBm,  $P_{out} = 28.5$  dBm).

IP5	$a_5$	Pmain	Pmainacp	Pout	Poutacp
70	-1e-7	28.0	-4.0	28.5	-27.2
60	-1e-5	28.0	-4.0	28.5	-27.2
50	-0.001	28.0	-3.75	28.5	-26.0
48	-0.0025	28.0	-3.4	28.5	-24.4
46	-0.006	28.0	-2.5	28.5	-21.7
44	-0.016	27.97	-1.0	28.5	-17.9
42	-0.040	27.8	1.2	28.47	-13.8

**Table 4.5** Equivalent third order model  $a_3$  coefficients and  $IP3^m$  values for the fifth order nonlinearities presented in Table 4.4 ( $C_1 = 10$  dB,  $C_2 = 20$  dB,  $C_3 = 10$  dB,  $C_4 = 10$  dB,  $G_m = 20$  dB,  $G_e = 40$  dB,  $IP3^e = 50$  dBm,  $P_{out} = 28.5$  dBm).

IP3	$a_3$	Pmain	Pmainacp	Pout	Poutacp
46	-0.25	28.0	-4.0	28.5	-27.2
46	-0.25	28.0	-4.0	28.5	-27.2
45.8	-0.263	28.0	-3.65	28.5	-26.0
45.7	-0.269	28.0	-3.4	28.5	-25.4
45.2	-0.302	27.97	-2.4	28.5	-22.6
44.4	-0.363	27.86	-0.9	28.5	-18.7
43.2	-0.479	27.66	1.25	28.47	-14.1

## CHAPTER 5

### RF SIMULATIONS

In Chapter 4 characterization of a simple feedforward circuit and verification of the model with MATLAB simulations have been performed. In this chapter, the model will be verified with RF simulations performed with real power amplifier models and system components. Simulations are realized in both DSP and Analog/RF environments suggested by ADS (Agilent Technologies). Application of the model to complex Gaussian processes and a wideband feedforward linearizer will also be demonstrated. The efficiency considerations and effect of the phase mismatches will be brought into consideration.

#### 5.1 Verification of the model using co-simulation

One of the RF simulation environments suggested by ADS (Agilent Technologies) is DSP simulation environment where analog amplifier models can be used as RF subcircuits in conjunction with DSP components, which constitute the overall feedforward circuit. This type of simulation is called *co-simulation*. The advantage of using a co-simulation is to make use of the convenient DSP tools for preparing the stimulus envelope data and processing the output data in both time and frequency domain. Figure 5.1 illustrates the schematic of the feedforward system in DSP environment. The input real envelope voltage data file (cdma615mtlb.tim) represents the band-limited white Gaussian noise (BWGN) and is the same file as the

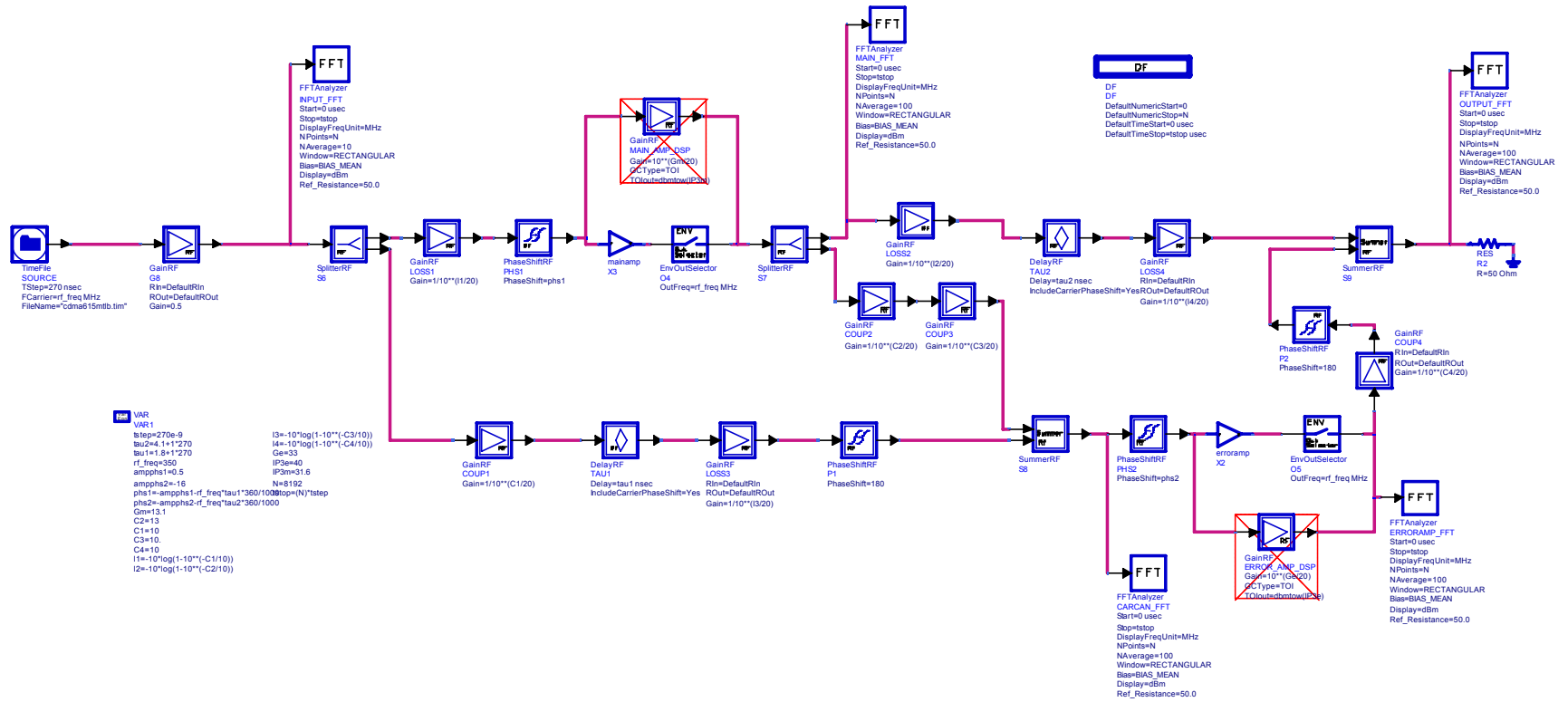


Figure 5.1 Schematic of the feedforward system in DSP co-simulation environment.

one used in MATLAB environment whose sidebands of the generated 615kHz BWGN noise data file in ADS-DSP environment, have been filtered out ideally. The sampling period and the number of samples have been chosen to be 270 nsec and 8192 respectively to monitor the power spectrum at a span of 3.7 MHz with a resolution bandwidth (RBW) of 451.8 Hz. The power of the input signal is adjusted with a gain block which is placed right after the time file so that the amplitude of the signal is scaled by the gain factor specified in the gain block. In our simulations input power ( $P_{in}$ ) is 2.17 dBm.

Losses of the couplers are directly related to the coupling coefficients of the couplers and are computed as following:

$$l_i = 10 * \log(1 - 10^{-C_i/10}) \quad (5.1)$$

The power spectrum at each node of the system is monitored using FFT analyzers whose window types are chosen to be rectangular. The monitored spectra can be smoothed by adjusting the parameter *Naverage*.

In co-simulation the system amplifiers are replaced with RF subcircuits. These subcircuits accept the discrete envelope data as input; perform the RF simulation using RF envelope simulation environment within the box and output the data suitable for DSP environment using the EnvOutSelector component placed right after the RF subcircuit. The subcircuits need to be terminated with termination load (50 Ohm). Figure 5.2 illustrates the schematic of the main amplifier subcircuit (d2001uk\_amp) which has been designed using an RF DMOS power transistor (SEMELAB D2001UK). The nonlinear simulation of the transistor is performed using its RF SPICE model which is illustrated in Figure 5.3. In order to compare the co-simulation and model results the actual main amplifier used in the simulation needs to be characterized in terms of IP3 ( $IP3^m$ ) and linear gain ( $G_m$ ).

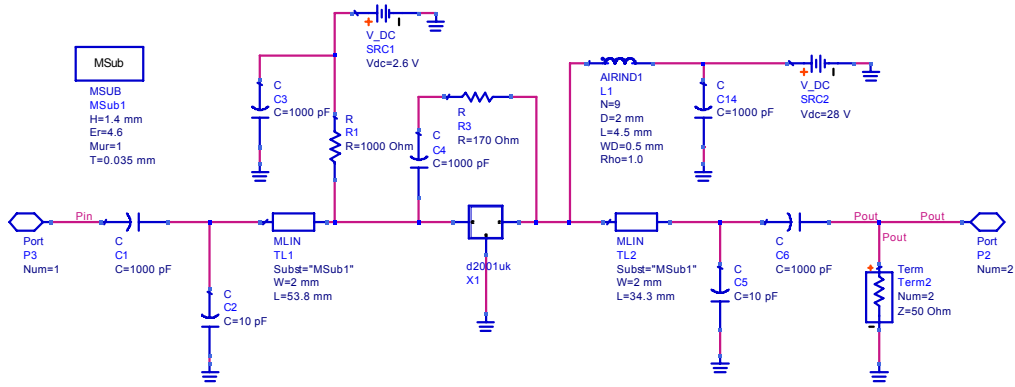


**Figure 5.2** Schematic of the main amplifier – d2001uk\_amp.

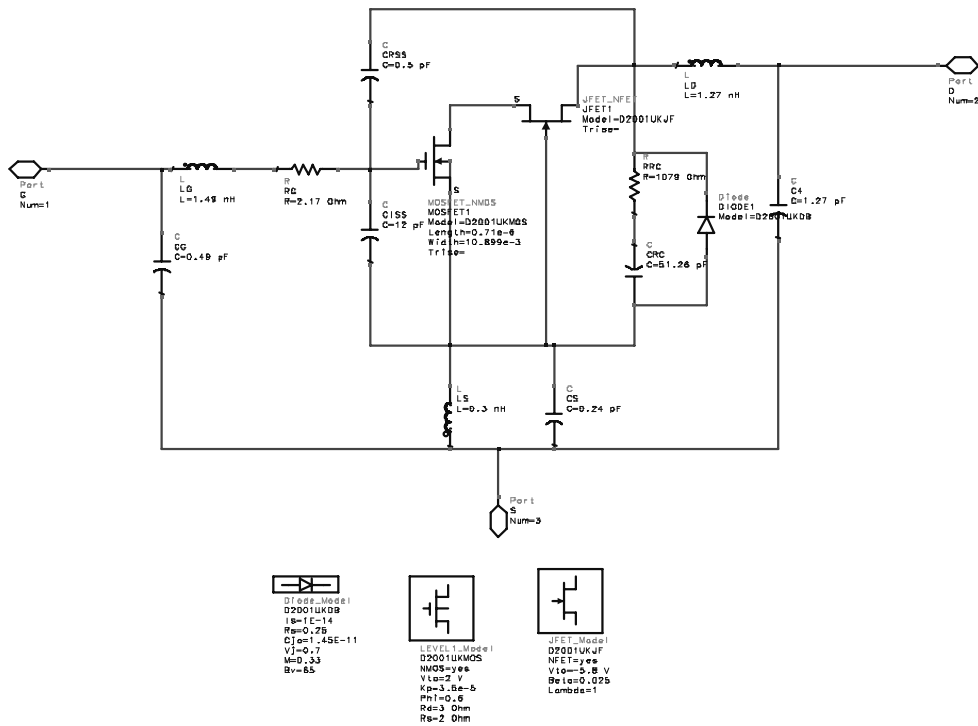


**Figure 5.3** SPICE model of D2001UK.

IP3 of the main amplifier is measured using a 2 tone (-0.8 dBm/tone) intermodulation test for different gate voltages ( $V_g$ ) with a 1 MHz frequency spacing at the specified frequency. Linear gain is measured using at a sufficiently low input power. Harmonic balance is used for both of the measurements. Table 5.1 tabulates the results for an operating frequency of 350 MHz.

**Table 5.1** Variation of gain and IP3 of the main amplifier for different gate voltages at 350MHz.

<b>Vg (V)</b>	2.4	2.6	3.0	3.2	3.4	3.6	3.8	4.0	4.2
<b>G (dB)</b>	11.8	13.1	14.1	14.4	14.7	14.8	14.9	15.0	15.0
<b>IP3(dBm)</b>	25	32	40	42.5	44.5	46.1	47.4	48.5	49.3

In our simulation  $V_g=2.6$  has been chosen as operating gate voltage. Phase introduced by the main amplifier can also be measured approximately by using a single-tone harmonic balance analysis. Figure 5.4 and Figure 5.5 illustrate the phase and gain variations with respect to input power for  $f=300$  and  $f=350$  MHz respectively. Note that as the input power increases, the amplifier is drawn to compression and the constant phase introduced by the amplifier deviates as a consequence of AM/PM conversion.

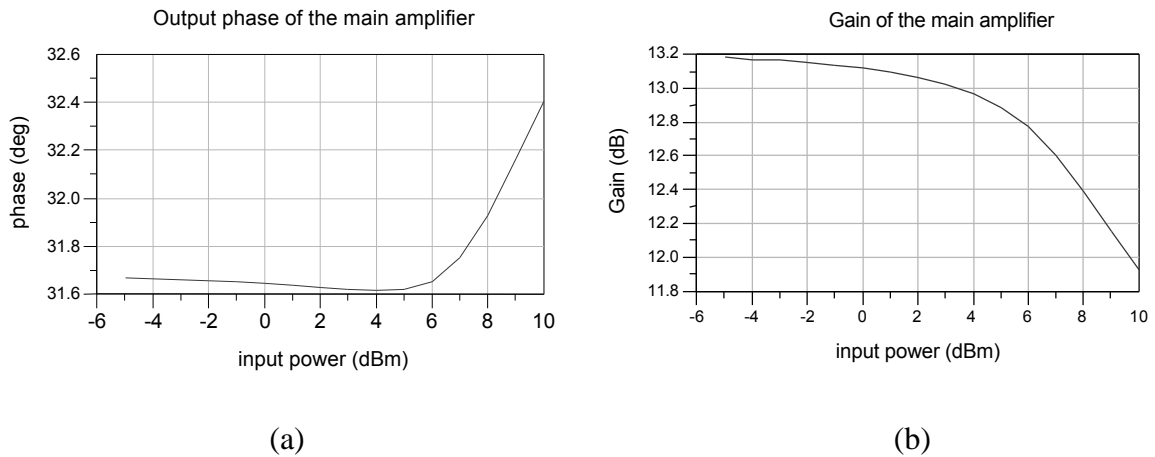
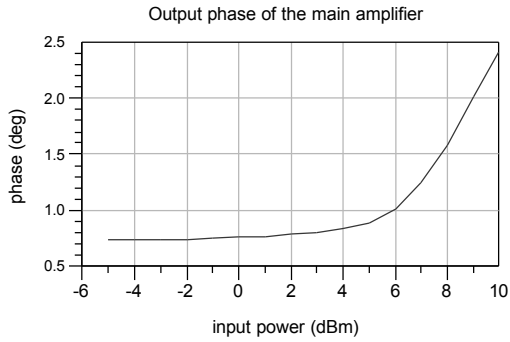
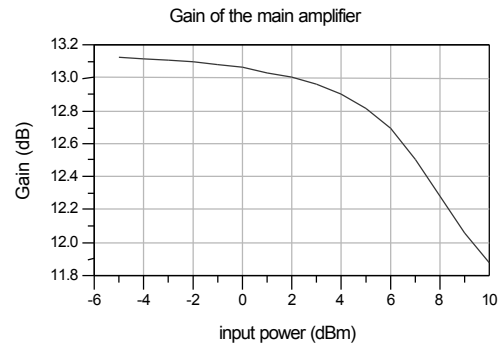


**Figure 5.4** (a) Phase variation (b) gain variation of the main amplifier at 300 MHz



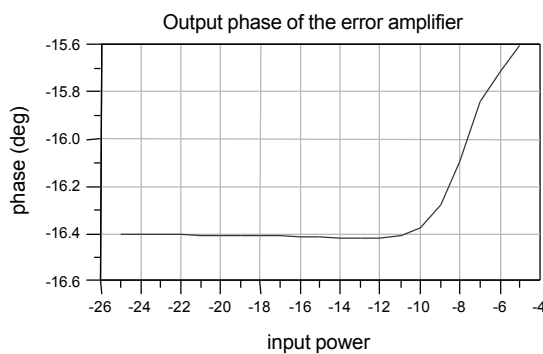
(a)



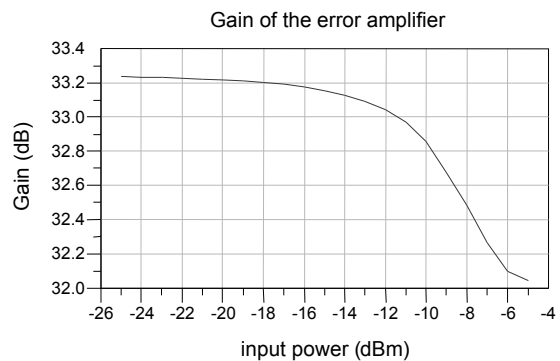
(b)

**Figure 5.5 (a) Phase variation (b) gain variation of the main amplifier at 350 MHz.**

The system error amplifier has also been replaced by an RF subcircuit whose schematic is illustrated in Figure 5.7. The amplifier has been designed using two stages of D2019UK Semelab DMOS transistors. Each stage has been biased with a gate voltage of 2.8V and optimized at 350 MHz for 50 Ohm system. The error amplifier IP<sub>3</sub> (IP<sub>3</sub><sup>e</sup>) and linear gain (G<sub>e</sub>) have been measured as 38 dBm and 33.3 dB respectively. G<sub>e</sub> has been adjusted to compensate for the attenuations caused by coupler couplings. Nominal values for coupler couplings are 10 dB for C<sub>1</sub>, C<sub>3</sub> and C<sub>4</sub> and 13 dB for C<sub>2</sub>. One of the criteria for choosing coupler couplings must be towards decreasing the required G<sub>e</sub> as much as possible. Figure 5.6 illustrates the variation of the phase and gain introduced by the error amplifier with respect to input power at f=350 MHz.



(a)



(b)

**Figure 5.6 (a) Phase variation (b) gain variation of the error amplifier at 350 MHz**

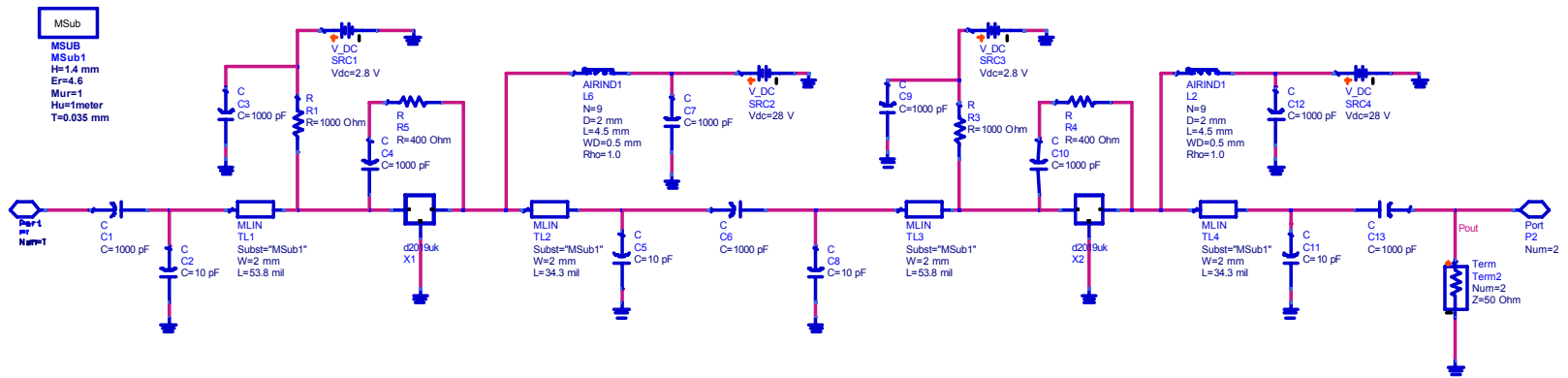
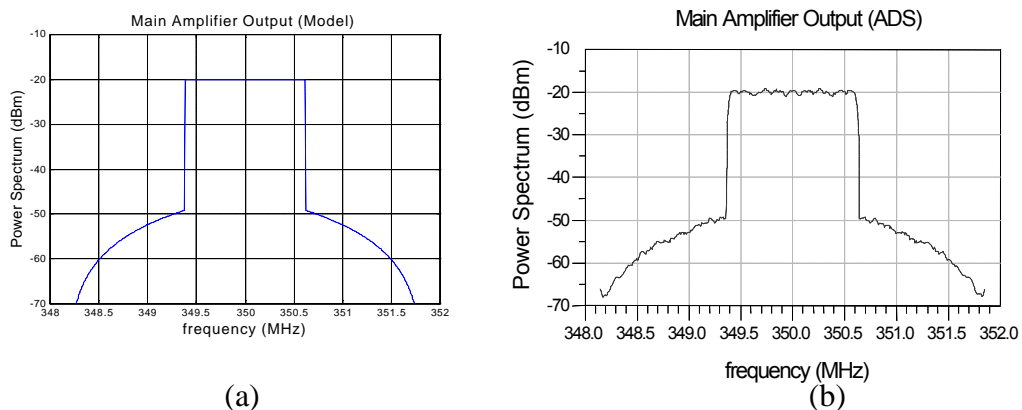


Figure 5.7 Schematic of the error amplifier.

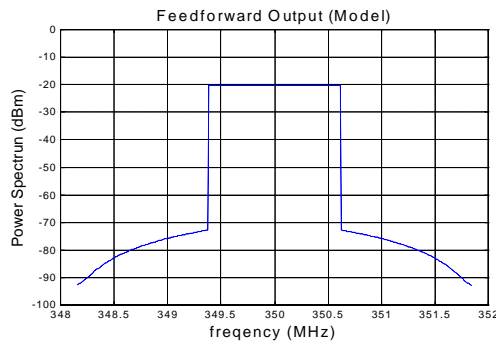
Delays of the main and error amplifiers are measured using linear S-parameter simulation test benches. Delay of the main amplifier for a frequency of 300 and 350 MHz is measured as 1.6 nsec and 1.8 nsec, respectively. On the other hand, that of error amplifier is measured as 4.1 nsec at 350MHz.

Our current model does not take phase mismatches into account. Therefore phase shifters have been replaced in front of the nonlinear amplifiers to compensate for the phase shifts introduced. Phase shifters placed for main and error amplifiers take values  $phsm$  and  $phse$ , respectively. Since co-simulation takes place in DSP environment the resolution for a delay component is the sampling period which is 270 nsec in our case. Main disadvantages of this simulation environment are the facts that the subcircuits have to be terminated with the reference impedance and the delay mismatch analysis is limited to the cases where delay is greater than or equal to the sampling period. Therefore impedance mismatches and subcircuit delays are not taken into account during the simulation.

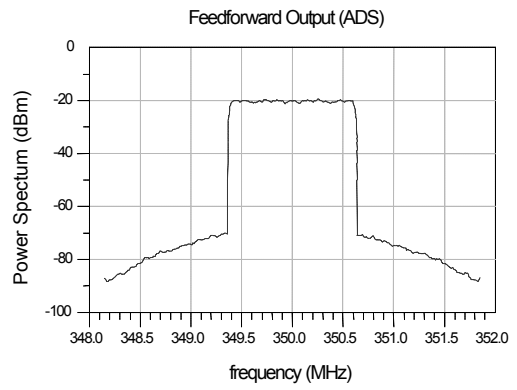
Figures 5.8-5.14 compare the co-simulation and model results for different cases. Note that  $phsm=-0.5$  and  $phse=16$  degrees during the simulations. For the cases where delay units are used, the carrier phase shifts are also compensated by adding  $-2pft$  to the quantities above. Table 5.2 tabulates the main amplifier output power ( $P_{main}$ ), main amplifier ACP ( $P_{mainacp}$ ), error amplifier input power ( $P_e$ ), feedforward output power ( $P_{out}$ ) and feedforward ACP ( $P_{outacp}$ ) for the cases illustrated in Figures. The predicted and measured main amplifier ACP ( $P_{mainacp}$ ) are -15.8 and -16.8 dBm respectively at an output power ( $P_{main}$ ) of 14.3 dBm.



**Figure 5.8** Main amplifier output power spectrum at 350 MHz for  $C_1=C_3=C_4=10$ ,  $C_2=13$ dB,  $t_1=t_2=0$  a) Model b) ADS co-simulation.

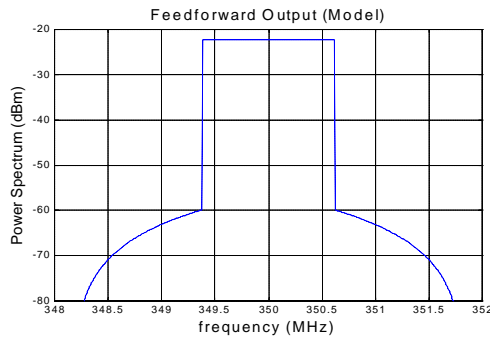


(a)

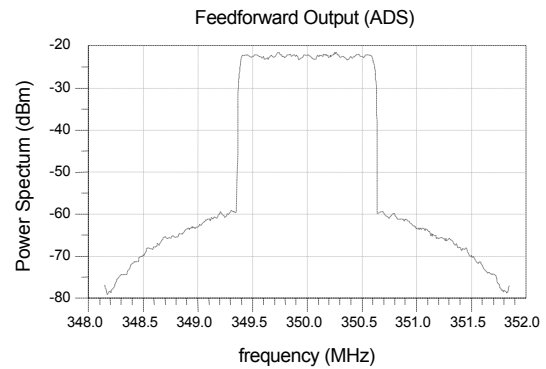


(b)

**Figure 5.9** Feedforward output power spectrum at 350 MHz for  $C_1=C_3=C_4=10$ ,  $C_2=13$  dB,  $t_1=t_2=0$  a) Model b) ADS co-simulation.

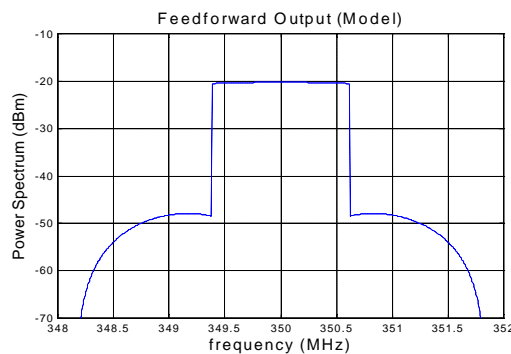


(a)

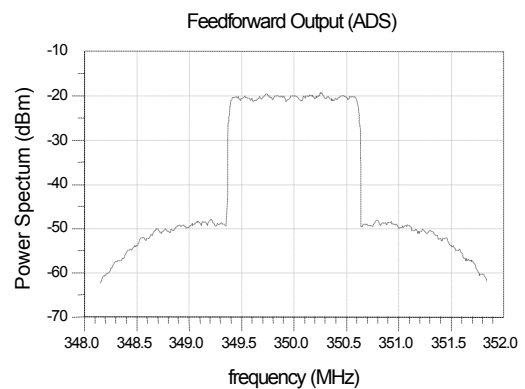


(b)

**Figure 5.10** Power spectrum at the feedforward output at 350 MHz for  $C_1=11$ dB,  $C_2=12$ dB,  $C_3=10.5$ dB,  $C_4=9$ dB,  $t_1=t_2=0$  a) Model b) ADS co-simulation

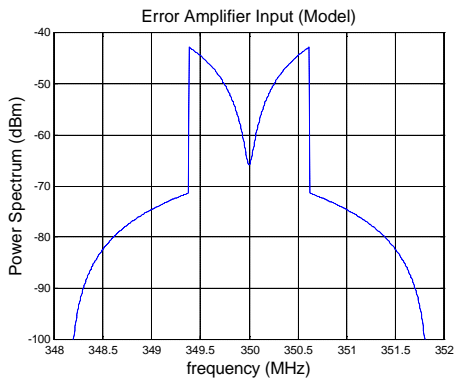


(a)

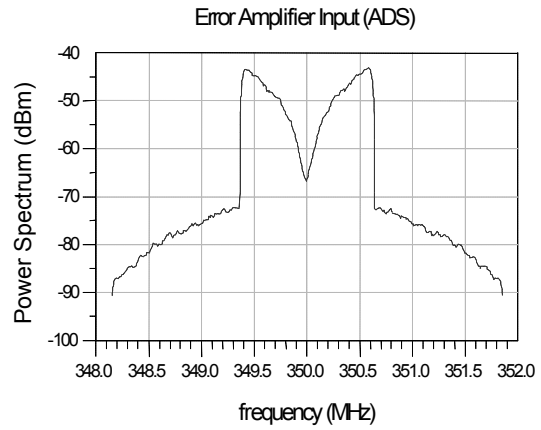


(b)

**Figure 5.11** Feedforward output power spectrum at the at 350 MHz for  $C_1=C_3=C_4=10$ ,  $C_2=13$ dB,  $t_1=0$ ,  $t_2=270$  nsec a) Model b) ADS co-simulation.

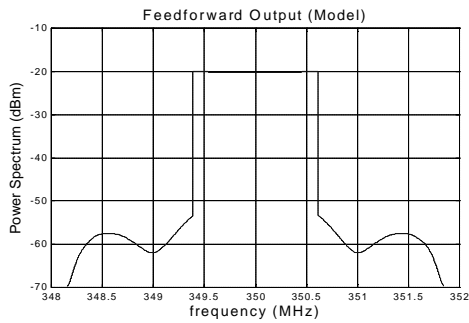


(a)

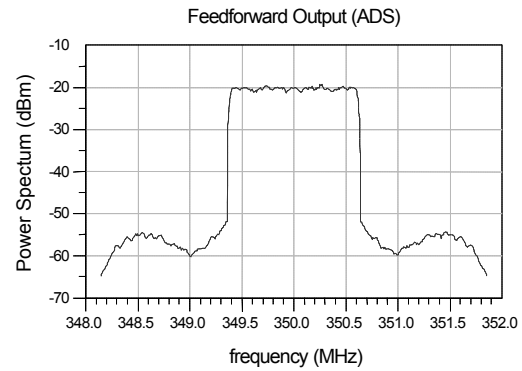


(b)

**Figure 5.12** Error amplifier input power spectrum at 350 MHz for  $C_1=C_3=C_4=10$ ,  $C_2=13\text{dB}$ ,  $t_1=270\text{ nsec}$ ,  $t_2=0\text{ nsec}$  a) Model b) ADS co-simulation.

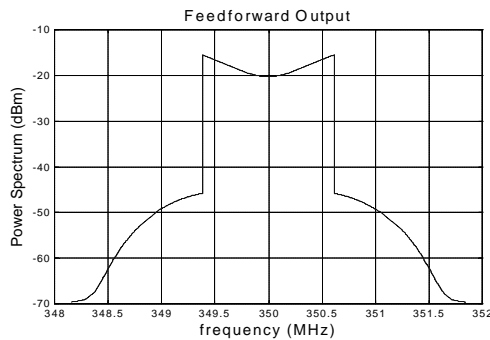


(a)

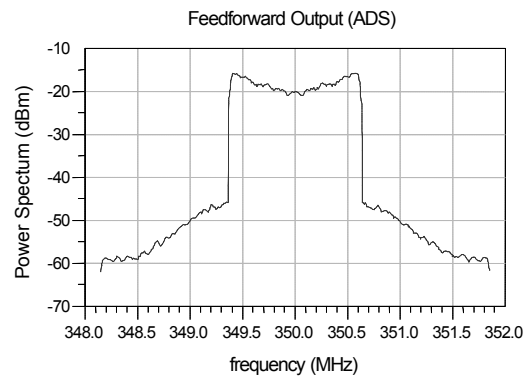


(b)

**Figure 5.13** Feedforward output power spectrum at 350 MHz for  $C_1=C_3=C_4=10$ ,  $C_2=13\text{dB}$ ,  $t_1=270\text{ nsec}$ ,  $t_2=0\text{ nsec}$  a) Model b) ADS co-simulation.



(a)



(b)

**Figure 5.14** Feedforward output power spectrum at 350 MHz for  $C_1=C_3=C_4=10$ ,  $C_2=13\text{dB}$ ,  $t_1=270\text{ nsec}$ ,  $t_2=270\text{ nsec}$  a) Model b) ADS co-simulation.

**Table 5.2** Comparison of the co-simulation and model results for different cases at 350 MHz.

<b>C<sub>1</sub></b> <b>(dB)</b>	<b>C<sub>2</sub></b> <b>(dB)</b>	<b>C<sub>3</sub></b> <b>(dB)</b>	<b>C<sub>4</sub></b> <b>(dB)</b>	<b>t<sub>1</sub></b> <b>(nsec)</b>	<b>t<sub>2</sub></b> <b>(nsec)</b>	<b>P<sub>out</sub></b> <b>ADS</b> <b>(dBm)</b>	<b>P<sub>out</sub></b> <b>Model</b> <b>(dBm)</b>	<b>P<sub>outacp</sub></b> <b>ADS</b> <b>(dBm)</b>	<b>P<sub>outacp</sub></b> <b>Model</b> <b>(dBm)</b>
10	13	10	10	0	0	14.1	14.1	-38.6	-36.0
11	12	10.5	9	0	0	12.0	12.0	-27.1	-25.5
10	13	10	10	0	270	14.0	14.0	-13.8	-13.0
10	13	10	10	270	0	14.1	14.1	-19.2	-21.4
10	13	10	10	270	270	16.3	16.3	-14.2	-13.5

During co-simulations channel power within a specified bandwidth is measured using the function *spec\_power(fft-analyzer-output, f\_start, f\_stop)*. *FFT-analyzer-output* is the data set representing the output of the FFT analyzer placed at the node whose spectrum is monitored. *F\_start* and *f\_stop* specify the frequency band where the spectral density is integrated.

In order to be able to use actual RF components such as couplers or delay lines, simulate the system for arbitrary delay mismatches (smaller portions of the sampling period) and take the impedance mismatches into account envelope simulation in Analog/RF environment needs to be used.

## 5.2 Verification of the model using Analog/RF envelope simulation

Processing the data and power spectra in envelope simulation is not as easy as in the co-simulation because of the lack of the convenient measurement tools such as FFT or spectrum analyzers. However, there exist some defined functions to monitor the power spectra and calculate the channel powers. These functions are defined in the schematic environment. Therefore the channel powers are calculated during the simulation. After the end of the simulation, one cannot change the channel limits to see the variations in the calculated power. On the other hand co-simulation provides this flexibility by defining the channel power measurement functions in the data display environment. The spectrum of the signal at a specified node is computed using the function *fs(node\_f)*. This function uses a rectangular window. For different

types of windowing functions such as Kaiser, Hanning or Hamming, the requested one must be defined in the arguments of the function.  $Node_f$  represents the voltage at the specified node at the fundamental frequency and is computed by the following relationship:  $node_f = node[1]$ . In envelope simulation environment there is no convenient tool to smooth the spectrum data. The function  $channel\_power\_vr(Node_f, 50, limits)$  calculates the power of the signal at the fundamental frequency in Watts for the frequency limits specified by the variable  $limits$  which is defined by  $limits = \{f\_start, f\_stop\}$ . While specifying  $f\_start$  and  $f\_stop$ , center frequency is ignored. For instance while computing the adjacent channel power at the upper channel  $f\_start$  and  $f\_stop$  are defined as B and 3B respectively where B is the baseband bandwidth.

In co-simulation an ASCII type of file (time versus voltage in *.tim* format) is used as the input data file. Unfortunately this data file cannot be used directly as a source file for envelope simulation. Instead, a new dataset (*.ds*) has to be created by accessing the File/Instrument server menu in the schematic, reading the *.tim* formatted file and converting it to a different format *.mdif*. The created dataset file (*cdmamatlab.ds* in our case) is used in the component palette *VtDataset* as a source file for our system. Figure 5.15 illustrates the schematic for the envelope simulation.

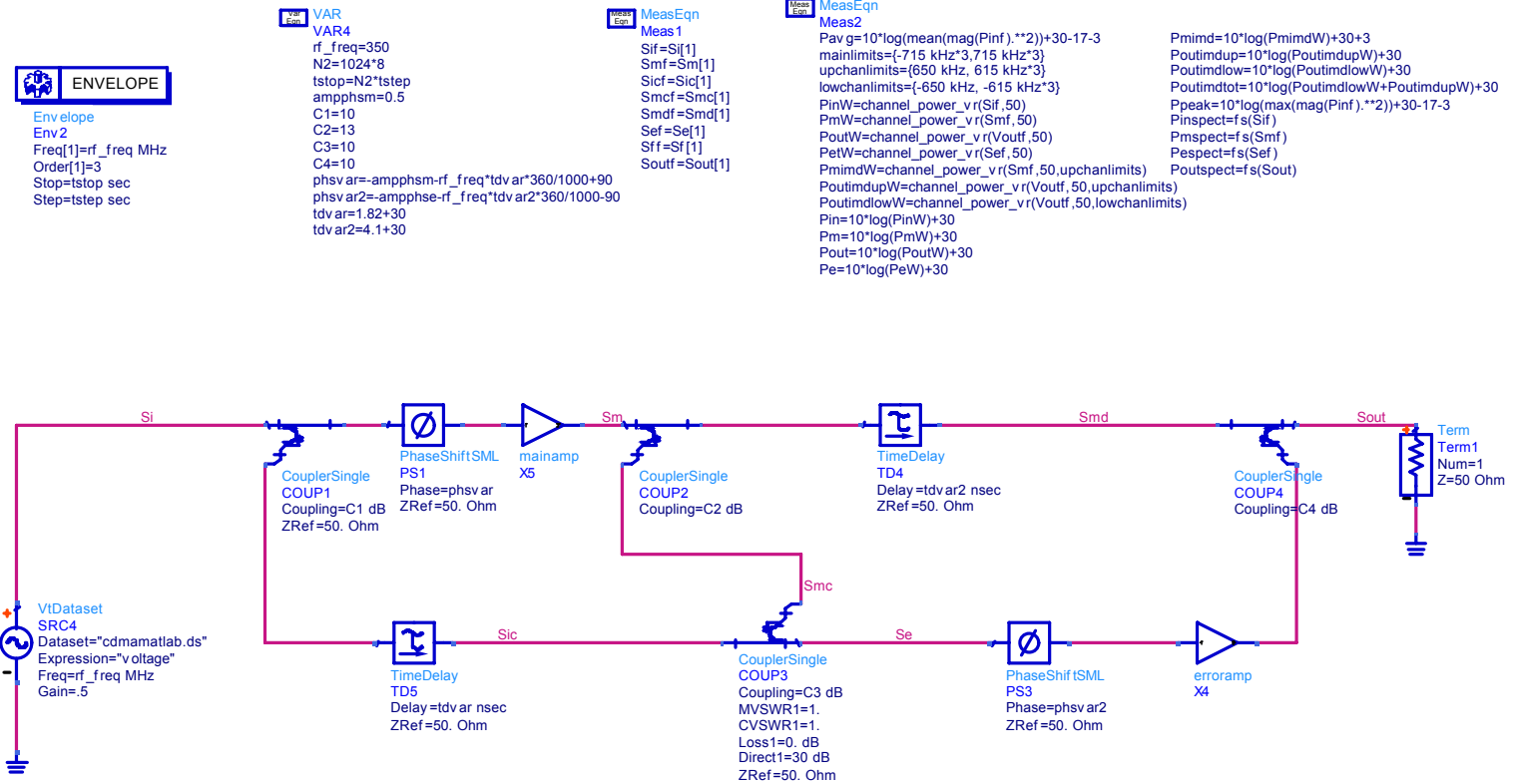


**Figure 5.15** Schematic of the feedforward system in Analog/RF envelope simulation environment.

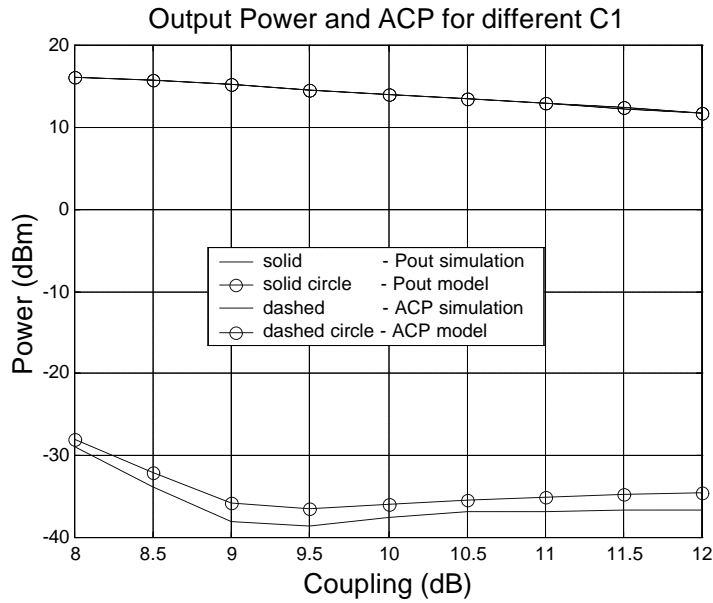
Figures 5.16-5.22 illustrate the comparisons of the model and envelope simulations for different parameter variations. Figure 5.16 compares feedforward output for different amplitude mismatches caused by varying coupling values of the first coupler. It can be observed that distortion correction decreases considerably as  $C_1$  extends from the nominal value towards smaller values, while a similar effect occurs for the output power as  $C_1$  increases.

Figure 5.17 illustrates the effect of  $C_4$ . Note that  $C_4$  has a drastic effect on the performance of the linearizer. The performance of the linearizer is very sensitive to  $C_4$ . The best performance is achieved for a  $C_4$  value 0.7 dB more than the estimated nominal value. This difference is possibly due to the coupler losses. Although model and simulation results agree with each other within 1 dB for most of the  $C_4$  values, they begin to deviate from each other within up-to 4 dB as the optimum performance is approached. However the trends coincide with each other. For the region where the cancellation performance is very high, the main and error amplifiers need to be modeled more accurately so that the model can catch the possible notches such as the case for  $C_4=10.5-11$  dB. It should be recalled that the main amplifier  $IP3$  is computed for a two tone input whose average power is same as that of the CDMA stimulus (2.2 dBm). However, for our case  $C_1$  is equal to 10 dB causing a loss of approximately 0.4 dB which means that average power at the input of the main amplifier is 0.4 dB less. This small decrement at the input power will increase the linearity of the amplifier and consequently increase the effective  $IP3$ . In our case  $IP3^m$  increases to 31.9 dBm. A similar effect occurs for the error amplifier and  $IP3^e$  increases to 38.5 dBm. These tiny increments in the  $IP3$  of the amplifiers have an essential impact on the model performance for the cases where a dramatic improvement is observed in the linearizer performance. Figure 5.17 illustrates this point. Figure 5.18 and 5.19 demonstrate the effect of the linearity of the error amplifier on the linearizer for two different cases. For the amplitude mismatch combination illustrated in Fig 5.18, as  $IP3^e$  increases the linearizer performance improves, whereas for the case illustrated in Figure 5.19 feedforward output is insensitive to  $IP3^e$ . These two figures clearly demonstrate the fact that increasing the linearity of the error amplifier might be a waste of efficiency if amplitude mismatches are not adjusted carefully. The

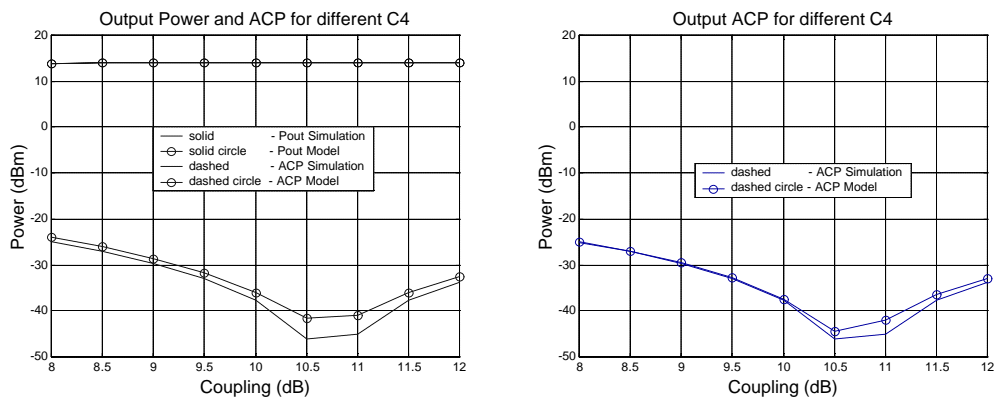
proposed model provides a fast and flexible tool to obtain parameter combinations for optimum linearity and efficiency.

Figure 5.20 and 5.21 illustrate the impact of the delay mismatch in the first loop,  $t_1$ , on the performance of the linearizer.  $IP3^e$  is taken as 34 dBm. Note that, for the proposed amplitude mismatches the average error power at the input of the error amplifier increases gradually with  $t_1$ . Although the delay mismatch in the first loop is not considered to have an impact on ACP of the error signal, as can be observed from (4.79), increment in the error power would expect to enforce the error amplifier to produce extra distortion products and deteriorate the performance of the linearizer. However it does not happen so and the ACP begins to increase after a delay mismatch of about 120 nsec. In order to be able to make a comment about this observation, the behavior of the peak error power should also be brought into consideration. For the case illustrated in Fig 5.20 peak error power, which is approximately 20 dB above the average error power, decreases up-to a  $t_1$  of 120 nsec and steps up afterwards. As much as the average power, peak power also has an important role on the distortion cancellation at the output. Although average power increases, it does not affect distortion cancellation much due to the fact that peak power, which is a limiting factor, decreases. For the case illustrated in Figure 5.21 the peak error power turns out to be much smaller than that of the first case. Hence the delay mismatch where the ACP begins to increase coincides with the mismatch some nanoseconds beyond the point where the peak error power begins to increase.

Fig 5.21 illustrates the comparison of the model and simulation results for various delay mismatches in the second loop ( $t_2$ ). It can be observed that ACP is directly related to the delay mismatch in the second loop on the contrary to first loop.



**Figure 5.16** Comparison of the model and envelope simulation results for varying  $C_1$  at 350MHz.  $C_3=C_4=10$  dB,  $C_2=13$ dB,  $t_1=0$ ,  $t_2=0$ .



**Figure 5.17** Comparison of the model and envelope simulation results for varying  $C_4$  at 350MHz.  $C_1=C_3=10$  dB,  $C_2=13$ dB,  $t_1=0$ ,  $t_2=0$  a)  $IP3^m=31.6$  dBm,  $IP3^e=38$  dBm b)  $IP3^m=31.9$  dBm,  $IP3^e=38.5$  dBm.

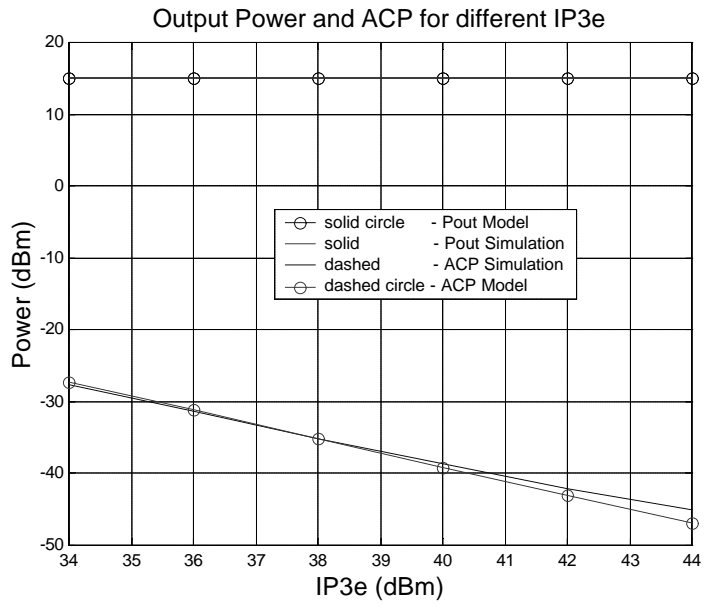


**Figure 5.18** Comparison of the model and envelope simulation results for varying  $IP3^e$  at 350MHz.  $C_1=C_4=10$  dB,  $C_3=11$  dB,  $C_2=13$ dB,  $t_1=0$ ,  $t_2=0$ .

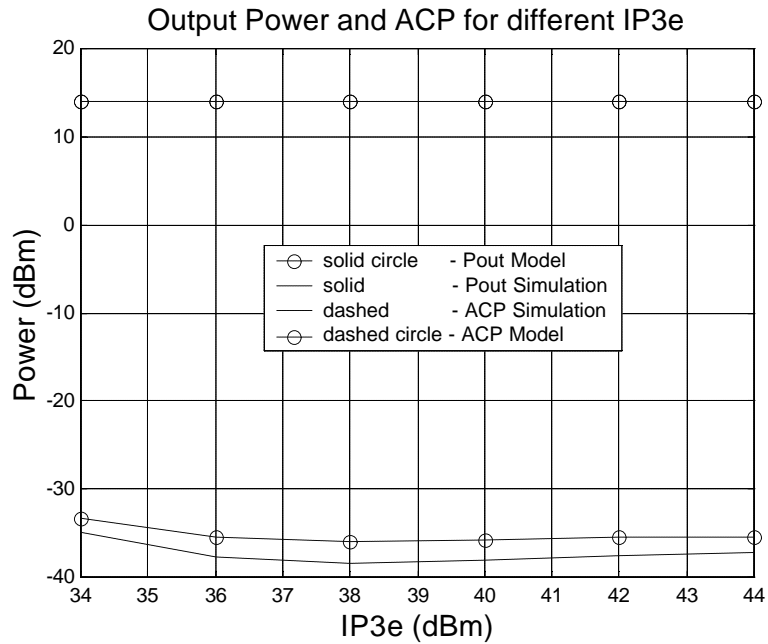


**Figure 5.19** Comparison of the model and envelope simulation results for varying  $IP3^e$  at 350MHz.  $C_1=C_4=C_3=10$  dB,  $C_2=13$ dB,  $t_1=0$ ,  $t_2=0$ .

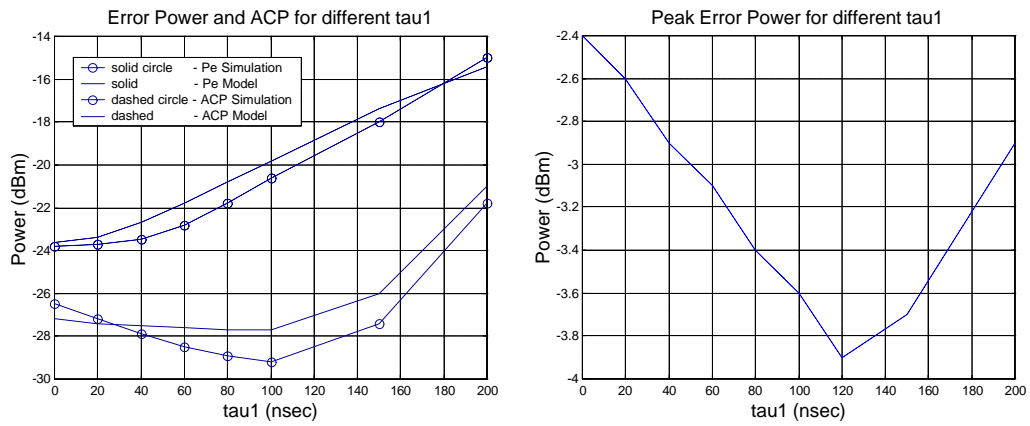


**Figure 5.20** Comparison of the model and envelope simulation results for varying  $t_1$  at 350MHz.  $C_1 = C_4 = 10$  dB,  $C_3 = 11$  dB, 9 dB,  $C_2 = 13$  dB,  $IP3^e = 34$  dBm,  $t_2 = 0$ .

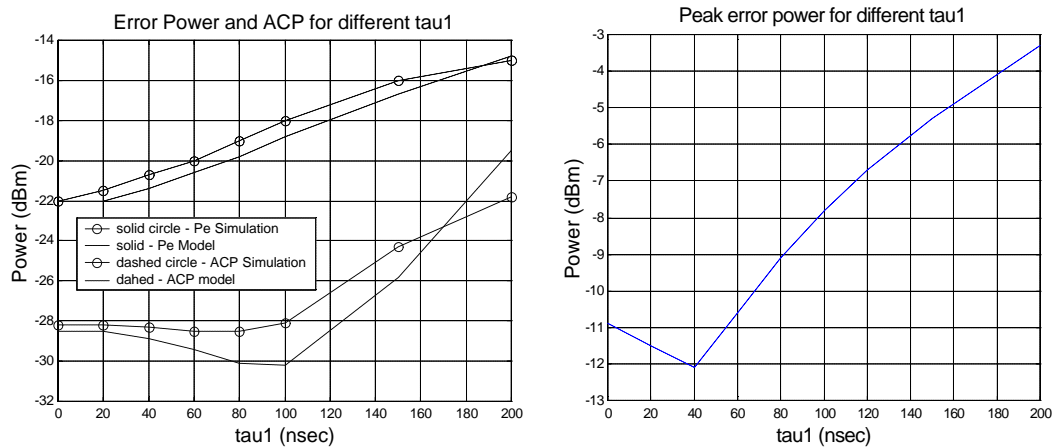


**Figure 5.21** Comparison of the model and envelope simulation results for varying  $t_1$  at 350MHz.  $C_1 = 11$  dB,  $C_3 = 9$  dB,  $C_4 = 10$  dB,  $C_2 = 13$  dB,  $IP3^e = 34$  dBm,  $t_2 = 0$ .

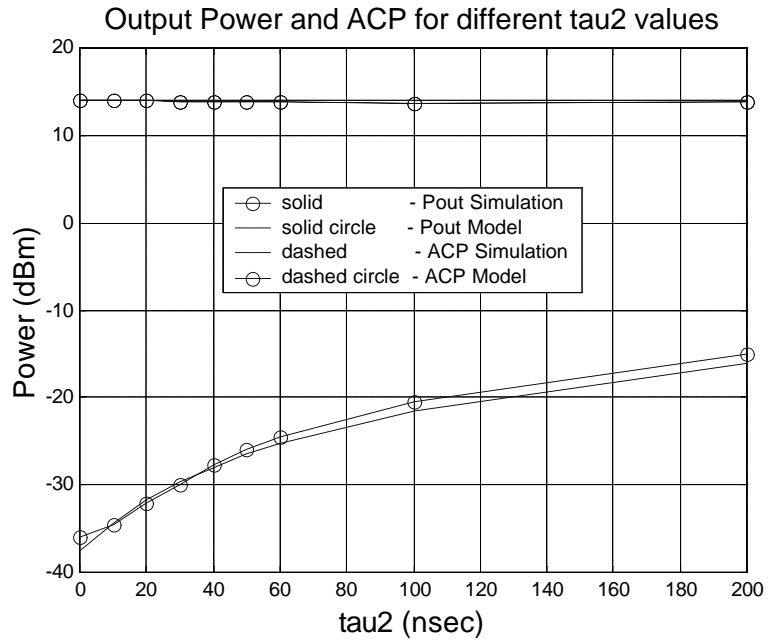


**Figure 5.22** Comparison of the model and envelope simulation results for varying  $t_2$  at 350MHz.  $C_1=C_4=C_3=10$  dB,  $C_2=13$ dB,  $t_1=0$ .

### 5.3 Phase mismatch considerations

Our current model does not account for phase mismatches within the loops. Tables 5.3-5.6 illustrate the deviations in the error power and output ACP for various phase mismatches. Results demonstrate the fact that a phase mismatch of 5 and 10 degrees within the first loop deviates the output ACP within 1 and 3 dB respectively. Phase mismatch in the second loop on the other hand is a little bit more effective. 10 degrees of phase mismatch causes a 4 dB increment in the output ACP.

**Table 5.3** Effect of the phase mismatch in the first loop at 350MHz -  $IP3^e=38$  dBm,  $IP3^m=31.6$  dBm,  $C_1=C_3=C_4=10$  dB,  $C_2=13$  dB.

phase (deg)	$P_{out}$ ADS (dBm)	$P_{outacp}$ ADS (dBm)	$P_e$ ADS (dBm)
0	14.09	-36.5	-30.5
5	14.09	-36.1	-27.1
10	14.1	-34.8	-22.8
15	14.1	-32.6	-19.8

**Table 5.4** Effect of the phase mismatch in the first loop at 350MHz -  $IP3^e=38$  dBm,  $IP3^m=31.6$  dBm,  $C_1=C_4=10$  dB,  $C_3=11$  dB,  $C_2=13$  dB.

phase (deg)	$P_{out}$ ADS (dBm)	$P_{outcap}$ ADS (dBm)	$P_e$ ADS (dBm)
0	15.1	-34.2	-23.4
5	15.1	-33.3	-22.5
10	15.1	-31.3	-20.7
15	15.09	-28.9	-18.8

**Table 5.5** Effect of the phase mismatch in the first loop at 350MHz -  $IP3^e=34$  dBm,  $IP3^m=31.6$  dBm,  $C_1=C_4=10$  dB,  $C_3=11$  dB,  $C_2=13$  dB,  $t_1=100$  nsec.

phase (deg)	$P_{out}$ ADS (dBm)	$P_{outcap}$ ADS (dBm)	$P_e$ ADS (dBm)
0	14.7	-29.2	-20.7
5	14.7	-28.5	-20.2
10	14.7	-26.7	-19.1
15	14.7	-24.7	-17.7

**Table 5.6** Effect of the phase mismatch in the second loop at 350 MHz -  $IP3^e=38$  dBm,  $IP3^m=31.6$  dBm,  $C_1=C_4=10$  dB,  $C_3=11$  dB,  $C_2=13$  dB.

phase (deg)	$P_{out}$ ADS (dBm)	$P_{outcap}$ ADS (dBm)	$P_e$ ADS (dBm)
0	15.1	-34.2	-23.4
5	15.1	-32.8	-23.4
10	15.1	-30.2	-23.4
15	15.08	-27.7	-23.4

## 5.4 Efficiency considerations

Average DC currents drawn from the supply by the whole linearizer and the main amplifier alone are compared for the same output power and output ACP. For the case  $C_1=C_3=C_4=10$  dB,  $C_2=13$  dB,  $G_e=33.3$  dB,  $IP3^e=38$  dBm,  $IP3^m=31.6$  dBm and  $G_m=13.1$  dB,  $P_{out}$  and  $P_{outacp}$  are equal to 14.1 dBm and -38.5 dBm respectively. For the linearizer parameters stated above, the main and error amplifiers draw 86 and 240 mA, respectively. Consequently the linearizer draws a total current of 326 mA At 350 MHz. The same  $P_{out}$  and  $P_{outacp}$  can be achieved using a single main amplifier with a gate voltage of 3.2V resulting with  $IP3^m$  and  $G_m$  of 42.5 dBm and 14.3 dB respectively. Note that  $G_m$  and  $IP3^m$  increase with the gate voltage. In order to achieve -38 dBm of  $P_{outacp}$  at  $P_{out}=14.1$  dBm an extra loss of 2.2 dB is introduced to the input signal and an average DC current of 220 mA is drawn from the supply of the main amplifier. Note that the current drawn from the linearizer is higher than that of the main amplifier alone. From Figure 5.19 it can be deduced that for the  $P_{out}$  and  $P_{outacp}$  goals stated above,  $IP3^e$  can be decreased to 34-35 dBm maintaining the same  $G_e$ . This decrement in  $IP3^e$  results with a current of 159 mA drawn from the supply of error amplifier. To accomplish this task, gate voltage of each stage and feedback resistor of each stage are switched to 2.6V and 500 Ohm respectively. Hence the total current has been decreased to 245 mA which is very closed to that of the single main amplifier case. This case emphasizes the fact that efficiency of the linearizer can be increased by careful adjustment of the parameters.

From Figure 5.17 it can be observed that changing  $C_4$  from 10 dB to 10.5 dB results with  $P_{out}$  and  $P_{outacp}$  of 14.1 and -46 dBm respectively. Since  $IP3^e$  is 38 dBm the total current drawn from the supply is 326 mA again. In order to achieve similar goals, a single main amplifier needs to be biased with 4V resulting with an  $IP3^m$  of 48.5 dBm,  $G_m$  of 14.8 dB and current of 436 mA drawn from the supply. This case illustrates the impact of amplitude matching on the overall efficiency.

## 5.5 Verification of the model using complex Gaussian CDMA noise

In previous sections the verification of the model using a real time BWGN has been presented. In this section the verification will be performed using another type of noise data, which is a complex Gaussian CDMA data. The stimulus signal has been generated using the component palette proposed by the ADS-DSP environment. The generated signal has a 9.5 dB peak-to-average ratio, which is lower than that of real time BWGN, 12 dB. The simulations are performed using the co-simulation tool where the main and error amplifiers are replaced with their Analog/RF counterparts. Figure 5.23 illustrates the spectra of the input signal and main amplifier output. The input average power is 2.2 dBm. The total distortion power at the adjacent channels decreases to -20.5 dBm from -16.8 dBm because of the fact that crest factor has decreased. Figure 5.24 to 5.29 illustrate the spectra of feedforward outputs for different cases. The comparison of the results with the model is summarized in Table 5.7. Although there is a discrepancy between the results, the deviation can be compensated by increasing  $IP3^m$  by an amount in dB, which is equal to crest factor difference between complex and white Gaussian noise (2.5 dB in this case).

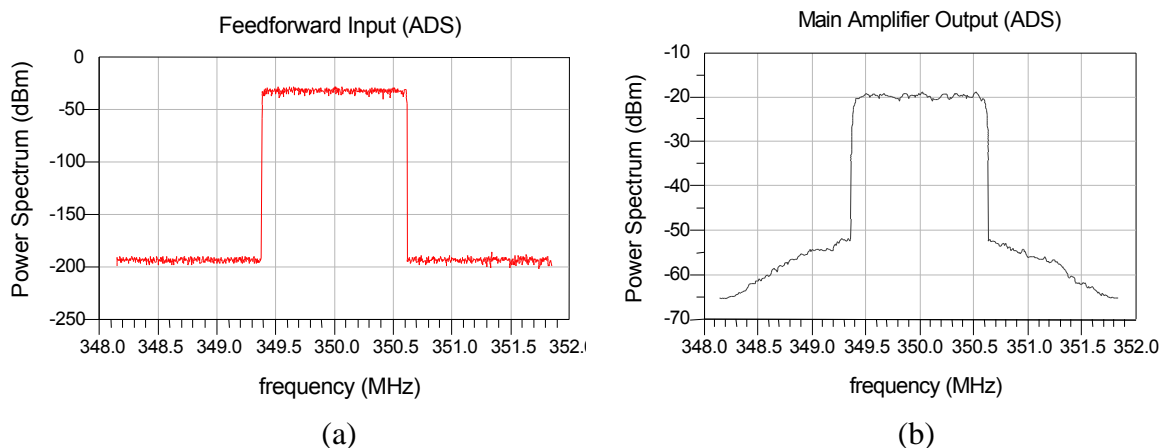


**Figure 5.23** Power spectrum **a)** at the feedforward input **b)** main amplifier output.

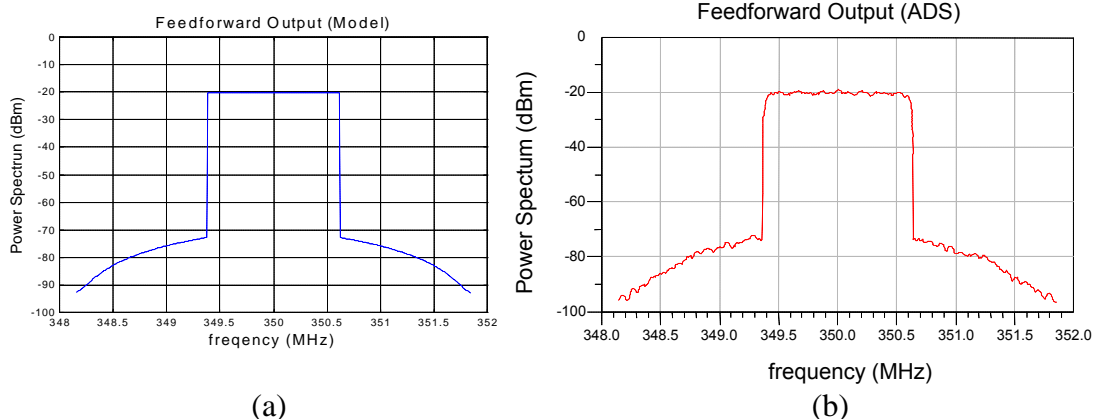


**Figure 5.24** Power spectrum at the feedforward output at 350 MHz for  $C_1=C_3=C_4=10$ ,  $C_2=13\text{dB}$ ,  $t_1=t_2=0$  **a)** Model **b)** ADS co-simulation.

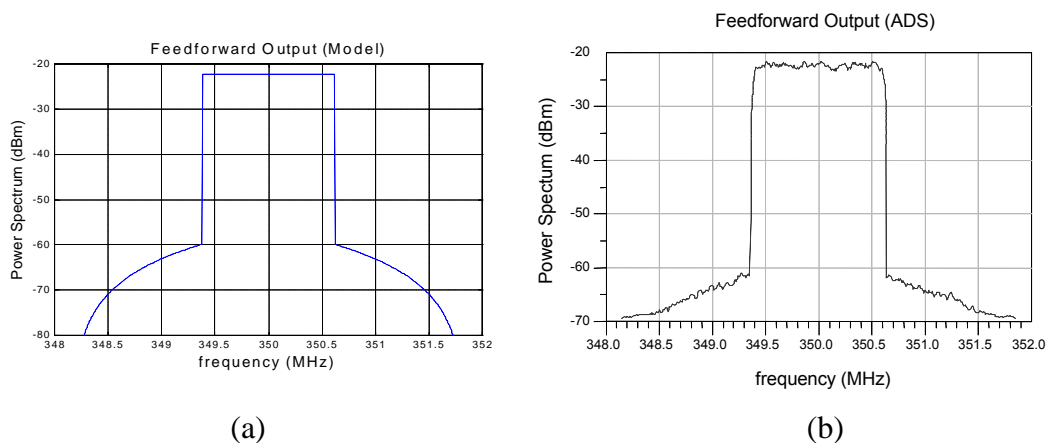


**Figure 5.25** Power spectrum at the feedforward output at 350 MHz for  $C_1=11\text{dB}$ ,  $C_2=12\text{dB}$ ,  $C_3=10.5\text{dB}$ ,  $C_4=9\text{dB}$ ,  $t_1=t_2=0$  **a)** Model **b)** ADS co-simulation.

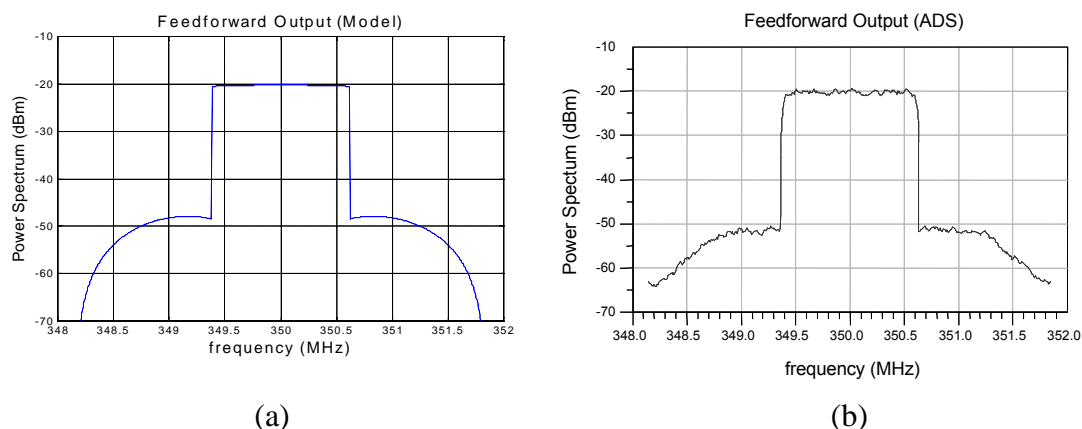
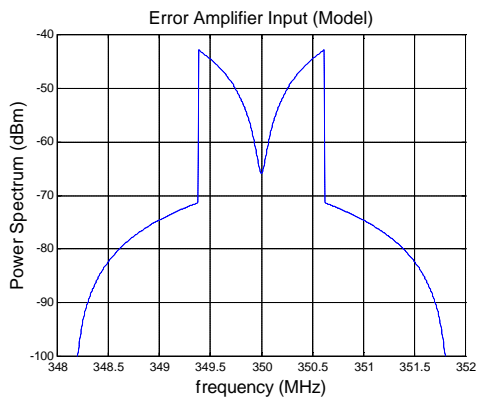
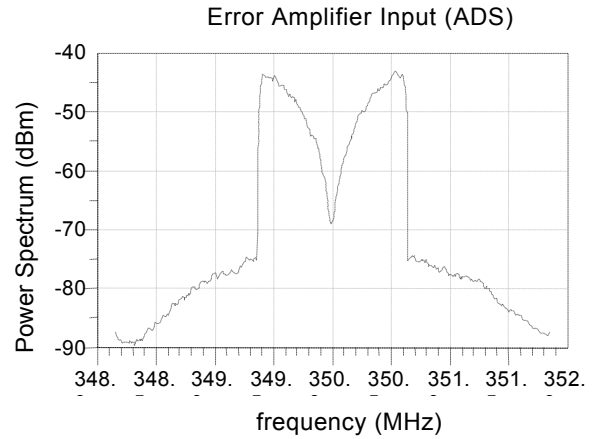


**Figure 5.26** Power spectrum at the feedforward output at 350 MHz for  $C_1=C_3=C_4=10$ ,  $C_2=13\text{dB}$ ,  $t_1=0$ ,  $t_2=270$  nsec **a)** Model **b)** ADS co-simulation.

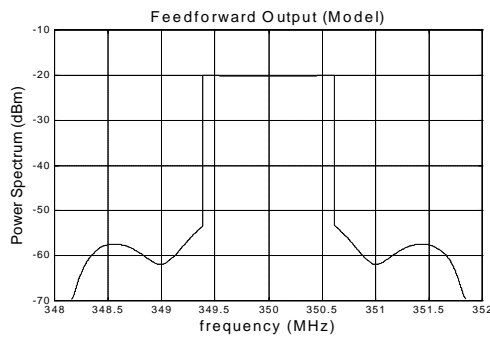


(a)

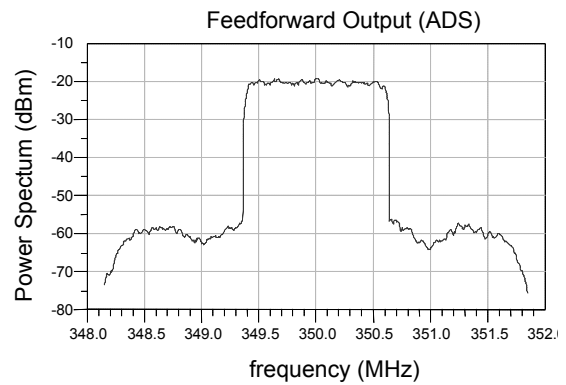


(b)

**Figure 5.27** Power spectrum at the error amplifier input at 350 MHz for  $C_1=C_3=C_4=10$ ,  $C_2=13\text{dB}$ ,  $t_1=270$  nsec,  $t_2=0$  nsec a) Model b) ADS co-simulation

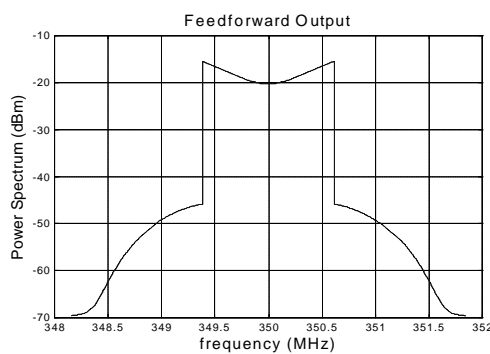


(a)

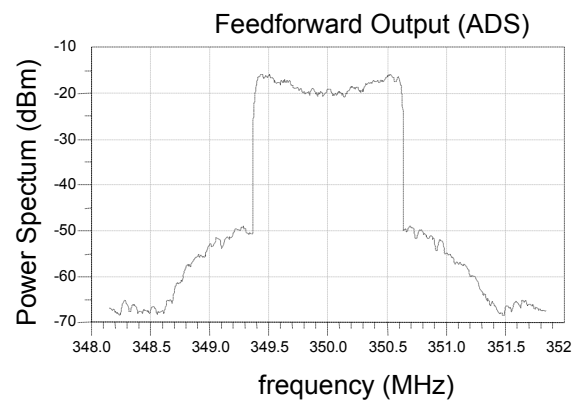


(b)

**Figure 5.28** Power spectrum at the feedforward output at 350 MHz for  $C_1=C_3=C_4=10$ ,  $C_2=13\text{dB}$ ,  $t_1=270$  nsec,  $t_2=0$  nsec a) Model b) ADS co-simulation



(a)



(b)

**Figure 5.29** Power spectrum at the feedforward output at 350 MHz for  $C_1=C_3=C_4=10$ ,  $C_2=13\text{dB}$ ,  $t_1=270$  nsec,  $t_2=270$  nsec a) Model b) ADS co-simulation.

**Table 5.7** Comparison of the co-simulation and model results for different cases at 350MHz.

C <sub>1</sub> (dB)	C <sub>2</sub> (dB)	C <sub>3</sub> (dB)	C <sub>4</sub> (dB)	t <sub>1</sub> (nsec)	t <sub>2</sub> (nsec)	P <sub>out</sub> ADS (dBm)	P <sub>out</sub> Model (dBm)	P <sub>outacp</sub> ADS (dBm)	P <sub>outacp</sub> Model IP3 <sup>m</sup> =31.6 (dBm)	P <sub>outacp</sub> Model IP3 <sup>m</sup> =34 (dBm)
10	13	10	10	0	0	14.1	14.1	-41.8	-36.0	-40.4
11	12	10.5	9	0	0	12.0	12.0	-30.5	-25.5	-30.2
10	13	10	10	0	270	14.0	14.0	-17.7	-13.0	-18.0
10	13	10	10	270	0	14.1	14.1	-23.0	-21.4	-21.3
10	13	10	10	270	270	16.3	16.3	-18.2	-13.5	-18.3

## 5.6 Application of the model to a CDMA wideband system design

In this section application of the developed analytical model to a wideband feedforward linearizer design for CDMA applications will be presented, and speed and accuracy aspects of the results are compared with RF simulations. Hence a fast, accurate and handy tool is aimed for the designer to make the initial parameter optimizations. To utilize the closed form formulations it is assumed that there is no phase mismatch within the loops and no delay mismatch within the first loop. Simulations over a frequency band 200-400 MHz are performed based on actual amplifier models, lumped components, couplers and delay units in RF Envelope Simulation environment. The input signal is the same as the one used in previous sections.

Nominal initial parameter values of the feedforward linearizer have been set for the midband frequency (300 MHz) where no delay or amplitude mismatch is assumed. For the lossless case (4.91) (recalled in (5.2)) can be used to determine rough values for the coupling coefficient of the output coupler (C<sub>4</sub>) and error amplifier IP3 (IP3<sup>e</sup>) for a given main amplifier IP3 (IP3<sup>m</sup>), linear main amplifier output power (P<sub>m</sub>) and output distortion power at the adjacent channel (P<sub>outacp</sub>):

$$IP_3^e + 3IP_3^m = 35.68 + \frac{9}{2}P_m - \frac{1}{2}P_{outacp} + C_4 \quad (5.2)$$

At 300 MHz  $IP3^m$ ,  $P_m$  and desired  $P_{outacp}$  are given as 32 dBm, 15.4 dBm and -38 dBm, respectively. Selecting a large  $C_4$  would increase error amplifier output power demands, whereas decreasing it too much would diminish the isolation within the second loop and increase the loss introduced in the main path. An optimum choice of 10 dB for  $C_4$  will consequently result with 38 dBm for  $IP3^e$  using (5.2). A nominal value of 13 dB is preferred for  $C_2$  since the main amplifier gain is around 13 dB. The choice for nominal values for  $C_1$  and  $C_3$  should be towards decreasing main path loss and the required error amplifier gain as much as possible. For our case 15 dB is set for  $C_1$  and  $C_3$ . The initial variations of  $G_m$ ,  $IP3^m$ ,  $G_e$ ,  $IP3^e$ , the coupling coefficients ( $C_1$ ,  $C_2$ ,  $C_3$  and  $C_4$ ), delay of the main amplifier ( $\tau_1$ ), delay mismatch in the second loop ( $\tau_2$ ), phase introduced by the main amplifier (phs), main amplifier output power ( $P_{main}$ ) and main amplifier adjacent channel power ( $P_{macp}$ ) for the stimulus signal over the frequency band are given in Table 5.8.

**Table 5.8** Initial parameter variations in the feedforward circuit.

Parameter	Min	Max	Parameter	Min	Max
$G_m$ (dB)	12.6	13.2	$C_2$ (dB)	11.5	14.5
$IP3^m$ (dBm)	31.5	34	$C_4$ (dB)	8.5	11.5
$G_e$ (dB)	37	39	$\tau_1$ (nsec)	1.6	2
$IP3^e$ (dBm)	35	40	$\tau_2$ (nsec)	-40	40
Phs (deg)	-30	90	$P_{main}$ (dBm)	14.2	14.9
$C_1, C_3$ (dB)	13.5	16.5	$P_{macp}$ (dBm)	-18	-16

Coupling coefficients,  $G_e$  and  $IP3^e$  are allowed to vary linearly in dB scale from the maximum value, which occurs at the beginning of the band to the minimum value, which occurs at the end. A similar variation is also allowed for  $\tau_2$ . Figure 5.30 illustrates ADS simulations for main amplifier and feedforward outputs for nominal parameter values at 300 MHz. Phase shifters have been injected in front of the main

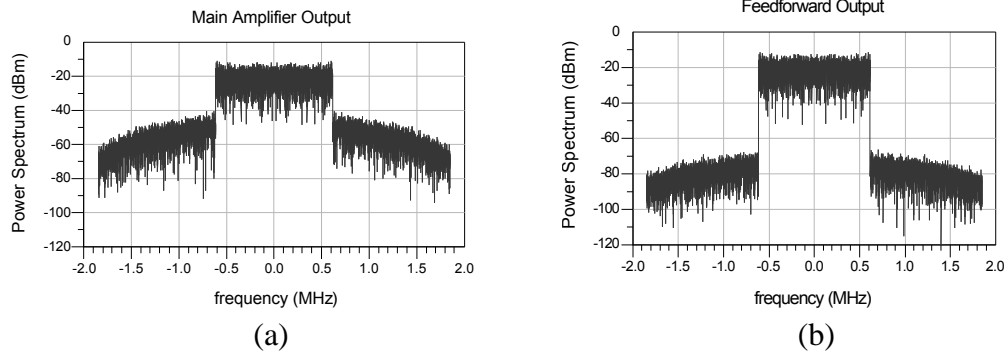


**Figure 5.30** a) Main amplifier output b) Feedforward output (ADS simulation for nominal parameter values around 300 MHz).

and error amplifiers to compensate for the phase mismatches due to the phase introduced by the main amplifier and phase due to the delay in the carrier frequency. To get an idea about the impact of the parameter variations listed in Table 5.8 on the feedforward linearizer, Figure 5.31 illustrates the comparison of the model and simulation results over a frequency band of 200-400 MHz. Note that the results are close to each other within 3 dB. Each simulation for a set of parameters takes about 3 minutes, i.e.; for 200-400 MHz bandwidth 11 simulations are required totaling in about 30 minutes of simulation time, whereas the model gives similar results instantly providing a powerful tool for the designer to observe the effect of any parameter change, determine the ultimate parameter tolerances and make the optimizations rapidly, particularly at the beginning of the design. As it is observed from Figure 5.31 the best distortion cancellation has been achieved at the mid-band, whereas there is a dramatic decrease in output power and distortion cancellation towards the end of the band.

A quick and handy methodology based on the analytical model given in Chapter 4 can be applied to rearrange the parameter tolerances for an efficient solution meeting design goals. Using the closed form equations (4.50) – (4.57) a number of parameters can be varied within the specified limits simultaneously and suitable combinations can be determined quickly. Let initial design goals for  $P_{out}$  be  $14.5 \pm 0.5$  dBm and for  $P_{outacp}$  be smaller than -33 dBm. The most important criteria that should be kept in mind for an efficient feedforward linearizer design are to allow the maximum delay mismatch in the second loop and minimum  $IP3^{\circ}$  that would meet

the design goals. Introducing a delay mismatch will result with a shorter and less lossy delay line, which would make the design less bulky and more efficient. Minimizing  $IP3^e$  will also increase efficiency since less DC current will be drawn from the power supply.

Since the initial performance of the linearizer is poor at the end of the band, we let the optimization begin from 400 MHz. The design goal for  $P_{outacp}$  has been extended to -35 dBm to have some margin in the design. In the first place let  $\tau_2$  be 40 nsec just like in the initial design and allow the coupler couplings,  $IP3^e$  (30 to 45 dBm) and  $G_e$  (33 to 39 dB) vary within a wide range to see whether any suitable solution is available meeting the design goals. While checking the availability of the solutions, it has to be tested that the proposed  $IP3^e$  is greater than or equal to the critical value computed from each swept set of parameters. In our case no solution was available for  $\tau_2=40$  nsec. Then we let  $\tau_2$  decrease until a solution is achieved. For  $\tau_2=25$  and 20 nsec some solutions exist for  $IP3^e$  beginning from 37 and 33 dBm respectively.

Since the other criterion is to decrease  $IP3^e$  as much as possible, a delay mismatch of 20 nsec and an  $IP3^e$  of 34 dBm are preferred. Now we have a set of solutions, which constitute different combinations of coupler couplings and  $G_e$ . We choose the one that has the limits closest to the initial design. One of the alternatives is the combination  $C_1=14$  dB,  $C_2=13.5$  dB,  $C_3=13.5$  dB,  $C_4=8.5$  dB,  $G_e=35$  dB. Assuming the same delay mismatch and  $IP3^e$  all over the band as a worst case, a similar set needs to be determined for the beginning of the band (200 MHz). By sweeping the parameters within the specified ranges, lots of combinations can be found. Among these alternatives, the solution, which would permit the largest tolerance for each parameter has to be selected. One of the alternatives is the set  $C_1=16.5$  dB,  $C_2=14$  dB,  $C_3=15.5$  dB,  $C_4=11$  dB,  $G_e=39$  dB. Assuming a linear variation in dB scale for these parameters over the band,  $P_{outacp}$  and  $P_{out}$  vary in the interval [-35,-31.5] and [14.1,14.5] respectively according to the model results. Note that limits for  $C_2$  are very tight. Extending its limits 0.5 dB more ([14.5,13.5]) would change the limits of the  $C_4$  and  $G_e$  to [10.5,8.5] and [39,36], respectively. These limits can be figured out by fast trial and errors using closed form expressions. Table 5.9 summarizes the parameter limits and Figure 5.32 illustrates the comparison of the

model and ADS results for the new parameter tolerances. Note that, increasing  $IP3^e$  or decreasing  $\tau_2$  can improve the overall ACP performance.

**Table 5.9** Optimized parameter variations in the feedforward circuit.

Parameter	Min	Max	Parameter	Min	Max
$G_e$ (dB)	36	39	$C_3$ (dB)	13.5	15.5
$IP3^e$ (dBm)	34	-	$C_4$ (dB)	8.5	10.5
$C_1$ (dB)	13.5	16.5	$\tau_2$ (nsec)	-	20
$C_2$ (dB)	13.5	14.5			

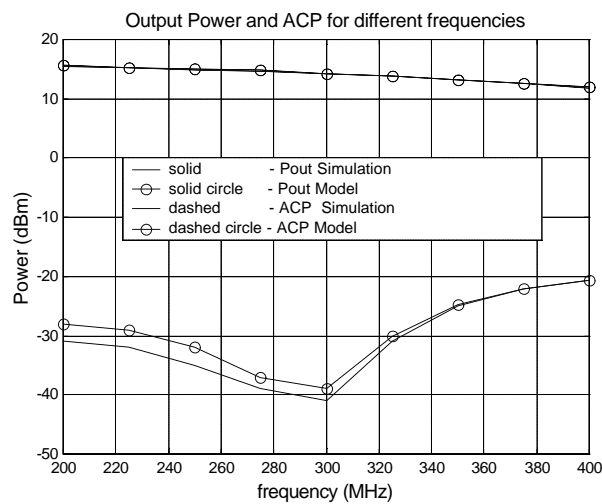


**Figure 5.31** Comparison of the model and simulation results for  $P_{out}$  and  $P_{outacp}$  for the parameter variations listed in Table 5.8.

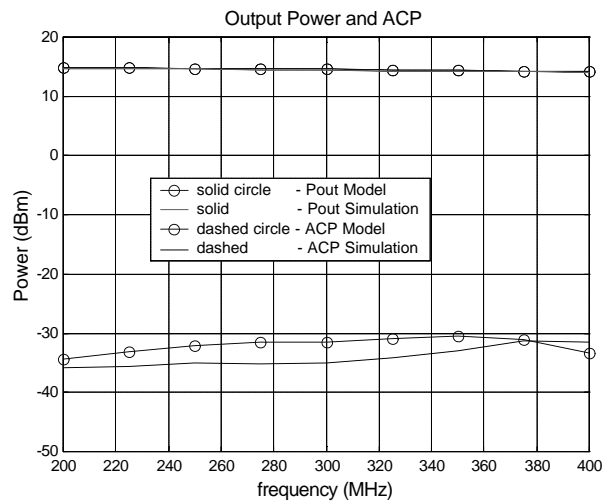


**Figure 5.32** Comparison of the model and simulation results for  $P_{out}$  and  $P_{outacp}$  for the parameter variations listed in Table 5.9.

## CHAPTER 6

### APPLICATION OF A MULTITONE MODEL TO ANALYZE FEEDFORWARD CIRCUITS

In previous chapters, we developed an analytical model to characterize a simple feedforward system for an input of CDMA signal with a large number of codes without taking phase mismatches into account. Such a signal has a well known PSD and is a suitable stimulus to characterize a nonlinear system analytically. In this chapter we are going to develop an alternative analysis to analyze a simple feedforward circuit for an arbitrary input complex signal whose stochastic properties are not well defined or difficult to handle to include in an analytical model. We are going to investigate whether an arbitrary signal can be represented with a certain number of sinusoidal signals having the same average power and a peak power determined by an effective envelope peak-to-average ratio. Developing such an alternative tool would help the designer to analyze a feedforward circuit with amplitude, phase and delay mismatches in a more convenient way, since one will have to deal with a series of tones rather than complex envelopes. In this chapter, first, expressions for mean and peak power of an equal amplitude two tone signal will be recalled. Then these expressions will be generalized for an arbitrary number of tones with different amplitudes. A simple feedforward circuit illustrated in Figure 4.1 will be analyzed using the developed model and expressions for main channel power and distortion power at the adjacent channels at the output of the main amplifier and the feedforward circuit will be derived. Later the application and the verification of the model will be presented. Finally, discussions regarding the analysis will be presented. Although the developed model is expected to be a

convenient tool to analyze phase mismatches, for the sake of simplicity, only amplitude mismatches are brought into consideration in this chapter.

## 6.1 Representation of signals with various envelopes

Time domain expression of an equal amplitude two tone signal can be written as follows:

$$v_s(t) = v \cos(\omega_1 t) + v \cos(\omega_2 t) \quad (6.1)$$

which is equivalent to:

$$v_s(t) = 2v \left[ \cos\left(\frac{\omega_1 - \omega_2}{2} t\right) \right] \left[ \cos\left(\frac{\omega_1 + \omega_2}{2} t\right) \right] \quad (6.2)$$

or

$$v_s(t) = 2v \cos(\omega_m t) \cos(\omega t) \quad (6.3)$$

where

$$\begin{aligned} \omega &= \frac{\omega_1 + \omega_2}{2} \\ \omega_m &= \frac{\omega_1 - \omega_2}{2} \end{aligned} \quad (6.4)$$

The envelope peak and average power expressions for the signal in (6.2) are

$$P_{pk} = \left( \frac{2v}{\sqrt{2}} \right)^2 = 2v^2 \quad (6.5)$$

and

$$P_m = 2 \left( \frac{v}{\sqrt{2}} \right)^2 = v^2 \quad (6.6)$$

respectively for 1  $\Omega$  load.. Note that envelope power peak-to-average ratio for the equal amplitude two-tone signal is 3 dB as expected.

It is possible to obtain different envelopes with different peak-to-average ratio and distributions by increasing the number of harmonics of  $\omega_m$  in (6.3). A general signal with the following representation:

$$v_s(t) = v \left[ \sum_{n=1}^p m_n \cos(n\omega_m t) \right] \cos(\omega t) \quad (6.7)$$

has a peak envelope power:

$$P_{pk} = \left( \frac{v^2}{2R} \right) \left( \sum_{n=1}^p m_n \right)^2 \quad (6.8)$$

Mean power for periodic signals with the following form

$$v_s(t) = vf(\omega_m t) \cos(\omega t) \quad (6.9)$$

can be computed using the following relationship [4]:

$$P_m = \frac{\omega_m}{2\pi} \int_0^{2\pi/\omega_m} \frac{1}{2} [f(\omega_m t)v]^2 dt \quad (6.10)$$

Hence mean power for the signal defined in (6.7) is:

$$P_m = \left( \frac{v^2}{4R} \right) \left( \sum_{n=1}^p m_n^2 \right) \quad (6.11)$$

Combining (6.8) and (6.11) yields us an expression for peak-to-average ratio [4]:

$$\Psi = \frac{P_{pk}}{P_m} = 2 \frac{\left( \sum_{n=1}^p m_n \right)^2}{\left( \sum_{n=1}^p m_n^2 \right)} \quad (6.12)$$

Different sets of  $m_n$  can be chosen to obtain different envelope power distributions for an arbitrary peak-to-average ratio. Note that, maximum envelope peak-to-average ratio of  $2p$  can be obtained for  $p$  harmonics. A nonlinear amplifier would be expected to produce different amount of IMD for different envelope power distributions even if their maximum peak to average ratio is same.

For an arbitrary time domain signal  $v_s(t)$ , peak and mean power can be found numerically by using the following expressions:

$$P_{pk} = \frac{(\max\{env\{v_s(t)\}\})^2}{2R} \quad (6.13)$$

$$P_m = \frac{avg\{env^2\{v_s(t)\}\}}{2R} \quad (6.14)$$

## 6.2 Modeling the feedforward system

$V_{out} - V_{in}$  characteristic of a memoryless amplifier with third order nonlinearity can be expressed as follows:

$$V_{out} = a_1'V_{in} + a_3'V_{in}^3 \quad (6.15)$$

In order to be able to compute  $V_{out}$ , we have to compute  $V_{in}^3$  for the signal of the form (6.7). One possible way to accomplish this task is to compute the inverse Fourier transform of the Fourier transform of  $V_{in}^3$ . This tedious task can be handled using MATHCAD upto p=4 or 5. The resulting expression will again be in the form of (6.7) but now the number of components will be three times as much as input signal. Hence the following can be written:

$$\left[ \sum_{n=1}^p m_n \cos(n\omega_m t) \right]^3 = \left[ \sum_{n=0}^{3p} m_n' \cos(n\omega_m t) \right] \quad (6.16)$$

for p=4 the new m' coefficients are listed in Appendix C. Note that cube of a series of sinusoids contains a DC component. Hence while modeling the whole system, (6.16) needs to be extended to take the DC component into consideration. The m' coefficients have been computed using MATHCAD for up to p=4. A function has been written in MATLAB to compute closed form m' expressions for higher harmonics.

Assuming (6.7) represents the input signal, for a general feedforward system, envelope expressions at the output of the main amplifier, carrier cancellation loop and feedforward circuit can be represented as follows:

$$s_m(t) = \sum_{n=0}^{3p} d_n \cos(n\omega_m t) \quad (6.17)$$

$$s_e(t) = \sum_{n=0}^{3p} e_n \cos(n\omega_m t) \quad (6.18)$$

$$y(t) = \sum_{n=0}^{3p} y_n \cos(n\omega_m t) \quad (6.19)$$

where

$$d_n = a_1 l_1 v m_n + a_3 l_1^3 v^3 m_n' \quad (6.24)$$

$$e_n = \left[ \frac{a_1 l_1}{C_2 C_3} - \frac{l_3}{C_1} \right] v m_n + \frac{a_3 l_1^3}{C_2 C_3} v^3 m_n' \quad (6.25)$$

$$y_n = l_2 l_4 d_n - \frac{b_1}{C_4} e_n - \frac{b_3}{C_4} f_n \quad (6.26)$$

$$a_1 = a_1', \quad a_3 = \frac{3}{4} a_3' \quad (6.27)$$

Note that ‘b’ coefficients stand for the error amplifier nonlinearity parameters, which were defined in previous chapters. The  $f_n$  coefficients arise from the cubic expansion of (6.25). Once the harmonic coefficients are determined by using (6.24) – (6.26), the main and adjacent channel power at the output of the main amplifier and feedforward system can be computed using the following relationships which are similar to (6.11).

$$P_{main} = \left( \frac{1}{4R} \right) \left( \sum_{n=1}^p d_n^2 \right) \quad (6.28)$$

$$P_{maincp} = \left( \frac{1}{4R} \right) \left( \sum_{n=p+1}^{3p} d_n^2 \right) \quad (6.29)$$

$$P_{out} = \left( \frac{1}{4R} \right) \left( \sum_{n=1}^p y_n^2 \right) \quad (6.30)$$

$$P_{outcp} = \left( \frac{1}{4R} \right) \left( \sum_{n=p+1}^{3p} y_n^2 \right) \quad (6.31)$$

### 6.3 Application of the model to real time signals and discussions

In this section we are going to investigate whether an arbitrary real or complex enveloped signal can be represented with a series of deterministic signals and whether this representation can be used to predict main and distorted adjacent channel power at the output of the main amplifier and feedforward system. Our first example is a randomly generated signal in MATLAB environment. The second and third examples focus on a Wideband CDMA data generated in ADS environment.

### 6.3.1 Random signal

A 8192 sample random signal at a sampling rate of 60 nsec has been generated in MATLAB environment using the built-in function *randn*. The generated signal has an average input power of 10.15 dBm with an envelope peak-to-average ratio of 7.55 dB and a bandwidth of 5 MHz. The time domain waveform of the envelope and the envelope histogram are illustrated in Figure 6.1. Also main amplifier and feedforward output power spectra are illustrated for  $C_1=C_2=C_3=C_4=10$  dB,  $IP3^m=33$  dBm,  $IP3^e=33$  dBm,  $G_m=10$  dB and  $G_e=30$  dB in Figure 6.2.

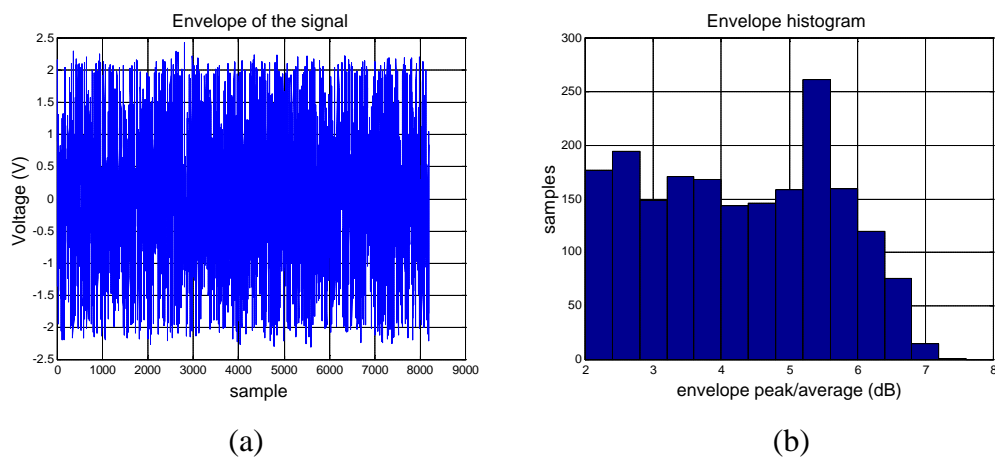


**Figure 6.1** a) Time domain envelope b) Envelope histogram of the generated random signal.

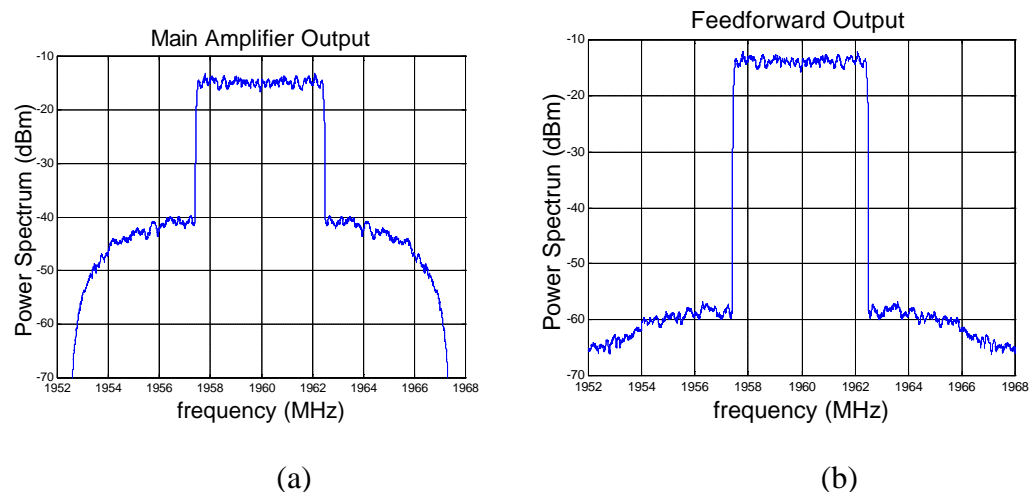


**Figure 6.2** Power spectrum of the random signal a) Main amplifier output b) Feedforward output -  $C_1=C_2=C_3=C_4=10$  dB,  $IP3^m=33$  dBm,  $IP3^e=33$  dBm,  $G_m=10$  dB and  $G_e=30$  dB.

From Figure 6.1-b it can be deduced that the distribution of the instantaneous envelope peak-to-average ratios is even to some extent until a peak-to-average ratio of about 5.3 dB. Between 5.3 and 5.6 dB the number of peaks increases considerably and beyond 5.6 dB the probability of the occurrence of the peaks decreases monotonically. Although the ultimate peak-to-average ratio is 7.55 dB, the number of peaks that correspond to a ratio of beyond 7 dB is negligible. The distribution of the envelope peaks is an important factor in determining the linearity characteristics of the main amplifier and the feedforward system since it may lead different values for effective envelope peak-to-average ratio. Table 6.1 tabulates feedforward output power and distorted ACP for different sets of harmonic coefficients, which correspond to different peak-to-average ratios with different distributions. System parameters are as stated above. Simulation values for  $P_{\text{main}}$ ,  $P_{\text{mainacp}}$ ,  $P_{\text{out}}$  and  $P_{\text{outacp}}$  are 19.05 dBm, -6.7 dBm, 20.1 dBm and -23.2 dBm respectively. Note that for three harmonics, closer results are obtained as peak-to-average ratio ( $\psi$ ) is reduced from 7.4 dB down to 6.3 dB. Since our model represents the input random signal with a series of deterministic signals, maximum peaks occur periodically. Consequently the maximum peaks of the model signal drives to amplifier to nonlinearity more frequently compared to a random signal. This results with higher ACP. Therefore  $\psi$  for the model signal has to be decreased leading to an effective envelope peak-to-average ratio,  $\psi_{\text{eff}}$ . For our case  $\psi_{\text{eff}}$  turns out to be somewhere 1 dB below actual  $\psi$ . Although the majority of the harmonic sets with the same  $\psi$  yield the same  $P_{\text{outacp}}$  and  $P_{\text{out}}$  for a specific set of system parameters, there might also exist some of them which result with different ACPs like the one seen in the table ( $m_1=0.6$ ,  $m_2=0.1$ ,  $m_3=0.9$ ). The number of harmonics can be increased to achieve more evenly distributed histograms and in this way the effective  $\psi$  used in the model signal can be increased with the cost of increased computational complexity. An example of this case is seen in the last two rows of Table 6.1. Note that with 4 harmonics, the  $\psi$  is set to 7.1-7.2 dB and main amplifier ACP is very closed to that of obtained by simulation. However ACP for the feedforward output does not coincide. This observation points out the fact that not only the main amplifier output but also the

feedforward system output need to be considered as a reference while determining  $\Psi_{\text{eff}}$  and the number of harmonics.

For the harmonic set ( $m_1=0.55$ ,  $m_2=0.9$ ,  $m_3=0.1$ ) simulation and model results are compared by sweeping the system parameters  $C_1$ ,  $C_3$ ,  $C_4$ ,  $\text{IP3}^e$  and  $\text{IP3}^m$ . The results are illustrated in Figure 6.3 - 6.5 and Tables 6.2 – 6.3. Note that model and simulation results coincide with each other.

**Table 6.1** Different harmonic sets to model the random signal  $C_1=C_2=C_3=C_4=10$  dB,  $\text{IP3}^m=33$  dBm,  $\text{IP3}^e=33$  dBm,  $G_m=10$  dB,  $G_e=30$  dB.

<b>M1</b>	<b>M2</b>	<b>M3</b>	<b>M4</b>	<b>y</b> <b>(dB)</b>	<b>P<sub>main</sub></b> <b>(dBm)</b>	<b>P<sub>mainacp</sub></b> <b>(dBm)</b>	<b>P<sub>out</sub></b> <b>(dBm)</b>	<b>P<sub>outacp</sub></b> <b>(dBm)</b>
0.7	0.35	0.5	-	7.4	18.6	-2.0	19.9	-12.9
0.5	0.95	0.4	-	7.2	18.7	-3.4	20.0	-15.5
0.55	0.35	0.15	-	6.9	18.8	-4.4	20.0	-17.7
0.45	0.85	0.2	-	6.7	18.9	-5.2	20.1	-19.8
0.65	0.3	0.15	-	6.5	18.9	-6.0	20.1	-21.0
0.55	0.9	0.1	-	6.3	19.0	-6.5	20.1	-23.1
0.4	0.75	0.1	-	6.3	19.0	-6.5	20.1	-23.3
0.4	0.95	0.2	-	6.4	19.0	-6.2	20.1	-22.5
0.6	0.1	0.9	-	6.4	19.0	-4.0	20.1	-22.9
0.8	0.55	0.1	0.15	7.2	18.8	-6.5	20.0	-16.5
0.95	0.4	0.1	0.25	7.1	18.8	-7.0	20.0	-17.6

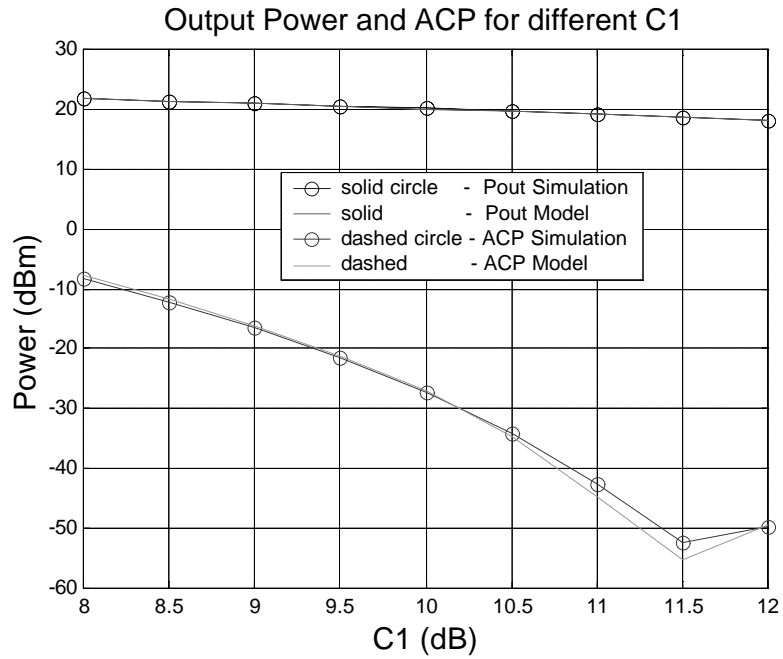


**Figure 6.3** Feedforward output power and ACP for various  $C_1$  –  $m_1=0.55$ ,  $m_2=0.9$ ,  $m_3=0.1$  –  $C_2=C_3=C_4=10$  dB,  $G_m=10$  dB,  $IP3^m=33$  dBm,  $G_e=30$  dB,  $IP3^e=35$  dBm.

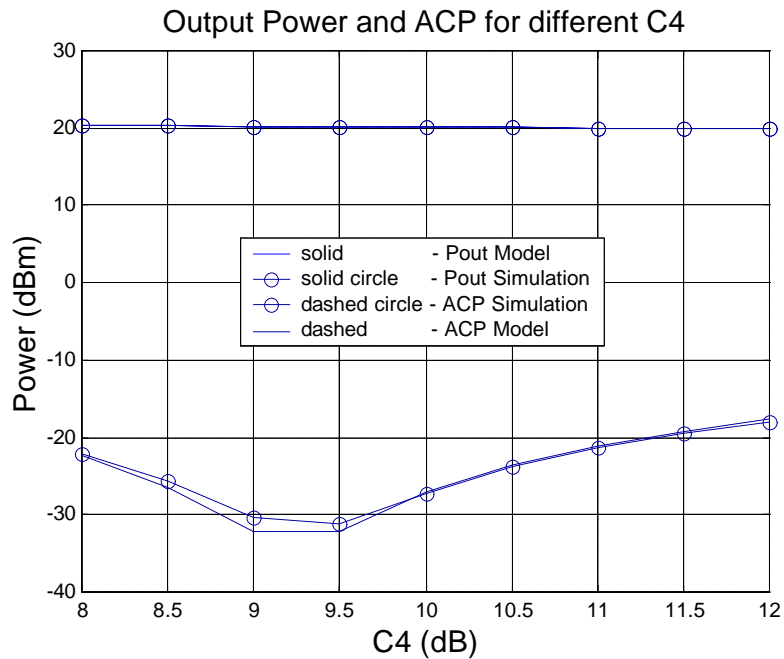


**Figure 6.4** Feedforward output power and ACP for various  $C_4$  –  $m_1=0.55$ ,  $m_2=0.9$ ,  $m_3=0.1$  –  $C_1=C_2=C_3=10$  dB,  $G_m=10$  dB,  $IP3^m=33$  dBm,  $G_e=30$  dB,  $IP3^e=35$  dBm.

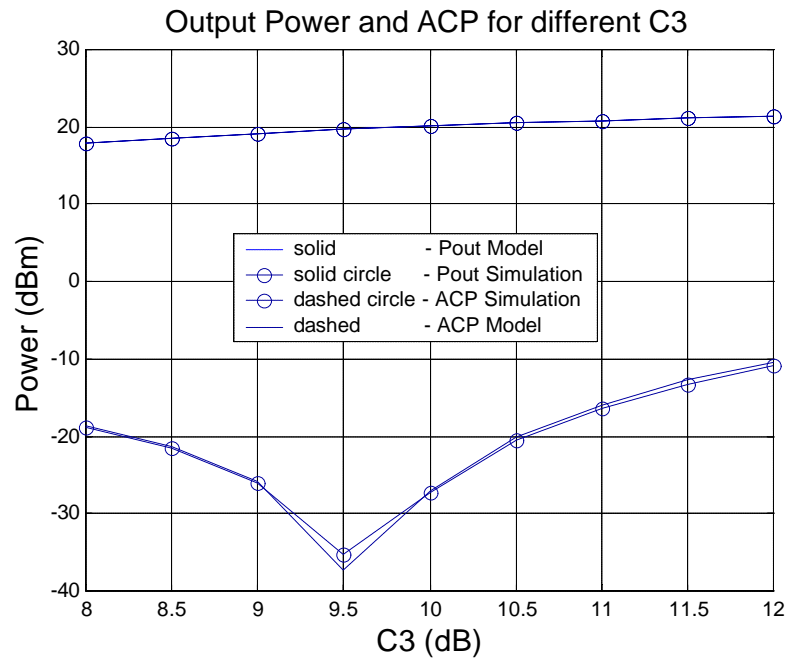


**Figure 6.5** Feedforward output power and ACP for various  $C_3$  –  $m_1=0.55$ ,  $m_2=0.9$ ,  $m_3=0.1$  –  $C_1=C_2=C_4=10$  dB,  $G_m=10$  dB,  $IP3^m=33$  dBm,  $G_e=30$  dB,  $IP3^e=35$  dBm.

**Table 6.2** Comparison of the simulation and model results for different  $IP3^e$  values,  $C_1=C_2=C_3=C_4=10$  dB,  $IP3^m=33$  dBm,  $G_m=10$  dB,  $G_e=30$  dB.

$IP3^e$	Sim.	Sim.	Model	Model
	$P_{out}$	$P_{outacp}$	$P_{out}$	$P_{outacp}$
33	20.1	-23.2	20.1	-23.1
35	20.1	-27.2	20.1	-27.1
37	23.2	-31.2	23.2	-31.1
39	23.3	-35.2	23.3	-35.1
41	20.1	-39.2	20.1	-39.1

**Table 6.3** Comparison of the simulation and model results for different  $IP3^m$  values,  $C_1=C_2=C_3=C_4=10$  dB,  $IP3^e=33$  dBm,  $G_m=10$  dB,  $G_e=30$  dB.

$IP3^m$	Sim. $P_m$	Sim. $P_{macp}$	Model $P_m$	Model $P_{macp}$	Sim. $P_{out}$	Sim. $P_{outacp}$	Model $P_{out}$	Model $P_{outacp}$
33	19.1	-6.7	19.0	-6.5	20.1	-23.2	20.1	-23.1
34	19.3	-8.7	19.3	-8.5	20.1	-29.2	20.1	-29.1
35	19.5	-10.7	19.5	-10.5	20.1	-35.2	20.1	-35.1
36	19.6	-12.7	19.6	-12.5	20.1	-41.2	20.1	-41.1

### 6.3.2 Wideband CDMA

In this section application of the model to a Wideband CDMA data will be presented. The stimulus signal has been generated using ADS example design file which generates a wideband CDMA at a sampling rate  $1/(4*16.384)$  microseconds. The resulting signal has a base-bandwidth of 8.192 MHz. First only the real part of this signal will be modeled. Later the analysis will be extended to the complex enveloped signal.

#### Real envelope data:

The real part of the generated wideband CDMA data has been processed in MATLAB environment. The time domain envelope data and the corresponding envelope histogram are illustrated in Figure 6.6. Input average power is 11.5 dBm with  $\psi$  of 8.5 dB. Main amplifier and feedforward output power spectra are illustrated for  $C_1=C_2=C_3=C_4=10$  dB,  $IP3^m=36$  dBm,  $IP3^e=35$  dBm,  $G_m=10$  dB and  $G_e=30$  dB in Figure 6.7.

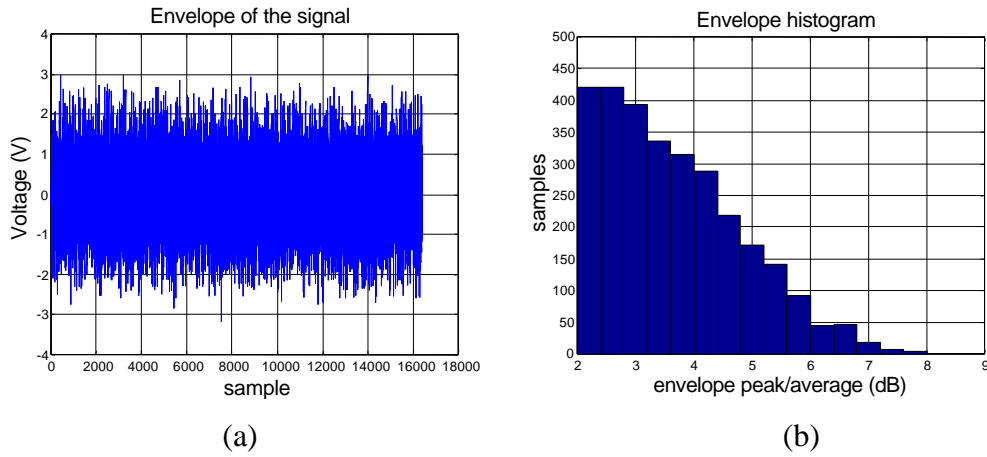


**Figure 6.6** a) Time domain envelope b) Envelope histogram of the generated real WCDMA data.

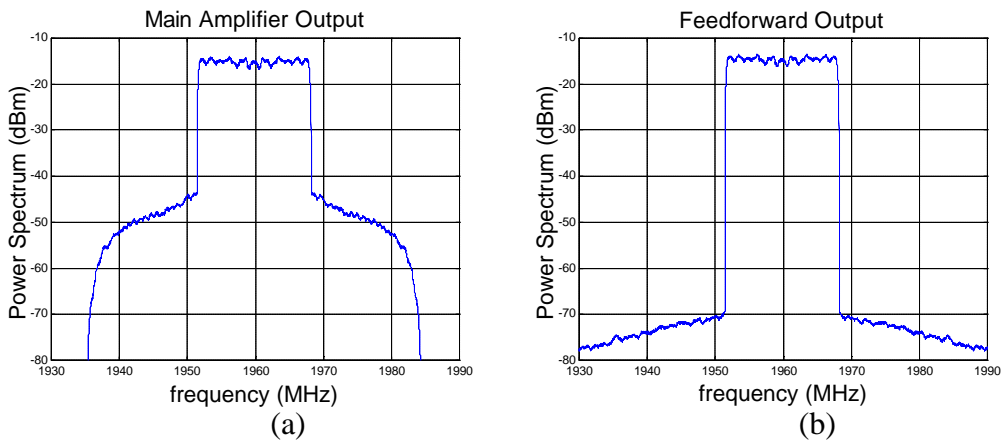


**Figure 6.7** Power spectrum of the real WCDMA signal a) Main amplifier output b) Feedforward output -  $C_1=C_2=C_3=C_4=10$  dB,  $IP3^m=36$  dBm,  $IP3^e=35$  dBm,  $G_m=10$  dB and  $G_e=30$  dB.

Simulation values of  $P_m$ ,  $P_{macp}$ ,  $P_{out}$  and  $P_{outacp}$  for the system parameters stated above are 21.0 dBm, -9.7 dBm, 21.5 dBm and -33.4 dBm respectively. Table 6.4 tabulates various sets of harmonic coefficients at different  $\psi$  values. Observations similar to the previous case can be done. ACP distortion power decreases and gets closer to the simulation values as  $\psi$  decrements from  $\psi_{max}$  (8.5 dB) to  $\psi_{eff}$  (6.3 dB) for a 3 harmonic representation. With a representation with 4 harmonics, the same main amplifier ACP can be achieved for a higher  $\psi$ , whereas linearizer output ACP prediction is not as good as the representation at a lower  $\psi$ . Figure 6.8 – 6.10 compare the simulation results and the model ( $m_1=0.9$ ,  $m_2=0.4$ ,  $m_3=0.15$ ) for a sweep of  $C_1$ ,  $C_4$  and  $C_3$ . In Figure 6.8, it seems that model and

simulation results deviate from each other for  $C_1=11$  dB. This deviation is possibly due to the limitation in simulation measurements. Apart from that, results agree with each other. Table 6.5 displays a comparison for varying  $IP3^e$ , which confirms the successful prediction of the model.

**Table 6.4** Different harmonic sets to model the real WCDMA signal  $C_1=C_2=C_3=C_4=10$  dB,  $IP3^m=36$  dBm,  $IP3^e=35$  dBm,  $G_m=10$  dB,  $G_e=30$  dB

M1	M2	M3	M4	y	$P_{main}$	$P_{mainacp}$	$P_{out}$	$P_{outacp}$
				(dB)	(dBm)	(dBm)	(dBm)	(dBm)
0.7	0.35	0.5	-	7.4	20.4	-4.0	21.4	-22.8
0.65	1.0	0.4	-	7.2	20.5	-5.1	21.4	-24.6
0.8	1.0	0.25	-	6.9	20.6	-6.3	21.4	-27.4
0.55	0.85	0.15	-	6.6	20.7	-7.4	21.5	-30.3
0.7	0.9	0.1	-	6.5	20.7	-8.1	21.5	-31.8
0.9	0.4	0.15	-	6.3	20.8	-9.2	21.5	-33.5
0.8	0.2	0.25	-	6.2	20.7	-9.4	21.5	-33.7
0.9	0.7	0.1	0.1	6.9	20.6	-9.7	21.5	-29.1
1.0	0.5	0.1	0.2	7.0	20.6	-9.7	21.5	-28.4

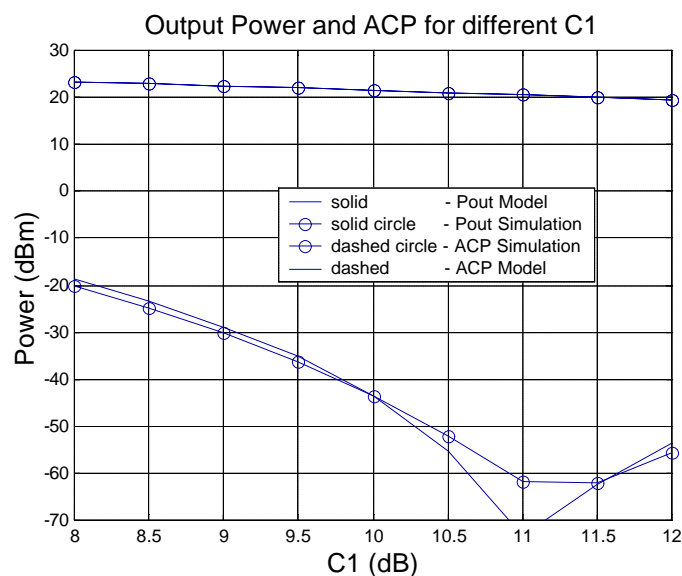


**Figure 6.8** Feedforward output power and ACP for various  $C_1$  –  $m_1=0.9$ ,  $m_2=0.4$ ,  $m_3=0.15$  -  $C_2=C_3=C_4=10$  dB,  $G_m=10$  dB,  $IP3^m=36$  dBm,  $G_e=30$  dB,  $IP3^e=40$  dBm.

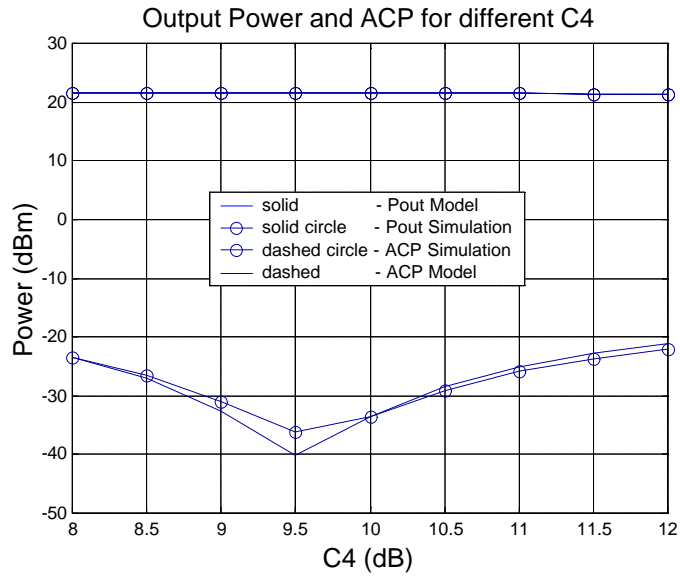


**Figure 6.9** Feedforward output power and ACP for various  $C_4$  –  $m_1=0.9$ ,  $m_2=0.4$ ,  $m_3=0.15$  –  $C_1=C_2=C_3=10$  dB,  $G_m=10$  dB,  $IP3^m=36$  dBm,  $G_e=30$  dB,  $IP3^e=35$  dBm.

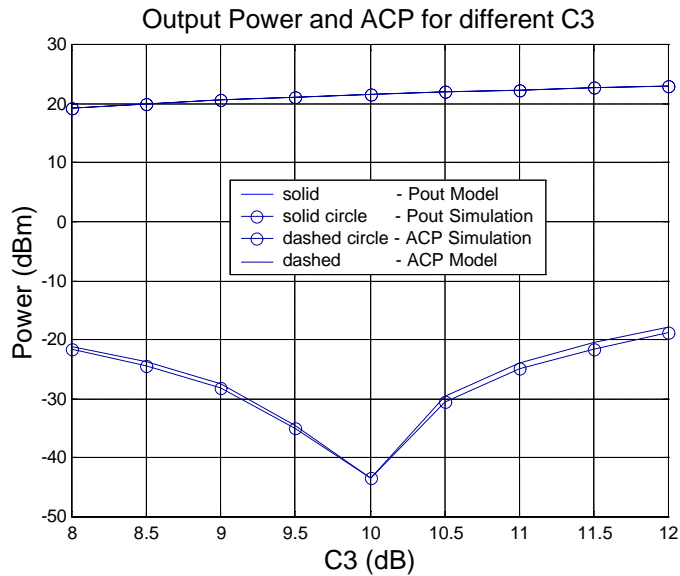


**Figure 6.10** Feedforward output power and ACP for various  $C_3$  –  $m_1=0.9$ ,  $m_2=0.4$ ,  $m_3=0.15$  –  $C_1=C_2=C_4=10$  dB,  $G_m=10$  dB,  $IP3^m=36$  dBm,  $G_e=30$  dB,  $IP3^e=40$  dBm.

**Table 6.5** Comparison of the simulation and model results for different  $IP3^e$  values,  $C_1=C_2=C_3=C_4=10$  dB,  $IP3^m=36$  dBm,  $G_m=10$  dB,  $G_e=30$  dB.

$IP3^e$	Sim $P_{out}$	Sim $P_{outacp}$	Model $P_{out}$	Model $P_{outacp}$
33	21.5	-29.5	21.5	-29.5
35	21.5	-33.5	21.5	-33.5
37	21.5	-37.5	21.5	-37.5
39	21.5	-41.5	21.5	-41.5
41	21.5	-45.5	21.5	-45.5

### Wideband CDMA Complex:

Time domain magnitude of the envelope data generated in the ADS environment and the corresponding envelope histogram are illustrated in Figure 6.11. Input average power is 14.5 dBm with an envelope peak-to-average ratio of 6.5 dB. Main amplifier and feedforward output power spectra are illustrated for  $C_1=C_2=C_3=C_4=10$  dB,  $IP3^m=36$  dBm,  $IP3^e=40$  dBm,  $G_m=10$  dB and  $G_e=30$  dB in Figure 6.12. Simulations are performed in DSP environment of ADS.

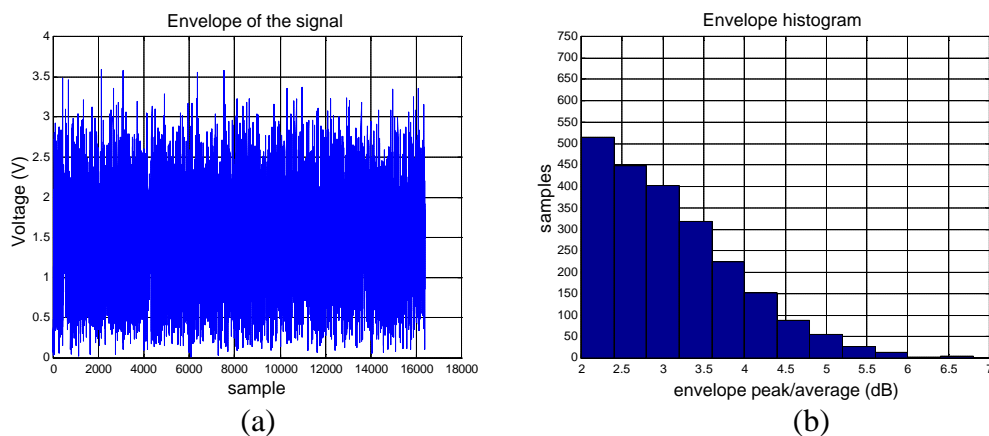


**Figure 6.11** a) Time domain envelope b) Envelope histogram of the generated complex WCDMA data.

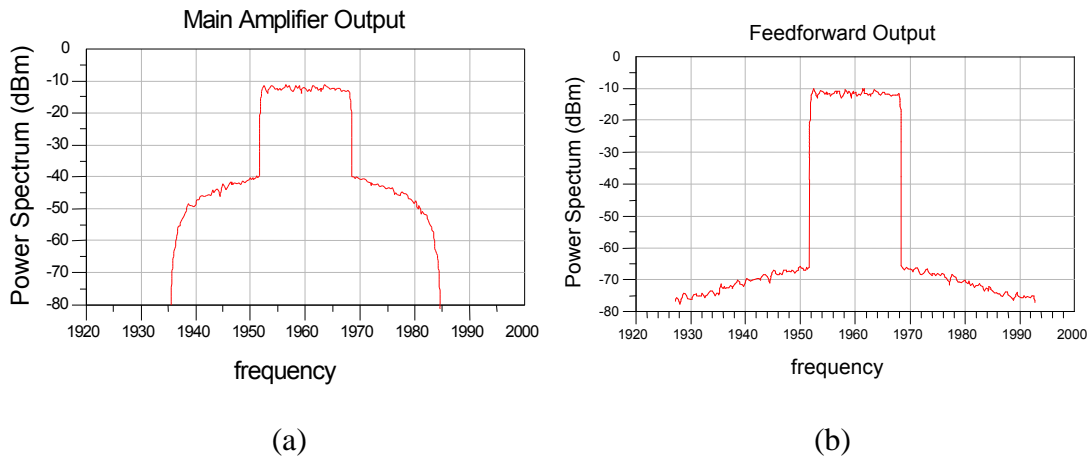


**Figure 6.12** Power spectrum of the complex WCDMA signal **a)** Main amplifier output **b)** Feedforward output -  $C_1=C_2=C_3=C_4=10$  dB,  $IP3^m=36$  dBm,  $IP3^e=40$  dBm,  $G_m=10$  dB and  $G_e=30$  dB.

Simulation values of  $P_m$ ,  $P_{macp}$ ,  $P_{out}$  and  $P_{outacp}$  for the system parameters stated above are 23.7 dBm, -4.9 dBm, 24.5 dBm and -29.8 dBm respectively. Table 6.6 tabulates various sets of harmonic coefficients at different  $\psi$  values. It can be deduced that  $\psi_{eff}$  for this case is somewhere between 5 and 5.4 dB which is about 1 – 1.5 dB lower than  $\psi_{max}$ . Although the entire combinations yield main amplifier ACP closed to the simulation results, they differ from each other at linearizer output ACP within 3 dB. The best result is achieved with the 4 harmonic representation, whose second and third harmonic coefficients are zero ( $m_1=0.95$ ,  $m_2=m_3=0$ ,  $m_4=0.3$ ). Figure 6.13 – 6.15 compare simulation and model results for various coupler couplings. Results agree with each other.

**Table 6.6** Different harmonic sets to model the complex WCDMA signal  $C_1=C_2=C_3=C_4=10$  dB,  $IP3^m=36$  dBm,  $IP3^e=40$  dBm,  $G_m=10$  dB,  $G_e=30$  dB.

M1	M2	M3	M4	y	$P_{main}$	$P_{mainacp}$	$P_{out}$	$P_{outacp}$
				(dB)	(dBm)	(dBm)	(dBm)	(dBm)
0.95	0.2	0.15	-	5.4	23.2	-4.3	24.5	-23.7
0.85	0.25	0.05	-	5.3	23.3	-4.7	24.5	-25.5
0.9	0.25	0.05	-	5.2	23.3	-5.2	24.5	-26.4
0.95	0.25	0.05	-	5.1	23.3	-5.6	24.5	-27.2
0.85	0.05	0.2	-	5.0	23.2	-5.6	24.5	-27.6
0.9	0.05	0.2	-	4.9	23.2	-6.2	24.5	-28.4
0.9	0.0	0.0	0.3	5.0	23.4	-5.2	24.5	-29.0

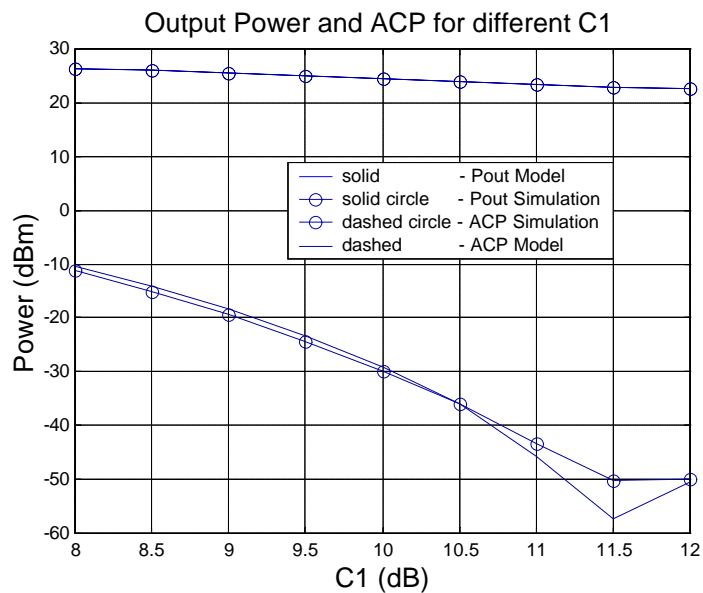


**Figure 6.13** Feedforward output power and ACP for various  $C_1$  -  $m_1=0.9$ ,  $m_2=m_3=0$ ,  $m_4=0.3$  -  $C_2=C_3=C_4=10$  dB,  $G_m=10$  dB,  $IP3^m=36$  dBm,  $G_e=30$  dB,  $IP3^e=40$  dBm.

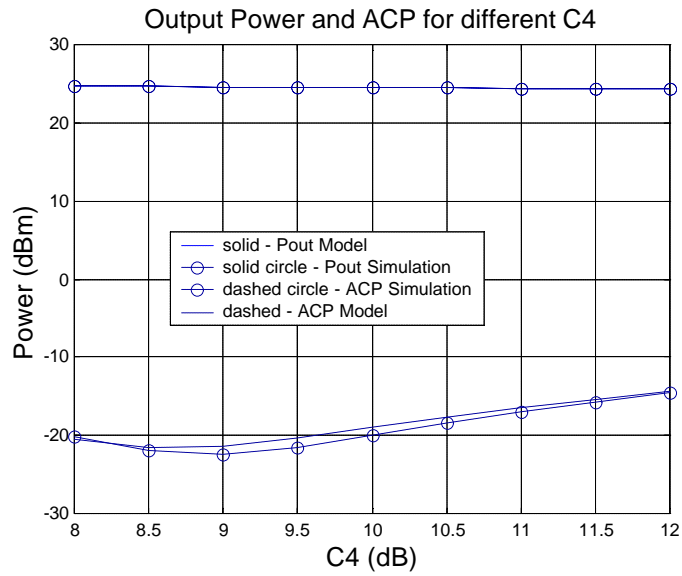


**Figure 6.14** Feedforward output power and ACP for various  $C_4$  –  $m_1=0.9$ ,  $m_2=m_3=0$ ,  $m_4=0.3$  –  $C_1=C_2=C_3=10$  dB,  $G_m=10$  dB,  $IP3^m=36$  dBm,  $G_e=30$  dB,  $IP3^e=35$  dBm.

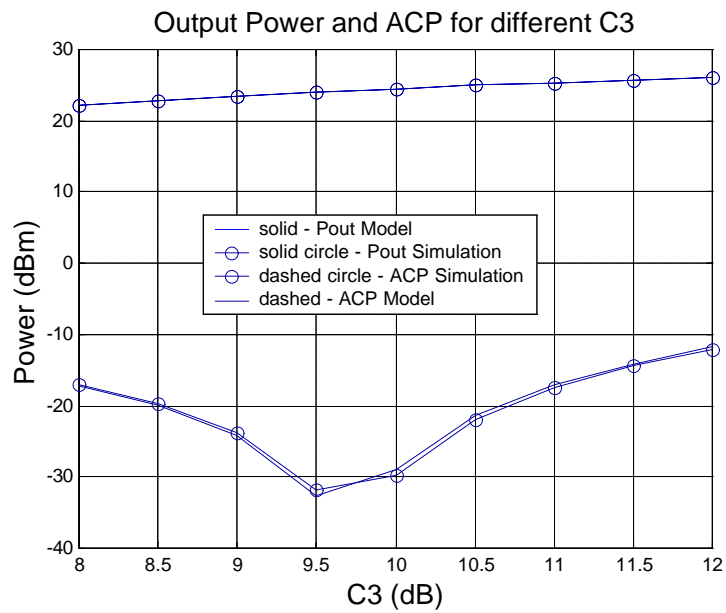


**Figure 6.15** Feedforward output power and ACP for various  $C_3$  –  $m_1=0.9$ ,  $m_2=m_3=0$ ,  $m_4=0.3$  –  $C_1=C_2=C_3=10$  dB,  $G_m=10$  dB,  $IP3^m=36$  dBm,  $G_e=30$  dB,  $IP3^e=40$  dBm.

## 6.4 Discussions and future research

In this chapter, we brought an aspect to model a feedforward circuit for an arbitrary real or complex enveloped signal. We represented signals with a combination of tones whose magnitudes are adjusted such that the average power of the model signal is the same as that of the original signal and envelope peak-to-average ratio is effectively the same to perform similar nonlinear characteristics. Since an arbitrary time domain signal has an envelope histogram randomly distributed, the probability of occurrence of the high peaks will probably be too small. On the other hand, the model signal is periodic and so are the peaks. This observation leads us to define an effective peak-to-average ratio for the original signal such that the nonlinearity at the output of the main amplifier and feedforward system are similar to that obtained with the model signal. The effective peak-to-average turned out to be about 1 dB lower than the maximum one for the above cases. Another observation is that, different combinations of tones having the same peak-to-average ratio yield similar nonlinear characteristics at the output of the main amplifier and the linearizer as long as the number of tones are same.

The most crucial point regarding this analysis is the criteria to choose the correct effective envelope peak-to-average ratio. In the examples above we showed the existence of a model signal that would replace the actual one. One criterion could be to take the main amplifier output power and ACP for a particular case as a reference and to keep the number of harmonics of the model envelope as small as possible. The examples above showed that a similar main amplifier output ACP could also be obtained for a higher number of harmonics with a higher peak-to-average ratio but then the feedforward output deviated to some extent. In the complex enveloped (third) example it can be observed that three and four harmonic combinations with the same peak-to-average ratios yield results for the feedforward output within 2 dB. Once the coefficients for the harmonics are set for the overall system, the model and simulation results agree with each other for all amplitude mismatches and IP3 variations. The selection criteria to choose the correct number of harmonics and corresponding coefficients is still an area of research.

The approach presented in this chapter provides a nice tool to analyze phase and delay mismatches in addition to AM/PM nonlinearities. A series of sinusoidal is relatively simple to deal with when phase issue is in consideration. This analysis needs to be extended and verified to include phase aspects.

## **CHAPTER 7**

### **CONCLUSION**

In modern communication systems issue of designing linear transmitters is an important concept and designing linear power amplifiers and power amplifier linearization are inevitable parts of this concept. Digital modulation involves bits and symbols of finite duration whose spectra spread within a wide frequency range. In order to increase the spectral efficiency, the pulses, which are finite in time domain, are usually raised cosine filtered. Modulation of these pulses on the carrier frequency causes a non-constant enveloped signal. Another source of non-constant envelope is multi carrier transmission, which is particularly used in base station applications. Amplification of a non-constant enveloped signal is a real challenge for power amplifiers. Although power amplifier are usually planned to produce average output power, they also have to be linear enough to handle peak powers. Hence they have to be designed at an output back off power whose back off factor is determined by the envelope peak to average ratio of the signal, namely crest factor. Failure to do so, will cause intermodulation products for multi carrier transmission and spectral regrowth for digitally modulated signals in addition to the in band distortion. Spectral regrowth means allocation in adjacent channels leading to sensitivity deterioration of the cellular radios communicating at those allocated channels. These limitations severely affect the frequency planning in a cellular application and physical structures of the cells. Designing linear power amplifiers brings the problems of efficiency and implementation into consideration. To overcome these problems, auxiliary systems that are called linearizers are used in conjunction with nonlinear power amplifiers.

Among several techniques feedforward suggests the most stable broadband operation and ultra linear performance with the drawback of relatively poor efficiency. Linearity performance of the system is highly dependent upon how well is the carrier and distorted signal is cancelled in the carrier and error cancellation loops, respectively. In order to achieve a good cancellation, amplitude, phase and delay matching need to be maintained within the loops. To accomplish this task, couplers, variable attenuators and phase shifters (vector modulators), delay units and linear error amplifiers are integrated in the system. Hence, there are lots of components, which affect the overall system. The coupler and delay line losses, main and error amplifier efficiencies and envelope peak-to-average ratio at the output of the main amplifier are the main factors that affect the overall efficiency of the system. Under the light of these observations, it can be deduced that it is essential to develop an analytical model, which characterizes the complexity of the system. Such a mathematical tool would help the system designer a lot in making the parameter optimizations and relaxations for optimum efficiency and a given linearity performance, particularly at the beginning of design.

The main aspect of this thesis is the stochastic characterization of a simple feedforward circuit using autocorrelation analysis. Due to the complexity of the structure, this task has been accomplished assuming that the main and error amplifier are modeled with third order AM/AM nonlinearities and there is no phase mismatch within the loops. Hence amplitude and delay mismatches are the main concerns of this analysis. The analysis has been performed for CDMA applications. The choice of CDMA rises from its popularity in modern communication systems and its simple stochastic characterization due to its convergence to an equivalent band limited white Gaussian noise when a large number of channels are superimposed together. To characterize the overall system, time domain envelope function and consequently autocorrelation function at any point in the system has been expressed in terms of those of the input envelope. Later the autocorrelation expressions have been Fourier transformed to obtain power spectral density at any point in the system. The analysis concludes by integrating the spectral density functions to obtain some closed form equations which relate the total main and adjacent channel power at any point to the system parameters which are coupler couplings and losses, main and error amplifier

linear gain and IP3s and delay mismatches within the loops. Although the amplifiers are modeled with third order nonlinearities, due to the transmission of the distortion products via error amplifier, the order of the system increases to ninth order which makes the autocorrelation analysis of the system very complex. Taking the delay mismatches in the first loop into account makes the overall analysis even more tedious and some of the components contributing to the output spectral density had to be calculated computationally. However, completely closed form expressions can be achieved by ignoring the delay mismatch in the first loop. Additionally, a compact equation has been derived for lossless perfect matching case, which clearly demonstrates the trade-off between the nonlinearities of the main and error amplifiers for a given output power and linearity.

In order to verify the model, a stimulus signal representing a band limited white Gaussian noise, has been generated using Advanced Design Suit tools. The system has been simulated in DSP environment of ADS using system amplifiers whose gain and IP3 can be specified. A similar system has also been simulated in MATLAB environment to understand the signal processing and to verify the equations used to model the transfer function of the system. There was an excellent agreement between these two environments. Later, the derived closed form expressions have been verified using these environments. Since the amplifiers are modeled with third order polynomials, the model diverges from the saturation point beyond a critical input voltage. This limitation led us define a critical IP3 for the main and error amplifier in terms of maximum input voltage, in order to maintain the compatibility between the model and simulation results. Nevertheless, we showed that higher orders of main amplifier nonlinearities can also be handled by representing them with an equivalent third order system which gives rise to the concept of equivalent IP3.

The simulations have further been improved to a more real case by RF modeling the main and error amplifiers using SPICE models of the RF MOSFETs used and lumped components for matching. The co-simulation and envelope simulation features of ADS have been used for RF simulation of the system. Both AM/AM and AM/PM nonlinearities of the amplifiers have been measured. The simulation results have been compared with model results for various cases and a

very good agreement has been achieved. The phase mismatches which result from the amplifiers and delay units have been compensated by injecting phase shifters at the inputs of the amplifiers. The effect of phase mismatches has been observed for various cases and simulations have shown that the output power and ACP vary within 3 dB for up to a phase mismatch of 10 degrees within the loops. The model has also been observed to give compatible results with simulations for complex Gaussian processes. Some deviations have been detected due to the decrement in the peak-to-average ratio relative to a band-limited white Gaussian noise. However these deviations can be compensated by increasing IP3 of the main amplifier by an amount in dB equal to the difference between the peak-to-average ratios of the complex and white Gaussian noise. To utilize the flexibility of the developed model, an optimum wide-band CDMA feedforward linearizer system has been designed based on the analytical tool.

While comparing the model with RF simulations some important observations have been pointed out. Overall feedforward performance is limited by amplitude mismatches. Hence, unless proper amplitude and delay matchings are maintained increasing the linearity of the error amplifier does not help very much with improving the feedforward performance. In other words, increasing the linearity of the error amplifier might be a waste of DC power depending on the parameter combination. Another important observation is that, delay mismatch in the second loop has a deeper impact on the overall performance compared with the first loop. Time domain analysis has shown that even though a good carrier cancellation is achieved in the first loop, peak-to-average ratio at the input of the error amplifier can increase to very high levels. Hence, minimizing the average power may not be sufficient and the linearity requirement of the error amplifier is usually determined by the distribution of the peaks at its input. Introducing a delay mismatch in the first loop does not deteriorate the adjacent channels, but may cause increment in the distortion mean power with a decrement in the peak power. Thus, the overall linearity performance of will not deteriorate with the injection of delay mismatch up to a certain value. This result will provide some relaxation in the parameter tolerances and even increase the overall efficiency by decreasing the linearity requirement of the error amplifier. This observation also emphasizes the impact of

the peak to average ratio of the signal and distribution of the peaks on the overall efficiency of the feedforward linearizer. Our model predicts all these phenomena and thus it is a powerful and flexible tool particularly for design purposes.

Another aspect of the thesis is to develop an alternative model to characterize the feedforward systems for arbitrary complex enveloped signals whose stochastic characteristics are not so well defined or difficult to handle analytically. In this approach, an arbitrary signal has been represented with a series of tones whose mean power is the same as that of the signal and peak-to-average ratio is the same as an effective envelope peak-to-average ratio of the signal which is determined by using envelope histogram of the signal. This tool computes the output power and ACP quantitatively but has the flexibility of dealing with sinusoidal signals. The model has been verified with different types of random signals taking only amplitude mismatches into account. The results are quite promising and this model is believed to be a flexible tool particularly for taking AM/PM nonlinearities and phase mismatches into consideration.

In summary, in this thesis characterization of a simple feedforward system for CDMA applications along with the verifications by RF simulations has been presented. This work involves characterization of systems with high orders and delay mismatches using autocorrelation analysis. Hence computation tools to perform expectations of up to 4 different Gaussian random variables with different orders have been developed. To verify the developed model RF simulation tools have been developed extensively using DSP and RF/Analog environments suggested by the RF simulator ADS. As a result a flexible, handy, mathematical and accurate model has been developed and consequently closed form expressions have been obtained to relate the main and adjacent channel power at any point to system parameters. Hence a fast tool is achieved to make rapid parameter optimizations for optimum efficiency and linearity particularly for broadband applications. Such a tool will decrease the design durations dramatically and give an insight to the designer to work out the complexity of the system. Additionally, an alternative approach has been brought into consideration to model feedforward systems for arbitrary complex enveloped signals.

Possible future research activities can be summarized as follows. The CDMA model can be improved to include higher orders of nonlinearities with the drawback of increased complexity. The real Taylor series coefficients used to model the amplifiers can be modified to complex ones by measuring single tone AM/AM and AM/PM characteristics. Thus AM/PM effects and phase mismatches can be included to the developed model. The current research activities on feedforward systems are concentrated on optimization of the error cancellation loop without the requirement of a pilot signal and minimization of the peaks produced in the carrier cancellation loop attempting to increase the overall efficiency. A possible research area would be contribution to these aspects. Finally, the proposed alternative model, which involves representation of arbitrary signals with a series of deterministic signals, needs to be developed to include phase and delay analysis.

## REFERENCES

- [1] J. Staudinger, “An examination of two measures of power amplifier linearity – Intermodulation distortion and channel spectral regrowth,” *Wireless Communications Conference*, 1996.
- [2] N. Pothecary, *Feedforward Linear Power Amplifiers*, Artech House, 1999.
- [3] A. Katz, “Linearizer Basics,” in *IEEE MTT-S Workshop*, Baltimore, MD, June 1998.
- [4] S. C. Cripps, *RF Power Amplifiers for Wireless Communications*, Artech House, 1999.
- [5] Dye – Granberg, *Radio Frequency Transistors*, Butterworth-Heinemann, 1993.
- [6] Q. Wu, H. Xiao, and F. Li, “Linear RF power amplifier design for CDMA signals: A spectrum analysis approach,” *Microwave Journal*, pp. 22-40, Dec. 1998.
- [7] S. A. Maas, “Third-order intermodulation distortion in cascaded stages,” *IEEE Microwave and Guided Wave Letters*, vol. 5, no. 6, pp. 189-191, June 1995.
- [8] M. J. Toolin, “A simplified approach to determining AM/PM conversion coefficient in microwave low noise amplifiers and systems,” *Microwave Journal*, pp. 80-90, Aug. 2000.
- [9] F. M. Ghannouchi, H. Wakana, and M. Tanaka, “A new unequal three-tone signal method for AM-AM and AM-PM distortion measurements suitable for characterization of satellite communication transmitters/transponders”, *IEEE Transactions on Microwave Theory Tech.*, vol. 48, no. 8, pp. 1404-1407, August 2000.
- [10] N. Suematsu, Y. Iyama, and O. Ishida, “Transfer characteristic of IM3 relative phase for a GaAs FET amplifier”, *IEEE Transactions on Microwave Theory Tech.*, vol. 45, no.12, pp. 2509-2514, December 1997.

- [11] T. R. Turlington, *Behavioral Modeling of Nonlinear RF and Microwave Devices*, Artech House, 2000.
- [12] N. B. Carvalho and J.C. Pedro, "Compact formulas to relate ACPR and NPR to two-tone IMR and IP3," *Microwave Journal*, pp. 70-84, Dec. 1999.
- [13] J.C. Pedro and N. B. Carvalho, "On the use of multitone techniques for assessing RF components' intermodulation distortion," *IEEE Transactions on Microwave Theory Tech.*, vol. 47, no.12, pp. 2393-2402, Decemeber 1999.
- [14] Q. Wu, M. Testa, and R. Larkin, "Linear RF power amplifier design for CDMA Signals," in *IEEE MTT-S Symp. Dig.*, vol 2, June 1996.
- [15] J. K. Cavers, "The effect of data modulation format on intermodulation power in nonlinear amplifiers," in *IEEE Vehicular Technology Conference*, vol.1, June 1994.
- [16] W. Bösch and G. Gatti, "Measurement and simulation of memory effects in predistortion linearizers," *IEEE Transactions on Microwave Theory Tech.*, vol. 37, no.12, pp. 1885-1890, December 1989.
- [17] A. Katz and R. Dorval, "Evaluation and correction of time dependent amplifier nonlinearity," in *IEEE MTT-S Digest*, 1996.
- [18] J. H. K. Vuolevi, T. Rahkonen, and J. P. A. Manninen, "Measurement technique for characterizing memory effects in RF power amplifiers," *IEEE Transactions on Microwave Theory Tech.*, vol. 49, no. 8, pp. 1383-1389, August 2001.
- [19] M. Eron, E. Martony, Y. Fogel, E. Jeckeln, and M. Hrybenko, "Accurate, wideband characterization and optimization of high power LDMOS amplifier memory properties", in *IEEE MTT-S Digest*, Philadelphia , PA, June 2003. pp 1729-1732.
- [20] S. Boumaiza, J. Gauthier, and F. M. Ghannouchi, "Dynamic electro-thermal behavioral model for RF power amplifiers," in *IEEE MTT-S Digest*, Philadelphia , PA, June 2003, pp. 351-354.
- [21] S.A. Maas, *Nonlinear Microwave Circuits*, Artech House, 1988.
- [22] T. Wang and T. Brazil, "The estimation of Volterra transfer functions with applications to RF Power amplifier behavior evaluation for CDMA digital communications," in *IEEE MTT-S Digest*, 2000.
- [23] A. Leke and J. S. Kenney, "Behavioral modeling of narrowband microwave power amplifiers with applications in simulating spectral regrowth," in *IEEE MTT-S Digest*, 1996.

- [24] S. A. Maas, "Volterra analysis of spectral regrowth," *IEEE Microwave and Guided Wave Letters*, vol. 7, no. 7, pp 192-193, July 1997.
- [25] R. A. Minasian, "Intermodulation distortion analysis of MESFET amplifiers using the Volterra series representation," *IEEE Transactions on Microwave Theory Tech.*, vol. 28, no. 1, pp. 1-8, January 1980.
- [26] P. K. Kenington, "Linearized RF Transmitter Techniques," in *IEEE MTT-S Workshop*, Baltimore, ML, June 1998.
- [27] P. K. Kenington, "Linearisation in Base-station Equipment," in *IEEE MTT-S Workshop*, Boston, MA, June 2000.
- [28] P. B. Kenington and A. Bateman, "RF Linear Amplifier Design," *Technical Paper*.
- [29] D. Jing and W. S. Chan, "New linearization method using interstage second harmonic enhancement," *IEEE Microwave and Guided Wave Letters*, vol. 8, no. 11, pp. 402-404, November 1998.
- [30] Y. K. G. Hau, V. Postoyalko and J. R. Richardson, "Effects of impedance mismatch and imperfect isolation on distortion cancellation in feedforward amplifiers," *IEE Proc.- Circuits Devices Syst.*, vol. 145, no. 1, pp. 35-39, February 1998.
- [31] L. Silverman and C. D. Plato, "Vector modulator enhances feedforward cancellation," *Microwaves & RF*, pp. 83 – 90, March 1998.
- [32] W. T. Thornton and L. E. Larson, "An improved 5.7 GHz ISM-Band feedforward amplifier utilizing vector modulators for phase and attenuation control", *Microwave Journal*, pp. 96 – 106, December 1999.
- [33] E. E. Eid and F. M. Ghannouchi, "Adaptive nulling loop control for 1.7-GHz feedforward linearization systems," *IEEE Transactions on Microwave Theory Tech.*, vol. 45, no.1, pp. 83-86, January 1997.
- [34] Q. Cheng, C. Yiyuan and Z. Xiaowei, "A 1.9 GHz adaptive feedforward power amplifier," *Microwave Journal*, pp. 86-96, November 1998.
- [35] B. Arntz, "Second order effects in feedforward amplifiers," *Applied Microwave and Wireless*, pp. 66-75, January 2000.
- [36] D. Wills, "A control system for a feedforward amplifier," *Microwave Journal*, pp. 24-34, April 1999.
- [37] J. K. Cavers, "Adaptation behavior of a feedforward amplifier linearizer," *IEEE Trans. On Vehicular Technology*, vol. 44, no.1, February 1995.

- [38] S. J. Grant and J. K. Cavers, "A DSP controlled adaptive feedforward amplifier linearizer," *Technical Paper*.
- [39] A. M. Smith, J. K. Cavers, "A wideband architecture for adaptive feedforward linearization," in *IEEE Vehicular Technology Conference*, 1998.
- [40] P. B. Kenington, "Efficiency of feedforward amplifiers," *IIE Proceedings-G*, vol. 139, no. 5, pp. 591-593, October 1992.
- [41] R. J. Wilkinson and P. B. Kenington, "Specification of error amplifiers for use in feedforward transmitters," *IIE Proceedings-G*, vol. 139, no. 4, pp. 477-480, August 1992.
- [42] E. E. Eid, F. M. Ghannouchi, and F. Beaugard, "Optimal feedforward linearization system design," *Microwave Journal*, pp. 78-86, November 1995.
- [43] K. J. Parsons and P.B. Kenington, "The efficiency of a feedforward amplifier with delay loss", *IEEE Trans. Vehicular Technology*, vol. 43, no. 2, pp. 407-412, May 1994.
- [44] K. J. Parsons and P. B. Kenington, "Effect of delay mismatch on a feedforward amplifier", *IIE Proceedings-Circuits Devices Syst.*, vol. 141, no. 2, pp. 140-144, April 1994.
- [45] P. K. Kenington, "Achieving high efficiency in multicarrier basestation power amplifiers," in *Microwave Engineering Europe*, pp. 83-90, August/September 1999.
- [46] C. L. Larose and F. M. Ghannouchi, "Optimization of feedforward amplifier power efficiency on the basis of drive statistics," *IEEE Transactions on Microwave Theory Tech.*, vol. 51, no. 1, pp 41-54, January 2003.
- [47] Y. Suzuki, T. Hirota, and T. Nojima, "Highly efficient feed-forward amplifier using a Class-F Doherty amplifier," in *IEEE MTT-S Digest*, Philadelphia, PA, June 2003. pp 77-80.
- [48] P. K. Kenington and D.W. Bennett, "Linear distortion correction using a feedforward system", *IEEE Trans. On Vehicular Technology*, vol. 45, no.1, pp. 74 – 81, February 1996.
- [49] K. D. Tiepermann, "CDMA signals: A challenge for power amplifiers," *RF Design*, pp. 72-78, September 1996.
- [50] K. G. Gard, H. M. Gutierrez, and M. B. Steer, "Characterization of spectral regrowth in microwave amplifiers based on the nonlinear transformation of a complex Gaussian process," *IEEE Transactions on Microwave Theory Tech.*, vol. 47, no. 7, pp 1059-1069, July 1999.

- [51] K. M. Gharaibeh, K. Gard, and M. B. Steer, "Statistical modeling of the interaction of multiple signals in nonlinear RF Systems," in *IEEE MTT-S Digest*, June 2002, pp. 143-146.
- [52] S. Yi, S. Nam, S. Oh, and J. Han, "Prediction of a CDMA output spectrum based on intermodulation products of two-tone test", *IEEE Transactions on Microwave Theory Tech.*, vol. 49, no. 5, pp 938-946, May 2001.
- [53] T.T. Ha, *Solid-state Microwave Amplifier Design*, John Wiley and Sons, 1981.
- [54] S. Haykin, *Communication Systems*, John Wiley and Sons, 1983.
- [55] A. Papoulis, *Probability, Random Variables, and Stochastic Processes*, New York: McGraw-Hill Book Company, 1984, pp.155-159.
- [56] M. Jeruchim, P.Balaban, and K. Shanmugan, *Simulation of Communication Systems*, Plenum Press, 1994.

## APPENDIX A

### COEFFICIENTS FOR THE MODEL PRESENTED IN CHAPTER 4

Expressions for the coefficients indicated in (4.17) are listed as follows:

$$D_1 = l_1 l_2 l_4 a_1 + \frac{b_1 l_3}{C_1 C_4} - \frac{a_1 b_1 l_1}{C_2 C_3 C_4} \quad (\text{A.1})$$

$$D_3 = l_1^3 l_2 l_4 a_3 - \frac{a_3 b_1 l_1^3}{C_2 C_3 C_4} + \frac{b_3 l_3^3}{C_1^3 C_4} - \frac{3b_3 a_1 l_1 l_3^2}{C_1^2 C_2 C_3 C_4} + \frac{3a_1^2 b_3 l_1^2 l_3}{C_1 C_4 C_2^2 C_3^2} - \frac{a_1^3 b_3 l_1^3}{C_4 C_2^3 C_3^3} \quad (\text{A.2})$$

$$D_5 = \frac{-3b_3 a_3 l_3^2 l_1^3}{C_1^2 C_2 C_3 C_4} + \frac{6a_1 a_3 b_3 l_1^4 l_3}{C_1 C_2^2 C_3^2 C_4} - \frac{3a_1^2 a_3 b_3 l_1^5}{C_2^3 C_3^3 C_4} \quad (\text{A.3})$$

$$D_7 = \frac{3a_3^2 b_3 l_3 l_1^6}{C_1 C_2^2 C_3^2 C_4} - \frac{3a_1 a_3^2 b_3 l_1^7}{C_2^3 C_3^3 C_4} \quad (\text{A.4})$$

$$D_9 = \frac{-b_3 a_3^3 l_1^9}{C_2^3 C_3^3 C_4} \quad (\text{A.5})$$

Expressions for the coefficients indicated in (4.38) are listed as follows:

$$\begin{aligned} M_1 = & D_1^2 + 6D_1 D_3 K + 30D_1 D_5 K^2 + 9D_3^2 K^2 + 90D_3 D_5 K^3 + 225D_5^2 K^4 + 210D_1 D_7 K^3 + \\ & 1890D_1 D_9 K^4 + 630D_3 D_7 K^4 + 5670D_3 D_9 K^5 + 3150D_5 D_7 K^5 + 28350D_5 D_9 K^6 + \\ & 11025D_7^2 K^6 + 198450D_7 D_9 K^7 + 893025D_9^2 K^8 \end{aligned} \quad (\text{A.6})$$

$$M_3 = 6D_3^2 + 120D_3D_5K + 600D_5^2K^2 + 1260D_3D_7K^2 + 15120D_3D_9K^3 + 12600D_5D_7K^3 + 151200D_5D_9K^4 + 66150D_7^2K^4 + 1587600D_7D_9K^5 + 9525600D_9^2K^6 \quad (\text{A.7})$$

$$M_5 = 120D_5^2 + 5040D_5D_7K + 90720D_5D_9K^2 + 52920D_7^2K^2 + 1905120D_7D_9K^3 + 17146080D_9^2K^4 \quad (\text{A.8})$$

$$M_7 = 5040D_7^2 + 362880D_7D_9K + 6531840D_9^2K^2 \quad (\text{A.9})$$

$$M_9 = 362880D_9^2 \quad (\text{A.10})$$

Expressions for the coefficients indicated in (4.53) are listed as follows:

$$D_1'' = l_1l_2l_4a_1 \quad (\text{A.11})$$

$$D_3'' = l_1^3l_2l_4a_3 \quad (\text{A.12})$$

$$D_1' = D_1 - D_1'' \quad (\text{A.13})$$

$$D_3' = D_3 - D_3'' \quad (\text{A.14})$$

$$D_5' = D_5, D_7' = D_7, D_9' = D_9 \quad (\text{A.15})$$

Expressions for coefficients indicated in (4.54) are listed as follows:

$$M_1' = D_1'^2 + 6D_1'D_3'K + 30D_1'D_5'K^2 + 9D_3'^2K^2 + 90D_3'D_5'K^3 + 225D_5'^2K^4 + 210D_1'D_7'K^3 + 1890D_1'D_9'K^4 + 630D_3'D_7'K^4 + 5670D_3'D_9'K^5 + 3150D_5'D_7'K^5 + 28350D_5'D_9'K^6 + 11025D_7'^2K^6 + 198450D_7'D_9'K^7 + 893025D_9'^2K^8 + D_1''^2 + 9D_3''^2K^2 + 6D_1''D_3''K \quad (\text{A.16})$$

$$M_3' = 6D_3'^2 + 120D_3'D_5'K + 600D_5'^2K^2 + 1260D_3'D_7'K^2 + 15120D_3'D_9'K^3 + 12600D_5'D_7'K^3 + 151200D_5'D_9'K^4 + 66150D_7'^2K^4 + 1587600D_7'D_9'K^5 + 9525600D_9'^2K^6 + 6D_3''^2 \quad (\text{A.17})$$

$$M_1'' = 945D_9'D_1''K^4 + 2835D_9'D_3''K^5 + 105D_7'D_1''K^3 + 315D_7'D_3''K^4 + 15D_5'D_1''K^2 + 45D_5'D_3''K^3 + 3D_3'D_1''K + 9D_3'D_3''K^2 + D_1'D_1'' + 3D_1'D_3''K \quad (\text{A.18})$$

$$M_3'' = 7560D_9' D_3'' K^3 + 630D_7' D_3'' K^2 + 60D_5' D_3'' K + 6D_3' D_3'' \quad (\text{A.19})$$

$$M_5 = 120D_5'^2 + 5040D_5' D_7' K + 90720D_5' D_9' K^2 + 52920D_7'^2 K^2 + 1905120D_7' D_9' K^3 + 17146080D_9'^2 K^4 \quad (\text{A.20})$$

$$M_7 = 5040D_7'^2 + 362880D_7' D_9' K + 6531840D_9'^2 K^2 \quad (\text{A.21})$$

$$M_9 = 362880D_9'^2 \quad (\text{A.22})$$

The modified D Coefficients indicated in (4.60) are listed as follows:

$$D_1 = -\frac{a_1 b_1 l_1}{C_2 C_3 C_4}, \quad D_{13} = \frac{b_1 l_3}{C_1 C_4}, \quad D_{10} = l_1 l_2 l_4 a_1 \quad (\text{A.23})$$

$$D_3 = -\frac{a_3 b_1 l_1^3}{C_2 C_3 C_4} - \frac{a_1^3 b_3 l_1^3}{C_4 C_2^3 C_3^3}, \quad D_{11} = l_1^3 l_2 l_4 a_3, \quad D_4 = \frac{3a_1^2 b_3 l_1^2 l_3}{C_1 C_4 C_2^2 C_3^2}, \quad D_{12} = \frac{b_3 l_3^3}{C_1^3 C_4} \quad (\text{A.24})$$

$$D_2 = -\frac{3b_3 a_1 l_1 l_3^2}{C_1^2 C_2 C_3 C_4} \quad (\text{A.25})$$

$$D_5 = -\frac{3a_1^2 a_3 b_3 l_1^5}{C_2^3 C_3^3 C_4}, \quad D_{14} = \frac{-3b_3 a_3 l_3^2 l_1^3}{C_1^2 C_2 C_3 C_4}, \quad D_6 = \frac{6a_1 a_3 b_3 l_1^4 l_3}{C_1 C_2^2 C_3^2 C_4} \quad (\text{A.26})$$

$$D_7 = -\frac{3a_1 a_3^2 b_3 l_1^7}{C_2^3 C_3^3 C_4}, \quad D_8 = \frac{3a_3^2 b_3 l_3 l_1^6}{C_1 C_2^2 C_3^2 C_4} \quad (\text{A.27})$$

$$D_9 = \frac{-b_3 a_3^3 l_1^9}{C_2^3 C_3^3 C_4} \quad (\text{A.28})$$

## APPENDIX B

### CALCULATED EXPECTED VALUES FOR GAUSSIAN MULTI RANDOM VARIABLES

Modeling of feedforward systems considering delay mismatches in the first loop requires computation of expected values in the form  $E\{s_1^{m_1} \dots s_n^{m_n}\}$  where  $n$  is the number of distinct Gaussian random variables. For the model presented in Chapter 4  $n$  can increase up to 4. For  $n = 2$  a compact formula has been derived and presented in (4.30). However for greater  $n$  values the procedure outlined in 4.2.4 (Equations 4.61 – 4.63) needs to be followed. Following equations are the results for the expectations that are used in our analysis.

$$\begin{aligned} E\{s_1^9 s_2^6 s_3\} = & \\ & 85050K^6 R_1 R + 453600K^4 R_1 R^3 + 340200K^5 R_2 R^2 + 680400K^3 R_2 R^4 + \\ & 181440KR_2 R^6 + 272160K^2 R_1 R^5 + 14175K^7 R_2 \end{aligned} \quad (B.1)$$

$$\begin{aligned} E\{s_1^9 s_2^4 s_3\} = & \\ & 45360K^2 R_2 R^4 + 2835K^6 R_2 + 45360K^4 R_2 R^2 + 30240K^3 R_1 R^3 + \\ & 11340K^5 R_1 R \end{aligned} \quad (B.2)$$

$$\begin{aligned} E\{s_1^9 s_2^3 s_3^2\} = & \\ & 2835K^6 R + 45360K^2 R_2 R^3 + 7560K^4 R^3 + 5670K^4 R_1^2 R + 22680K^4 R_2 R^2 + \\ & 45360K^3 R_1 R_2 R^2 + 5670K^5 R_1 R_2 \end{aligned} \quad (B.3)$$

$$E\{s_1^9 s_2 s_3^2\} = 1890K^4 R_2 R_1 + 7560K^3 R_2^2 R + 945K^5 R \quad (\text{B.4})$$

$$E\{s_1^7 s_2^6 s_3\} = 37800K^2 R_2 R^4 + 5040R_2 R^6 + 1575K^6 R_2 + 9450K^5 R_1 R + 28350K^4 R_2 R^2 + 37800K^3 R_1 R^3 + 15120KR_1 R^5 \quad (\text{B.5})$$

$$E\{s_1^7 s_2^4 s_3\} = 315K^5 R_2 + 2520KR_2 R^4 + 3780K^3 R_2 R^2 + 2520K^2 R_1 R^3 + 1260K^4 R_1 R \quad (\text{B.6})$$

$$E\{s_1^7 s_2^3 s_3^2\} = 1890K^3 R_2^2 R + 3780K^2 R_1 R_2 R^2 + 2520KR_2^2 R^3 + 630K^3 R_1^2 R + 315K^5 R + 630K^3 R^3 + 630K^4 R_1 R_2 \quad (\text{B.7})$$

$$E\{s_1^7 s_2 s_3^2\} = 630K^2 R_2^2 R + 210K^3 R_1 R_2 + 105K^4 R \quad (\text{B.8})$$

$$E\{s_1^5 s_2^6 s_3\} = 720R_1 R^5 + 225K^5 R_2 + 1350K^4 R_1 R + 1800KR_2 R^4 + 2700K^3 R_2 R^2 + 3600K^2 R_1 R^3 \quad (\text{B.9})$$

$$E\{s_1^5 s_2^4 s_3\} = 240KR_1 R^3 + 180K^3 R_1 R + 120R_2 R^4 + 360K^2 R_2 R^2 + 45K^4 R_2 \quad (\text{B.10})$$

$$E\{s_1^5 s_2^3 s_3^2\} = 45K^4 R + 120K^2 R_2^2 R^3 + 360KR_1 R_2 R^2 + 180K^2 R_2^2 R + 90K^2 R_1^2 R + 60K^2 R^3 + 90K^3 R_1 R_2 \quad (\text{B.11})$$

$$E\{s_1^5 s_2 s_3^2\} = 15K^3 R + 30K^2 R_1 R_2 + 60KR_2^2 R \quad (\text{B.12})$$

$$E\{s_1^3 s_2^6 s_3\} = 270K^3 R_1 R + 360KR_1 R^3 + 45K^4 R_2 + 270K^2 R_2 R^2 \quad (\text{B.13})$$

$$E\{s_1^3 s_2^4 s_3\} = 24R_1 R^3 + 36K^2 R_1 R + 36KR_2 R^2 + 9K^3 R_2 \quad (\text{B.14})$$

$$E\{s_1^3 s_2^3 s_3^2\} = 6KR^3 + 18KR_1^2 R + 9K^3 R + 18KR_2^2 R + 18K^2 R_2 R_1 + 36R_1 R_2 R^2 \quad (\text{B.15})$$

$$E\{s_1^3 s_2 s_3^2\} = 3K^2 R + 6KR_1 R_2 + 6R_2^2 R \quad (\text{B.16})$$

$$E\{s_1 s_2^6 s_3\} = 90K^2 R_1 R + 15K^3 R_2 \quad (\text{B.17})$$

$$E\{s_1 s_2^4 s_3\} = 12KR_1R + 3K^2R_2 \quad (\text{B.18})$$

$$E\{s_1 s_2^3 s_3^2\} = 3K^2R + 6KR_1R_2 + 6R_1^2R \quad (\text{B.19})$$

$$E\{s_1 s_2 s_3^2\} = KR + 2R_1R_2 \quad (\text{B.20})$$

$$E\{s_1^9 s_2^2 s_3\} = 945K^5R_2 + 1890K^4R_1R + 7560K^3R_2R^2 \quad (\text{B.21})$$

$$E\{s_1^7 s_2^2 s_3\} = 630K^2R_2R^2 + 105K^4R_2 + 210K^3R_1R \quad (\text{B.22})$$

$$E\{s_1^5 s_2^2 s_3\} = 30K^2R_1R + 15K^3R_2 + 60KR_2R^2 \quad (\text{B.23})$$

$$E\{s_1^3 s_2^2 s_3\} = 6KR_1R + 3K^2R_2 + 6R_2R^2 \quad (\text{B.24})$$

$$E\{s_1 s_2^2 s_3\} = 2R_1R + KR_2 \quad (\text{B.25})$$

where  $R = E\{s_1 s_2\}$ ,  $R_1 = E\{s_2 s_3\}$ ,  $R_2 = E\{s_1 s_3\}$ ,  $K = E\{s^2\}$ .

$$\begin{aligned} E\{s_1^4 s_2 s_3^6 s_4\} = & \\ & 720R_1R_3R^4 + 180K^4R_1R_2 + 540K^3R^3 + 360KR^5 + 45K^5R + \\ & 1080K^3R_2R_3R + 2160K^2R_1R_3R^2 + 1080K^3R_1^2R + 270K^4R_1R_3 + \\ & 1440KR_1^2R^3 + 1440KR_2R_3R^3 + 1080K^2R_1R_2R^2 \end{aligned} \quad (\text{B.26})$$

$$\begin{aligned} E\{s_1^3 s_2^2 s_3^6 s_4\} = & \\ & 540K^3R_3R^2 + 360K^4R_1R + 270K^3R_2R_3^2 + 720KR^4R_3 + 270K^3R_2R^2 + \\ & 1080K^2R_1R_2R_3R + 90K^3R_1^2R_2 + 45K^5R_2 + 900K^2R_1R^3 + 720R_1R_3^2R^3 + \\ & 2160KR_1^2R_3R^2 + 1080KR_2R_3^2R^2 + 1080K^2R_1R_3^2R + 540K^2R_1^3R + \\ & 540K^3R_1^2R_3 \end{aligned} \quad (\text{B.27})$$

$$\begin{aligned} E\{s_1^2 s_2 s_3^6 s_4\} = & \\ & 360KR_1R_3R^2 + 180K^2R_1^2R + 90K^3R_1R_3 + 180K^2R_2R_3R + 30K^3R_1R_2 + \\ & 15K^4R + 90K^2R^3 \end{aligned} \quad (\text{B.28})$$

$$\begin{aligned} E\{s_1 s_2^2 s_3^6 s_4\} = & \\ & 360KR_1R_3^2R + 180K^2R_3R^2 + 90K^2R_2R_3^2 + 15K^4R_2 + 180K^2R_1^2R_3 + \\ & 120K^3R_1R \end{aligned} \quad (\text{B.29})$$

$$\begin{aligned}
E\{s_1^6 s_2 s_3^6 s_4\} = & \\
& 10800KR_1R_2R^4 + 21600K^2R_1^2R^3 + 225K^6R + 720R^7 + 10800KR_1R_2R^4 + \\
& 16200K^3R_1R_3R^2 + 16200K^3R_1R_2R^2 + 5400K^2R^5 + 8100K^4R_1^2R + \quad (B.30) \\
& 4320R_2R_3R^5 + 1350K^5R_1R_2 + 21600K^2R_2R_3R^3 + 1350K^5R_1R_3 + \\
& 4320R_1^2R^5 + 4050K^4R^3 + 8100K^4R_2R_3R
\end{aligned}$$

$$\begin{aligned}
E\{s_1^4 s_2 s_3^4 s_4\} = & \\
& 24R^5 + 144KR_1R_2R^2 + 36K^3R_1R_2 + 72K^2R^3 + 9K^4R + 96R_1^2R^3 + \quad (B.31) \\
& 144KR_1R_3R^2 + 36K^3R_1R_3 + 144K^2R_1^2R + 96R_2R_3R^3 + 144K^2R_2R_3R
\end{aligned}$$

$$\begin{aligned}
E\{s_1^3 s_2^2 s_3^4 s_4\} = & \\
& 9K^4R_2 + 96KR_1R^3 + 144R_1^2R_3R^2 + 36K^2R_2R_3^2 + 48R_3R^4 + 72KR_1^3R + \quad (B.32) \\
& 72K^2R_1^2R_3 + 54K^3R_1R + 72K^2R_3R^2 + 72R_2R_3^2R^2 + 36K^2R_2R^2 + \\
& 72KR_1R_3^2R + 144KR_1R_2R_3R + 18K^2R_1^2R_2
\end{aligned}$$

$$\begin{aligned}
E\{s_1^2 s_2 s_3^4 s_4\} = & \\
& 24KR_1^2R + 24R_1R_3R^2 + 3K^3R + 12K^2R_1R_3 + 24KR_2R_3R + 12KR^3 + \quad (B.33) \\
& 6K^2R_1R_2
\end{aligned}$$

$$\begin{aligned}
E\{s_1 s_2^2 s_3^4 s_4\} = & 18K^2R_1R + 12KR_2R_3^2 + 3K^3R_2 + 24R_1R_3^2R + 24KR_1^2R_3 + \quad (B.34) \\
& 24KR_3R^2
\end{aligned}$$

$$\begin{aligned}
E\{s_1^3 s_2^2 s_3^3 s_4^2\} = & \\
& 36R_1^4R + 24K^2R^3 + 72R_1^2R^3 + 36KR_1^3R_2 + 36KR_1^3R_3 + 18K^2R_2^2R + \\
& 72K^2R_1^2R + 18K^3R_1R_2 + 9K^4R + 36KR_1R_3R_2^2 + 18K^3R_1R_3 + 12R^5 + \quad (B.35) \\
& 144R_1^2R_2R_3R + 18K^2R_3^2R + 36KR_1R_2R_3^2 + 108KR_1R_2R^2 + 36R_2^2R_3^2R + \\
& 36K^2R_2R_3R + 72R_2R_3R^3 + 108KR_1R_3R^2
\end{aligned}$$

$$\begin{aligned}
E\{s_1^2 s_2 s_3^3 s_4^2\} = & \\
& 12KR_1^2R_2 + 12K^2R_1R + 12R_1^3R + 3K^3R_3 + 6KR_1^2R_3 + 12KR_2R^2 + 12R_1R^3 + \quad (B.36) \\
& 5KR_3R_2^2 + 24R_1R_2R_3R + 6KR_3R^2
\end{aligned}$$

$$E\{s_1 s_2^2 s_3^3 s_4^2\} = 24R_1 R_3 R^2 + 6KR_3^2 R + 12KR_2 R_3 R + 12R_1 R_2 R_3^2 + 12R_1^3 R_3 + 6K^2 R_1 R_2 + 3K^3 R + 18KR_1^2 R + 6K^2 R_1 R_3 + 6KR^3 \quad (B.37)$$

$$E\{s_1^2 s_2 s_3^2 s_4\} = K^2 R + 2R^3 + 2KR_1 R_2 + 4R_1^2 R + 4RR_3 R_2 + 2KR_1 R_3 \quad (B.38)$$

$$E\{s_1 s_2^2 s_3^2 s_4\} = K^2 R_2 + 2R_2 R_3^2 + 4KR_1 R + 4R_3 R^2 + 4R_1^2 R_3 \quad (B.39)$$

$$E\{s_1 s_2^2 s_3 s_4^2\} = K^2 R + 2R^3 + 2KR_1 R_3 + 4R_1^2 R + 4RR_3 R_2 + 2KR_1 R_2 \quad (B.40)$$

where  $s_3(t)=s_1(t+\tau)$ ,  $s_4(t)=s_2(t+\tau)$ ,  $R=E\{s_1 s_3\}=E\{s_2 s_4\}$ ,  $R_1=E\{s_3 s_4\}=E\{s_1 s_2\}$ ,  $R_2=E\{s_2 s_3\}$ ,  $R_3=E\{s_1 s_4\}$ .

Using the computed expectations given above, feedforward output autocorrelation function coefficients can be determined. The coefficients for the closed form part of the output autocorrelation function (Equation 4.64) are given below. The matrix 'A' which is used for the computational part (Equation 4.66) is also presented just after the coefficients.

### Closed form coefficients:

$$M_1 = K^8(893025D_9^2) + 2*99225*D_9*D_7*K^7 +$$

$$K^6(170100*D_9*D_8*R_1 + 28350*D_9*D_5 + 5670*D_9*D_14 + 11025*D_7^2 + 225*D_8^2) +$$

$$K^5(22680*D_9*D_6*R_1 + 5670*D_9*D_3 + 1890*D_9*D_2 + 18900*D_8*D_7*R_1 + 3150*D_5*D_7 + 630*D_14*D_7 + 90*D_8*D_6) +$$

$$K^4(11340*D_9*D_14*R_1^2 + 3780*D_9*D_4*R_1 + 1890*D_9*D_1 + 30*D_8*D_4 + 2520*D_6*D_7*R_1 + 630*D_3*D_7 + 210*D_2*D_7 + 8100*D_8^2*R_1^2 + 2700*D_8*D_5*R_1 + 360*D_8*D_14*R_1 + 90*D_12*D_8 + 225*D_5^2 + 90*D_14*D_5 + 9*D_6^2 + 9*D_14^2) +$$

$$K^3(1260*D_14*D_7*R_1^2 + 420*D_4*D_7*R_1 + 270*D_3*D_8*R_1 + 210*D_1*D_7 + 2160*D_8*D_6*R_1^2 + 240*D_2*D_8*R_1 + 30*D_13*D_8 + 360*D_6*D_5*R_1 + 90*D_5*D_3 + 30*D_5*D_2 + 108*D_6*D_14*R_1 + 6*D_6*D_4 + 18*D_6*D_12 + 18*D_3*D_14 + 6*D_14*D_2) +$$

$$K^2(1080*D_8*D_14*R_1^3 + 360*D_8*D_4*R_1^2 + 180*D_8*D_1*R_1 + 180*D_14*D_5*R_1^2 + 60*D_5*D_4*R_1 + 30*D_5*D_1 + 144*D_6^2*R_1^2 + 72*D_6*D_3*R_1 + 24*D_6*D_1*R_1 + 36*D_6*D_2*R_1 + 6*D_6*D_13 + 9*D_3^2 + 36*D_3*D_14*R_1^2 + 6*D_3*D_2 + 72*D_14^2*R_1^2 + 24*D_14*D_4*R_1 + 6*D_14*D_1 + 36*D_14*D_12*R_1 + D_4^2 + 6*D_4*D_12 + D_2^2 + 9*D_11^2 + 9*D_12^2) +$$

$$K(144*D6*D14*R1^3+48*D6*D4*R1^2+12*D3*D4*R1+6*D3*D1+36*D14*D2*R1^2+12*D14*D13*R1+8*D2*D4*R1+2*D4*D13+2*D1*D2+12*D2*D12*R1+D10^2+6*D10*D11+6*D12*D13+36*D14^2*R1^4+24*D14*D4*R1^3+12*D14*D1*R1^2+4*D4^2*R1^2+4*D1*D4*R1+D1^2+4*D2^2*R1^2+4*D2*D13*R1 +D13^2);$$

$$M3=9525600*D9^2*K^6+2*793800*D9*D7*K^5+$$

$$K^4(907200*D9*D8*R1+151200*D9*D5+2*7560*D9*D14+66150*D7^2+4050*D8^2)$$

$$K^3(60480*D9*D6*R1+15120*D9*D3+75600*D8*D7*R1+12600*D5*D7+1260*D14*D7+1080*D8*D6)+$$

$$K^2(5040*D6*D7*R1+1260*D3*D7+180*D8*D4+21600*D8^2*R1^2+7200*D8*D5*R1+1800*D8*D14*R1+600*D5^2+120*D14*D5+72*D6^2+24*D14^2)+$$

$$K(2880*D8*D6*R1^2+720*D8*D3*R1+480*D5*D6*R1+120*D5*D3+192*D6*D14*R1+12*D3*D14+24*D6*D4+12*D14*D2)+$$

$$96*D6^2*R1^2+48*D6*D3*R1+6*D3^2+72*D14^2*R1^2+24*D14*D4*R1+2*D4^2+2*D2^2+6*D11^2+6*D12^2);$$

$$M5= K^4*(17146080*D9^2) + K^3*(1905120*D9*D7) +$$

$$K^2*(544320*D9*D8*R1+90720*D9*D5+52920*D7^2+5400*D8^2)+$$

$$K*(30240*D8*D7*R1+5040*D5*D7+720*D8*D6)+$$

$$4320*D8^2*R1^2+2*720*D8*D5*R1+120*D5^2+24*D6^2+12*D14^2;$$

$$M7=6531840*D9^2*K^2+362880*D9*D7*K+5040*D7^2+720*D8^2;$$

$$M9=362880*D9^2;$$

$$M2=14175*D9*D8*K^7+$$

$$K^6*(2835*D9*D6+1575*D8*D7)+$$

$$K^5*(945*D9*D4+45*D8*D14+2835*D9*D12+1350*D8^2*R1+315*D6*D7+225*D8*D5)+$$

$$K^4*(945*D9*D13+105*D4*D7+630*D14*D7*R1+315*D12*D7+180*D8*D6*R1+270*D8*D6*R1+45*D8*D3+15*D2*D8+45*D6*D5+9*D6*D14)+$$

$$K^3*(210*D2*D7*R1+90*D8*D4*R1+30*D8*D4*R1+105*D13*D7+15*D1*D8+90*D8*D14*R1^2+540*D8*D14*R1^2+270*D8*D12*R1+90*D14*D5*R1+15*D5*D4+36*D6^2*R1+9*D6*D3+45*D5*D12+3*D6*D2+18*D14^2*R1+3*D14*D4+9*D14*D12)+$$

$$K^2*(180*D8*D2*R1^2+90*D8*D13*R1+30*D5*D2*R1+15*D5*D13+72*D6*D14*R1^2+18*D6*D14*R1^2+12*D6*D4*R1+6*D6*D4*R1+3*D6*D1+36*D6*D12*R1+18*D3*D14*R1+3*D3*D4+9*D3*D12+6*D14*D2*R1+6*D14*D2*R1+3*D14*D13+ D2*D4+3*D2*D12)+$$

$$K*(24*D6*D2*R1^2+12*D6*D13*R1+6*D3*D2*R1+3*D3*D13+36*D14^2*R1^3+12*D14*D4*R1^2+6*D14*D4*R1^2+6*D14*D1*R1+18*D14*D12*R1^2+2*D4^2*R1+D1*D4+6*D4*D12*R1+3*D1*D12+ D2*D13+ D1*D13+2*D2^2*R1)+$$

$$12*D14*D2*R1^3+6*D14*D13*R1^2+4*D2*D4*R1^2+2*D4*D13*R1+2*D1*D2*R1$$

$$\begin{aligned}
M2' &= K^5 * 2835 * D9 * D11 + K^4 * (945 * D9 * D10 + 315 * D11 * D7) + \\
& K^3 * (105 * D10 * D7 + 270 * D11 * D8 * R1 + 45 * D5 * D11 + 9 * D14 * D11) + \\
& K^2 * (90 * D10 * D8 * R1 + 15 * D5 * D10 + 36 * D6 * D11 * R1 + 9 * D3 * D11 + 3 * D14 * D10 + 3 * D2 * D11) + \\
& K * (3 * D3 * D10 + 6 * D4 * D11 * R1 + 3 * D1 * D11 + D2 * D10 + 18 * D14 * D11 * R1^2 + 12 * D6 * D10 * R1) + \\
& 6 * D14 * D10 * R1^2 + 2 * D4 * D10 * R1 + D1 * D10
\end{aligned}$$

$$M4 = K^3 * 7560 * D9 * D12 + K^2 * 630 * D12 * D7 + K * (360 * D12 * D8 * R1 + 60 * D5 * D12 + 6 * D14 * D12) + 24 * D6 * D12 * R1 + 6 * D3 * D12;$$

$$M4' = K^3 * 7560 * D9 * D11 + K^2 * 630 * D11 * D7 + K * (360 * D11 * D8 * R1 + 60 * D5 * D11 + 6 * D3 * D11 + 6 * D14 * D11) + 24 * D6 * D11 * R1;$$

$$M6 = K^4 * 45 * D11 * D8 + K^3 * (15 * D10 * D8 + 9 * D6 * D11$$

$$K^2 * (3 * D6 * D10 + 18 * D14 * D11 * R1 + 3 * D4 * D11 + 9 * D11 * D12 +$$

$$K * (6 * D14 * D10 * R1 + D4 * D10 + 6 * D2 * D11 * R1 + 3 * D10 * D12 + 3 * D11 * D13) +$$

$$2 * D2 * D10 * R1 + D10 * D13;$$

$$M6' = 6 * D11 * D12$$

D coefficients are given in Appendix A (A.23 – A.28).

#### Matrix 'A' which is used in (4.66)

%	C1	C2	C3	K	R	R1	R2	R3	R4	R5	R6	R7
A=[	9	8	340200	5	2	0	1	0	0	0	0	0
	9	8	680400	3	4	0	1	0	0	0	0	0
	9	8	181440	1	6	0	1	0	0	0	0	0
	9	6	45360	2	4	0	1	0	0	0	0	0
	9	6	45360	4	2	0	1	0	0	0	0	0
	9	14	45360	2	3	0	2	0	0	0	0	0
	9	14	22680	4	1	0	2	0	0	0	0	0
	9	14	45360	3	2	1	1	0	0	0	0	0
	9	14	5670	5	0	1	1	0	0	0	0	0
	9	4	7560	3	2	0	1	0	0	0	0	0
	9	2	1890	4	0	1	1	0	0	0	0	0
	9	2	7560	3	1	0	2	0	0	0	0	0
	7	8	37800	2	4	0	1	0	0	0	0	0
	7	8	5040	0	6	0	1	0	0	0	0	0
	7	8	28350	4	2	0	1	0	0	0	0	0
	7	6	2520	1	4	0	1	0	0	0	0	0
	7	6	3780	3	2	0	1	0	0	0	0	0
	7	14	1890	3	1	0	2	0	0	0	0	0
	7	14	3780	2	2	1	1	0	0	0	0	0

7	14	2520	1	3	0	2	0	0	0	0	0
7	4	630	2	2	0	1	0	0	0	0	0
7	2	630	2	1	0	2	0	0	0	0	0
8	8	10800	1	4	1	0	1	0	0	0	0
8	8	10800	1	4	1	1	0	0	0	0	0
8	8	16200	3	2	1	0	1	0	0	0	0
8	8	16200	3	2	1	1	0	0	0	0	0
8	8	4320	0	5	0	1	1	0	0	0	0
8	8	21600	2	3	0	1	1	0	0	0	0
8	8	8100	4	1	0	1	1	0	0	0	0
5	8	1800	1	4	0	0	1	0	0	0	0
5	8	2700	3	2	0	0	1	0	0	0	0
6	8	720	0	4	1	1	0	0	0	0	0
6	8	1080	3	1	0	1	1	0	0	0	0
6	8	2160	2	2	1	1	0	0	0	0	0
6	8	1440	1	3	0	1	1	0	0	0	0
6	8	1080	2	2	1	0	1	0	0	0	0
3	8	270	2	2	0	1	0	0	0	0	0
8	14	540	3	2	0	0	1	0	0	0	0
8	14	270	3	0	0	1	2	0	0	0	0
8	14	720	1	4	0	0	1	0	0	0	0
8	14	270	3	2	0	1	0	0	0	0	0
8	14	1080	2	1	1	1	1	0	0	0	0
8	14	720	0	3	1	0	2	0	0	0	0
8	14	2160	1	2	2	0	1	0	0	0	0
8	14	1080	1	2	0	1	2	0	0	0	0
8	14	1080	2	1	1	0	2	0	0	0	0
8	4	360	1	2	1	0	1	0	0	0	0
8	4	180	2	1	0	1	1	0	0	0	0
8	2	360	1	1	1	0	2	0	0	0	0
8	2	180	2	2	0	0	1	0	0	0	0
8	2	90	2	0	0	1	2	0	0	0	0
8	11	270	2	0	0	0	0	2	0	1	0
8	12	270	2	1	0	0	2	0	0	0	0
5	6	120	0	4	0	1	0	0	0	0	0
5	6	360	2	2	0	1	0	0	0	0	0
5	14	120	0	3	0	2	0	0	0	0	0
5	14	360	1	2	1	1	0	0	0	0	0
5	14	180	2	1	0	2	0	0	0	0	0
5	4	60	1	2	0	1	0	0	0	0	0
5	2	60	1	1	0	2	0	0	0	0	0
6	6	144	1	2	1	1	0	0	0	0	0
6	6	144	1	2	1	0	1	0	0	0	0
6	6	96	0	3	0	1	1	0	0	0	0
6	6	144	2	1	0	1	1	0	0	0	0
6	3	36	1	2	0	1	0	0	0	0	0
6	14	144	0	2	2	0	1	0	0	0	0
6	14	36	2	0	0	1	2	0	0	0	0
6	14	48	0	4	0	0	1	0	0	0	0
6	14	72	2	2	0	0	1	0	0	0	0
6	14	72	0	2	0	1	2	0	0	0	0
6	14	36	2	2	0	1	0	0	0	0	0
6	14	72	1	1	1	0	2	0	0	0	0
6	14	144	1	1	1	1	1	0	0	0	0
6	4	24	0	2	1	0	1	0	0	0	0
6	4	24	1	1	0	1	1	0	0	0	0
6	2	12	1	0	0	1	2	0	0	0	0
6	2	24	0	1	1	0	2	0	0	0	0
6	2	24	1	2	0	0	1	0	0	0	0

6	11	36	1	0	0	0	0	2	0	1	0
6	12	36	1	1	0	0	2	0	0	0	0
3	14	18	1	1	0	2	0	0	0	0	0
3	14	36	0	2	1	1	0	0	0	0	0
3	4	6	0	2	0	1	0	0	0	0	0
3	2	6	0	1	0	2	0	0	0	0	0
14	14	18	2	1	0	2	0	0	0	0	0
14	14	36	1	0	1	2	1	0	0	0	0
14	14	144	0	1	2	1	1	0	0	0	0
14	14	18	2	1	0	0	2	0	0	0	0
14	14	36	1	0	1	1	2	0	0	0	0
14	14	108	1	2	1	1	0	0	0	0	0
14	14	36	0	1	0	2	2	0	0	0	0
14	14	36	2	1	0	1	1	0	0	0	0
14	14	72	0	3	0	1	1	0	0	0	0
14	14	108	1	2	1	0	1	0	0	0	0
14	4	12	1	2	0	1	0	0	0	0	0
14	4	6	1	0	0	2	1	0	0	0	0
14	4	24	0	1	1	1	1	0	0	0	0
14	4	6	1	2	0	0	1	0	0	0	0
14	2	24	0	2	1	0	1	0	0	0	0
14	2	6	1	1	0	0	2	0	0	0	0
14	2	12	1	1	0	1	1	0	0	0	0
14	2	12	0	0	1	1	2	0	0	0	0
14	11	18	1	0	0	0	0	1	0	2	0
14	11	36	0	0	1	0	0	2	0	1	0
14	12	18	1	2	0	0	1	0	0	0	0
14	12	36	0	1	1	0	2	0	0	0	0
4	4	4	0	1	0	1	1	0	0	0	0
4	2	2	0	0	0	1	2	0	0	0	0
4	2	4	0	2	0	0	1	0	0	0	0
4	11	6	0	0	0	0	0	2	0	1	0
4	12	6	0	1	0	0	2	0	0	0	0
2	2	4	0	1	0	1	1	0	0	0	0
2	11	6	0	0	0	0	0	1	0	2	0
2	12	6	0	2	0	0	1	0	0	0	0];

## APPENDIX C

### COEFFICIENTS FOR THE CUBE OF A TONE STREAM

The analysis presented in Chapter 6 involves computation of the cube of a series of sinusoidal signals with arbitrary weighting coefficients. The result of this computation is a new series of sinusoids with new coefficients. Hence, the following can be written:

$$\left[ \sum_{n=1}^p m_n \cos(n\omega_m t) \right]^3 = \left[ \sum_{n=0}^{3p} m'_n \cos(n\omega_m t) \right] \quad (\text{C.1})$$

Below  $m'$  coefficients for  $p=4$  in terms of  $m$  coefficients are given:

$$\begin{aligned} m'_0 &= \frac{3}{4}m_1^2m_2 + \frac{3}{2}m_1m_2m_3 + \frac{3}{2}m_1m_3m_4 + \frac{3}{4}m_2^2m_4 \\ m'_1 &= \frac{3}{4}m_1^2m_3 + \frac{3}{4}m_1^3 + \frac{3}{2}m_1m_2^2 + \frac{3}{2}m_1m_3^2 + \\ &\quad \frac{3}{4}m_2^2m_3 + \frac{3}{2}m_1m_2m_4 + \frac{3}{2}m_1m_4^2 + \frac{3}{2}m_2m_3m_4 \\ m'_2 &= \frac{3}{2}m_2m_3^2 + \frac{3}{2}m_1^2m_2 + \frac{3}{4}m_2^3 + \frac{3}{2}m_1m_2m_3 + \frac{3}{2}m_1m_3m_4 + \\ &\quad \frac{3}{2}m_2m_4^2 + \frac{3}{4}m_3^2m_4 + \frac{3}{4}m_1^2m_4 \\ m'_3 &= \frac{3}{2}m_1^2m_3 + \frac{3}{2}m_2^2m_3 + \frac{3}{4}m_3^3 + \frac{1}{4}m_1^3 + \frac{3}{4}m_1m_2^2 + \\ &\quad \frac{3}{2}m_2m_3m_4 + \frac{3}{2}m_3m_4^2 + \frac{3}{2}m_1m_2m_4 \end{aligned}$$

$$\begin{aligned}
m'_4 &= \frac{3}{4}m_1^2m_2 + \frac{3}{4}m_2m_3^2 + \frac{3}{2}m_1m_2m_3 + \frac{3}{2}m_1^2m_4 + \frac{3}{2}m_2^2m_4 + \frac{3}{2}m_3^2m_4 + \frac{3}{4}m_4^3 \\
m'_5 &= \frac{3}{4}m_1m_2^2 + \frac{3}{4}m_1m_3^2 + \frac{3}{4}m_1^2m_3 + \frac{3}{4}m_3m_4^2 + \frac{3}{2}m_1m_2m_4 + \frac{3}{2}m_2m_3m_4 \\
m'_6 &= \frac{1}{4}m_2^3 + \frac{3}{2}m_1m_2m_3 + \frac{3}{4}m_2m_4^2 + \frac{3}{4}m_1^2m_4 + \frac{3}{2}m_1m_3m_4 \\
m'_7 &= \frac{3}{4}m_1m_3^2 + \frac{3}{4}m_2^2m_3 + \frac{3}{4}m_1m_4^2 + \frac{3}{2}m_1m_2m_4 \\
m'_8 &= \frac{3}{4}m_2m_3^2 + \frac{3}{4}m_2^2m_4 + \frac{3}{2}m_1m_3m_4 \\
m'_9 &= \frac{1}{4}m_3^3 + \frac{3}{2}m_2m_3m_4 + \frac{3}{4}m_1m_4^2 \\
m'_{10} &= \frac{3}{4}m_2m_4^2 + \frac{3}{4}m_3^2m_4 \\
m'_{11} &= \frac{3}{4}m_3m_4^2 \\
m'_{12} &= \frac{1}{4}m_4^3
\end{aligned}$$

## VITA

Arslan Hakan Coskun was born in Ankara, Turkey on March 7, 1972. He received his B.Sc. degree (with high honors) in Electrical and Electronics Engineering from Middle East Technical University, Ankara, Turkey, in June 1993, his M.Sc. degree in Electrical and Electronics Engineering from Arizona State University, Tempe, AZ, in May 1996. From 1993 to 1994 he was with Turkish Scientific and Technical Research Institute (TUBITAK), Ankara, Turkey where he worked on modeling of inertial navigation systems. Since 1996 he has been with ASELSAN Electronics Industries, Inc, Ankara, Turkey, where he is a Senior Engineer responsible for the design and development of radio frequency wideband high power amplifiers for wireless products. His current research interests are in the areas of power amplifier design and power amplifier linearization for wireless applications.

Mr. Coskun received a Fulbright scholarship.

### Publications

- A. H. Coskun, and S. Demir “ A mathematical characterization and analysis of a feedforward circuit for CDMA applications,” *IEEE Trans. Microwave Theory Tech.*, vol. 51, pp. 766-777, March 2003.
- A. H. Coskun, and S. Demir “ A CDMA system wideband feedforward linearizer design based on an analytical model,” in *RAWCON Digest*, Boston, MA, August 2003, pp. 191-194.
- A. H. Coskun, and S. Demir “ Application of an analytical model to an actual CDMA system feedforward linearizer,” to be presented in *EUMW 2003*.